NISTIR 6750

Measurement Techniques for Low Heat Flux Exposures to Fire Fighters Protective Clothing

Robert L. Vettori
William H. Twilley
David W. Stroup

NIST
National Institute of Standards and Technology
Technology Administration, U.S. Department of Commerce

NISTIR 6750

Measurement Techniques for Low Heat Flux Exposures to Fire Fighters Protective Clothing

Robert L. Vettori
William H. Twilley
David W. Stroup

Building and Fire Research Laboratory
National Institute of Standards and Technology
Gaithersburg, MD 20899-8641

June 2001

U.S. Department of Commerce
Donald L. Evans, Secretary

National Institute of Standards and Technology
Karen H. Brown, Acting Director

Table of Contents

List of Figures

List of Tables

Measurement Techniques for Low Heat Flux Exposures to Fire Fighters Protective Clothing

Robert L. Vettori
William H. Twilley
David W. Stroup

Abstract

A series of experiments were conducted to investigate measurement technologies that are necessary and appropriate for evaluating the thermal performance of fire fighter protective clothing under low heat flux (≤5.0 kW/m^2) exposure conditions and for relatively long periods of time, up to 10 min. The 19 sensors were tested in six different configurations and exposed to three different levels of heat flux from a natural-gas fired radiant panel. The 6 different configurations were; (1) the sensor exposed to the radiant panel with no contact with anything other than the wires transmitting the sensor output signal, (2) the sensor mounted on a substrate such that the surface of the sensor is flush with the surface of the substrate and exposed to the radiant panel, (3) a section of fire fighter protective clothing is placed between the sensor and the radiant panel, the sensor is touching the back of the material, (4) a section of fire fighter protective clothing is placed between the sensor and the radiant panel, the sensor is placed 6 mm (0.25 in) behind the material, (5) a section of fire fighter protective clothing is placed between the sensor and the radiant panel, the sensor is mounted on the substrate and touching the back of the material, (6) a section of fire fighter protective clothing is placed between the sensor and the radiant panel, the sensor is mounted on the substrate and placed 6 mm (0.25 in) behind the material. The three levels of heat flux were 1.2 kW/m^2, 2.5 kW/m^2, and 5.0 kW/m^2. For a given configuration, there was a significant difference in the recorded measurement of heat flux and temperature. All sensors were affected by mounting them on the substrate. Based on the results from this experimental series the Schmidt-Boelter total heat flux gauge was deemed the most appropriate for measuring incident heat flux. For measuring the surface temperature of a fabric, the use of a thermal pad, made of a material with a high thermal conductivity to which is attached a thermocouple with lead wires made of a material with a low thermal conductivity, may be the most appropriate.

Keywords: burns, fire fighters, fire research, heat flux, protective clothing, sensors, temperature measuring instruments, temperature measurements, test methods

1.0 Introduction

The National Institute of Occupational Safety and Health (NIOSH) has been given the task of addressing the national problem of increasing occupational fire fighter injuries and fatalities. The objectives of the NIOSH program are: to define the magnitude and characteristics of work-related deaths and severe injuries among fire fighters, to develop recommendations for the prevention of these injuries and deaths, and to implement and disseminate prevention efforts. In an effort to prevent burn injuries NIOSH has identified the need to understand the thermal performance of fire fighter protective clothing under relatively low heat flux exposures, ≤ 5 kW/m^2 with extended exposure times of up to 10 min. Currently, there are no standardized test or measurement protocols that adequately address the performance of fire fighter protective clothing under these conditions.

Many workers are exposed to fire hazards in a variety of industrial settings. This is especially true for fire fighters that are exposed to many different thermal environments including flashover conditions. The protective clothing worn by fire fighters is designed to give them a degree of protection from the thermal environment produced by a fire. It allows fire fighters to work where they would be otherwise unable to survive. Fire fighters are at great risk in these environments and protective clothing worn by fire fighters has limitations in terms of thermal protection. The National Fire Protection Association (NFPA) 1971 Standard on Protective Ensemble for Structural Fire Fighting [1] gives minimum requirements for thermal insulation of protective clothing. While the thermal performance of fire fighter's protective clothing has been a point of interest and discussion for the last several decades, little scientific information is available on the technical issues. Much of the data is empirical or based on fire service field experience. Although an excellent source of qualitative data, field experience does not provide the necessary understanding of how to improve the performance of protective clothing. There is still a lack of quantitative data on thermal performance of fire fighter protective clothing. Very little research has been conducted to develop methods for predicting the thermal performance of protective clothing throughout the range of environments faced by a fire fighter. However, much data has been collected in an effort to characterize the thermal environments experienced by fire fighters [2,3,4]. The conditions ranged from pre and post flashover fires within burning structures to conditions on the fire ground outside of burning structures. Foster and Roberts [3] divided this thermal environment into four categories with the associated heat flux exposures that a fire fighter would experience as follows: routine up to 1 kW/m^2, hazardous from 1 kW/m^2 to 4 kW/m^2, extreme 4 kW/m^2 to 10 kW/m^2, and critical over 10 kW/m^2. Abbott [4], in turn, divides the thermal environment into three categories: routine, ordinary, and emergency. The associated heat fluxes associated with these divisions are: routine up to 1.7 kW/m^2, ordinary 1.7 kW/m^2 to 12.5 kW/m^2, and emergency greater than 12.5 kW/m^2. While both Foster et. al. and Abbott considered an exposure to a heat flux of 5 kW/m^2 as hazardous, it is considerably less than the Thermal Protective Performance Test exposure of 84 kW/m^2 described in NFPA 1971.

In order to predict the extent of injury to a human that would result in a heat exposure it is necessary to know the temperature history of the skin's basal layer. Many investigators have examined skin burning and developed criteria to predict the onset of irreversible damage [5,6].

For damage to occur the growing or basal layer temperature must reach 44 °C (112 °F). At this temperature, irreversible damage begins to occur to the basal layer and the longer it is at or above this temperature the greater the amount of damage.

For the temperature at the surface of the skin or a portion within it to be predicted, the heat transfer to the surface of the skin needs to be known. Once the heat transfer and its variation with location and times is known, a heat transfer model of human skin can be used to estimate the damage due to burning. Heat transfer from a heat source into the surface of the skin can be modeled as transient heat transfer into a semi-infinite solid [7,8]. For the case of a constant heat flux at the surface and constant thermal physical properties, the analytical solution can be shown to be:

$$T(x,t) - T_i = \frac{2q_o''\left(\frac{\alpha t}{\pi}\right)^{1/2}}{k}\exp\left(\frac{-x^2}{4\alpha t}\right) - \frac{q_o'' x}{k}\,erfc\left(\frac{x}{2\sqrt{\alpha t}}\right)$$

Equation 1

Where T = temperature K

T_i = initial temperature K

q_o'' = incident heat flux W/m^2

α = thermal diffusivity $\left(k/\rho c\right) m^2/s$

ρ = density kg/m^3

c = specific heat J/kgK

t = time s

k = thermal conductivity W/mK

x = distance into solid m

$erfc$ = complimentary error function

At the surface, i.e. $x = 0$ this reduces to

$$T(0,t) - T_i = \frac{2q\sqrt{t}}{\sqrt{\pi k \rho c}}$$

Equation 2

Physiological burn damage rate models are based on knowledge of the intensity and duration of incident heat flux on the skin surface. The purpose of a sensor is either to obtain a direct reading of the heat flux or to permit the heat flux to be predicted.

The objective of this experimental series is to examine the response of various thermal sensors[1], in different configurations, exposed to relatively low heat fluxes, ≤ 5 kW/m^2, for a period of 10 min. It will demonstrate that sensors made of various materials, placed in identical configurations and exposed to the same radiant heat flux will give different results. Also, that sensors made of the same material, placed in identical configurations and exposed to the same radiant heat flux will report different results based on the size of the sensor and lead wires that carry the sensor signal. Most of the sensors examined in this experimental series have been used in past research in a variety of configurations to measure the heat transfer through protective clothing.

2.0 Sensor Selection

The sensors chosen for this experimental series are listed in Table 1.

The copper disk sensor, Figure 1 and Figure 2, is presently used to measure the applied heat flux in the Thermal Protective Performance (TPP) Test as described in NFPA 1971. Type J thermocouples, such as those shown in Figure 3 and Figure 4, are used to measure the temperature rise of the copper disk used in the TPP test. The encapsulated thermocouple, Figure 5 and Figure 6, is one type of sensor that is presently used in full-scale experiments utilizing mannequins [9]. The encapsulated thermocouple used in these experiments consisted of a type T thermocouple buried below the exposed surface of a cast resin plug. Type K thermocouples, Figure 3 and Figure 4, and the water cooled Schmidt-Boelter total heat flux gauge have both been used for many years in fire research to measure temperatures and heat fluxes respectively [10]. For each type of thermocouple, four different wire sizes were tested. Only one encapsulated thermocouple was tested. The thin film heat flux sensor, Figure 7, like the water-cooled Schmidt-Boelter total heat flux gauge measures the incident heat flux at its surface. The thin film sensor measurement is obtained from a thermopile heat flux sensor that occupies most of the surface area on the sensor face. Two water-cooled radiometers were also chosen. Both are based on the Schmidt-Boelter principle of measuring heat flux. Radiometers are designed to measure only the radiative fraction of thermal energy. If radiation and convection are both present, the radiometer will only monitor the radiative component. Radiometers typically employ a window or lens placed between the heat source and the heat flux sensor. The window or lens can be fabricated in such a way as to allow radiation of specific wavelength to pass through. In the case of these two radiometers, one had a sapphire lens which had a spectral transmittance of 0.15 μm to 5.0 μm and one with a zinc selenide window, which had a spectral transmittance of 0.5 μm to 22 μm.

[1] Certain commercial equipment, instruments, or materials are identified in this paper in order to adequately specify the experimental procedure. Such identification does not imply recommendation or endorsement by the National Institute of Standards and Technology, nor does it imply that the materials or equipment identified are necessarily the best available for the purpose.

3.0 Experimental Set Up

The test apparatus and its components are the same as the apparatus used in reference 11 and is shown in Figure 8. Radiant heat energy for this test is produced by a premixed air natural gas fueled radiant panel with a radiating surface measuring 305 mm by 457 mm (12 in by 18 in). The radiant panel type is specified in ASTM E162, Standard Test Method for Surface Flammability of Materials using a Radiant Heat Energy Source [12]. This radiant panel is normally operated at an average surface blackbody temperature of 943 K with variation not to exceed ± 4 K.

A calibrated Schmidt-Boelter total heat flux gauge of the type specified in ASTM E1321, Standard Test Method for Determining Material Ignition and Flame Spread Properties [13] was used to measure the heat flux level. This water-cooled, thermopile, heat flux transducer has a nominal range of 0 kW/m^2 to 10 kW/m^2 with a corresponding voltage range of 0 mV to 9 mV. The time constant to reach 63 % of final value for this heat flux gauge is not more than 290 ms with a corresponding time to reach 95 % of the final output of not more than 1 s.

Since the radiant panel is always operated at a constant temperature, the incident heat flux is adjusted to the desired value by moving a trolley assembly that is attached to the radiant heat panel test frame. The sensor is attached to this moveable assembly. The distance from the radiant panel needed for each of the three desired heat fluxes was determined by the use of the Schmidt-Boelter total heat flux gauge and analytical methods. The energy incident on a surface a distance from a specific radiator, such as a radiant panel, may be found by use of the following:

$$q_o'' = \phi \varepsilon \sigma T^4$$

Equation 3

Where q_o'' = incident heat flux W/m^2

ϕ = configuration factor

ε = emissivity of sensor surface

σ = Stefan Boltzmann constant (5.67×10^{-8} W/m^2K^4)

T = temperature of the radiant panel K

The emissivity of the Schmidt-Boelter total heat flux gauge is 0.96. The temperature of the radiant panel is 943 K ± 4 K. The configuration factor is used to take into account the geometrical relationship between the radiator, in this case the radiant panel, and the receiving element. It may be defined as the ratio of the intensity at the receiving element to the intensity of the radiator and is a function of the size of the radiating surface, its distance from the receiving element, and the relative orientation of the receiving element and radiator. For example, the distance from the radiant panel that would produce incident radiation of 2.5 kW/m^2 was determined by the use of the Schmidt-Boelter gauge as 0.85 m (33.5 in). By use of Equation 3, a configuration factor obtained from McGuire (14), and the range of temperatures for the radiant

panel, the calculated incident heat flux at 0.85 m (33.5 in) from the radiant panel is in the range of 2.43 kW/m^2 to 2.52 kW/m^2.

Each sensor was tested in six different configurations. For each configuration, 10 experiments were conducted. The six different configurations are listed in Table 2

The first configuration, "exposed," Figure 9, was chosen to measure the response of each sensor when exposed to a radiant heat source. The second configuration, "substrate," Figure 10, was chosen to measure the response of each sensor when mounted on a substrate and exposed to a radiant heat source. The material used for the substrate was bakelite with dimensions of 100 mm by 100 mm by 13 mm (4 in by 4 in by 0.5 in). The thermal properties of the substrate are given in Table 3. This was done to simulate the placement of the sensor on a skin simulant or on a mannequin to determine what effect this placement has on the sensor response. The third configuration, "fabric-exposed-no space," Figure 11, measures the response of the sensor when placed behind protective clothing. This simulates the measurement of the heat transfer through protective clothing with the protective clothing touching the wearer's skin. The fourth configuration, "fabric-exposed-space," Figure 12, adds a space of approximately 6 mm (0.25 in) between the sensor and the protective clothing to simulate an air gap between the wearer and the protective clothing. The fifth configuration, "fabric-substrate-no space," Figure 13, again places the sensor on a substrate, to simulate the sensor placed on a skin simulant or mannequin to determine the impact this placement has on the sensor response. The sixth and last configuration, "fabric-substrate-space," Figure 14, is the same as the fifth configuration with a space of 6 mm (0.25 in) added between the sensors and the protective clothing to simulate an air gap between the wearer and the protective clothing.

The piece of protective clothing placed between the sensor and radiant panel was made of materials used in the construction of typical fire fighter protective clothing. The individual components, an outer shell, a breathable moisture barrier, and a thermal liner, are shown in Figure 15 before assembly into a test specimen. The surface dimensions of the protective clothing were 305 mm by 355 mm (12 in by 14 in) with the 355 mm (14 in) dimension in the vertical direction. For all the experiments conducted in this series, there was no air gap between the individual components. Figure 8 shows an experimental set up in which the protective clothing assembly is placed between the radiant panel and the sensor. Thermal properties of the individual components that make up the protective clothing are listed in Table 4 and came from reference 18. The specific heats of these components are not available at this time.

4.0 Experimental Procedure and Data Acquisition

The gas fired radiant panel was ignited and allowed to preheat for 45 min. This preheat period allowed the radiant panel's temperature to stabilize before calibration was attempted. Using the Schmidt-Boelter total heat flux transducer, the moveable assembly was positioned such that the incident heat flux was one of the three pre-determined levels. A thermal radiation shield which included a water cooled panel was placed between the assembly and the radiant panel. The sensor(s) was mounted on the assembly. The data acquisition system was started. After 60 s of background data the radiation shield was removed exposing the sensor(s) to the radiant panel.

After a 10 min exposure the radiation shield was put back into place, the sensor(s) allowed to cool to ambient temperature and the experiment repeated. A computer controlled data logger recorded data at one second intervals.

5.0 Data Presentation

Data from the experiments are presented in two formats, tabular and graphical. First, a tabular format in which the final temperature increase or heat flux is given after a 10 min exposure along with plus and minus two standard deviations. Table 7 through Table 25 gives this information for each sensor in each of the six tested configurations. The first column of each table lists the six experimental configurations. The second, third, and fourth columns are the reported sensor response for the 1.2 kW/m^2, 2.5 kW/m^2 and 5.0 kW/m^2 exposures, respectively. The graphical format presents the sensor response curves versus time for the entire 10 min exposure. Each graph has multiple curves. These curves represent the response of more than one sensor to an exposure or the response of one sensor to all three heat flux exposures. At a minimum, the curves represent the average response of the sensor(s) for the 10 experiments. Many of the graphs have error bars that represent plus and minus two standard deviations. The caption for each figure will indicate the sensor or sensors reported, the configuration the sensor(s) was in, the heat flux exposure, and if the figure contains error bars. If possible, labels were placed on the graph indicating which sensor each curve represents. Often the sensor responses were so close together that labeling the curves was difficult. In this case the labels were omitted. For comparison purposes the figures can be divided into the following categories:

Figure 16 through Figure 21	Response of one type of thermocouple to an exposure based on all four wire sizes in the “exposed” configuration.
Figure 22 through Figure 27	Response of one type of thermocouple to an exposure based on all four wire sizes in the “substrate” configuration.
Figure 28 through Figure 33	Response of one type of thermocouple to an exposure based on all four wire sizes in the “fabric-exposed-no space” configuration.
Figure 34 through Figure 39	Response of one type of thermocouple to an exposure based on all four wire sizes in the “fabric-exposed-space” configuration.
Figure 40 through Figure 45	Response of one type of thermocouple to an exposure based on all four wire sizes in the “fabric-substrate-no space” configuration.
Figure 46 through Figure 51	Response of one type of thermocouple to an exposure based on all four wire sizes in the “fabric-substrate-space” configuration.
Figure 52 through Figure 55	Response of all three thermocouple types to an exposure based on one wire size in the “exposed” configuration.
Figure 56 through Figure 59	Response of all three thermocouple types to an exposure based on one wire size in the “substrate” configuration.

Figure 60 through Figure 63	Response of all three thermocouple types to an exposure based on one wire size in the “fabric-exposed-no space” configuration.
Figure 64 through Figure 67	Response of all three thermocouple types to an exposure based on one wire size in the “fabric-exposed-space” configuration.
Figure 68 through Figure 71	Response of all three thermocouple types to an exposure based on one wire size in the “fabric-substrate-no space” configuration.
Figure 72 through Figure 75	Response of all three thermocouple types to an exposure based on one wire size in the “fabric-substrate-space” configuration.
Figure 76 through Figure 81	Response of encapsulated type T thermocouple.
Figure 82 through Figure 89	Response of copper disks.
Figure 90 through Figure 95	Response of thin film heat flux gauge.
Figure 96 through Figure 100	Response of water-cooled Schmidt-Boelter total heat flux gauge.
Figure 101 through Figure 105	Response of water-cooled sapphire window radiometer.
Figure 106	Response of water-cooled zinc selenide window radiometer.

6.0 Results

6.1 Temperature Measurement

Final Temperature Increases

The sensor configuration, thermal properties of the sensor itself, and the incident radiant flux all affected the final temperature increases. Sensors in the “substrate” configuration recorded higher temperature increases than in the “exposed” configuration. Once the sensors were placed behind the protective clothing the effect of mounting the sensors on the substrate was not as significant. In these configurations, several sensors recorded less of a temperature increase when placed on the substrate. The size and the thermal conductivity of the thermocouple wire influenced the temperature increases reported by the twelve thermocouple sensors. Both copper disks, and the encapsulated thermocouple monitored greater temperature increases than the twelve thermocouple sensors. As would be expected, the 5.0 kW/m^2 value of incident flux produced significantly higher temperature increases than did the 2.5 kW/m^2 or 1.2 kW/m^2 incident fluxes.

Thermocouples

All thermocouples recorded higher temperatures when in the “substrate” configuration then when in the “exposed” configuration. For the twelve thermocouples, the final temperature increases in the “exposed” configuration ranged from 1.6 °C to 2.7 °C (3 °F to 5 °F) at 1.2 kW/m^2 to 1.1 °C to 9.0 °C (2 °F to 16 °F) at 5.0 kW/m^2. When the thermocouples were

placed in the “substrate” configuration the temperature increases ranged from 18.6 °C to 31.3 °C (33 °F to 56 °F) at 1.2 kW/m^2 to 68.0 °C to 112.0 °C (122 °F to 202 °F) at 5.0 kW/m^2. When placed behind the protective clothing and having a space of 6 mm (0.25 in) between the sensor and the protective clothing, all 12 thermocouples again recorded higher temperature increases when placed on the substrate. However, when there is no space between the sensor and the protective clothing the effect of mounting the sensor on a substrate is not as clear. In the case of the thermocouples some recorded greater temperature increases when placed on the substrate and others less of a temperature increase when placed on the substrate.

The thermal conductivity, emissivity, and diameter of the thermocouple wire did appear to impact the increase in temperatures reported by the type J, K, and T thermocouple sensor packages. The effect of thermal conductivity is most readily seen in the temperature increases or actually the reduced temperature increases of the type T thermocouples in the "substrate" configuration as compared to the type J and K thermocouples in the "substrate" configuration. For the 0.81 mm (0.032 in) wire diameter and 5.0 kW/m^2 radiant flux, the type T, J and K thermocouples recorded temperature increases of 68 °C, 91 °C, and 99.1 °C (122 °F, 164 °F, and 178 °F), respectively. This would be consistent with the higher thermal conductivity of the type T thermocouple wire, see Table 5. The impact of wire diameter is apparent when comparing the four different wire diameters within a single type of thermocouple. For the type T thermocouple and 5 kW/m^2 of radiant flux the temperature increases for the 0.13 mm, 0.26 mm, 0.51 mm and 0.81 mm (0.005 in, 0.010 in, 0.020 in, and 0.032 in) wire diameters were 106 °C, 93.9 °C, 77.6 °C and 68 °C, (191 °F, 169 °F, 140 °F, and 122°F) respectively. As the wire diameter increased there was a reduction in the temperature increase. This would be consistent with the larger wire conducting more energy away from the thermocouple bead then that for a smaller diameter wire.

In the “exposed” configuration, all twelve thermocouples responded similarly. When exposed and placed 6 mm (0.25 in) behind the protective clothing (“fabric-exposed-space” configuration) the twelve thermocouples again responded in similar fashions. In these two configurations, the type of thermocouple or the diameter of the thermocouple wire did not appear to have a significant effect on the response. When the thermocouples are placed on a substrate the differences between type of thermocouple material and diameter of the thermocouple wire becomes more significant. In the “substrate” configuration the type J and type K thermocouples respond similarly. However, in all cases, the type T thermocouples consistently reported lower temperatures than the type J or K thermocouples and the difference becomes greater as the diameter of the thermocouple wire increases. The effect of thermal conductivity is not apparent at the smallest thermocouple wire size, 0.13 mm (0.005 in). At the two largest wire sizes, 0.51 mm and 0.81 mm (0.020 in and 0.032 in) the measured increase in temperature follows the ranking of the thermocouple wire thermal conductivity. The type K thermocouples, which have the lowest thermal conductivity reports the highest temperature increase, while the type T thermocouples with the highest thermal conductivity reported the least increase in temperature.

Copper Disks and Encapsulated Thermocouples

The two copper disks and the encapsulated thermocouple responded differently to the incident flux than the type J, K, and T thermocouples. In the "exposed" configuration, the copper disks recorded temperature increases of between 30.8 °C (55 °F) at 1.25 kW/m^2 and 105.3 °C (190 °F)

at 5 kW/m^2 while the encapsulated sensor reported temperature increases of 28.7 °C to 105.6 °C (52 °F to 190 °F). These temperature increases are ten to twenty times higher than for the twelve thermocouples in the "exposed" configuration. Of course much of the higher temperature increase would be consistent with the greater surface area of the disk and of the cast resin plug encapsulating the thermocouple. The larger surface area would allow these sensors to absorb more of the incident radiant flux. Mounting the sensor on a substrate did result in the sensor reporting higher temperature increases. The changes were in the range of 16 % to 29 % which was much less than the factor of ten or twenty observed in the twelve thermocouples.

The response of the two copper disks were almost identical in both the “exposed” and “substrate” configurations. No extra degree of accuracy was obtained by having four thermocouples attached to the copper disk. Therefore, for the configurations in which the sensor was placed behind the protective clothing only one of the copper disks was tested.

The copper disk and encapsulated thermocouple, when positioned behind the protective clothing, and having a gap between the sensor and the protective clothing, both recorded higher temperature increases when mounted on a substrate. However, when there is no space between the sensor and protective clothing both sensors recorded less of a temperature increase when mounted on the substrate.

6.2 Heat Flux Measurement

Table 22 through Table 25 give the final measurement for the four sensors whose output is recorded as heat flux. In the “exposed” configuration the response of the water cooled sapphire window radiometer is consistently less than that of the water-cooled Schmidt-Boelter total heat flux gauge. This is due to the sapphire window excluding some fraction of the spectral energy from the gas fired radiant panel. The spectral transmittance of the sapphire window is from 0.15 μm to 5.0 μm. For the “exposed” configuration the sapphire window radiometer measurements of 0.9 kW/m^2, 1.82 kW/m^2, and 3.8 kW/m^2, were respectively 71 %, 72 %, and 76 % of those recorded by the Schmidt-Boelter total heat flux gauge. This measured response of the sapphire window radiometer is reasonable since at 943 K, the average surface blackbody temperature of the radiant panel, approximately 70 % of the radiation falls at wavelengths below 5.8 μm [15]. The remaining radiation is excluded by the sapphire window.

The zinc selenide window with a spectral transmittance from 0.5 μm to 22 μm allows approximately 98 % of the incident radiation to pass through. This is also in line with measured values recorded when in the “exposed” configuration. Recorded measurements of the water-cooled zinc selenide radiometer of 1.18 kW/m^2, 2.40 kW/m^2, and 4.84 kW/m^2, were respectively 93 %, 95 %, and 97 % of those recorded by the water-cooled Schmidt Boelter total heat flux gauge. The zinc selenide window radiometer was only tested in the “exposed” configuration.

When placed behind the protective clothing (“fabric-exposed-space” configuration) the water-cooled sapphire window radiometer readings were only 19 % to 22 % of that recorded by the water-cooled Schmidt-Boelter total heat flux gauge. With the back of the protective clothing being much cooler than the radiant panel, there is not only less radiant energy given off by the

protective clothing, but it is also at a higher wavelength and therefore a greater percentage is excluded by the sapphire window. In the "fabric-exposed- no-space" configurations the sapphire window radiometer measurements were only 9 % of the Schmidt Boelter total heat flux gauge.

The Schmidt-Boelter total heat flux gauge and the sapphire window radiometer were only placed on substrates when tested behind the protective clothing. When there was a space between the sensor and the protective clothing the Schmidt-Boelter gauge recorded a higher heat flux when mounted on the substrate. When there was no space between the sensor and the protective clothing the Schmidt-Boelter gauge recorded a lesser heat flux when mounted on the substrate. There was no measurable difference in the values recorded by the sapphire window radiometer when placed on a substrate.

In the "exposed" configuration, the thin film heat flux gauge measurements of 0.9 kW/m^2, 1.82 kW/m^2, and 3.8 kW/m^2 were respectively 58 %, 63 %, and 68 % of those recorded by the Schmidt-Boelter total heat flux gauge. When placed on a substrate the thin film heat flux gauge initially recorded higher heat flux measurements than when in the "exposed" configuration (Figure 91), but the recorded output decreased as the experiment continued. This was most noticeable at the 5 kW/m^2 exposure. No other total heat flux gauge or radiometer was tested in the "substrate" configuration.

When placed behind the protective clothing sample, the thin film heat flux gauge recorded lower heat fluxes than the Schmidt-Boelter gauge ranging from 51 % to 82 % of the values recorded by the Schmidt-Bolter gauge. When there was a space between the thin film heat flux gauge and the protective clothing there was a slight increase in the reported heat flux when the sensor was mounted on the substrate. When there was no space there was no difference in the reported heat fluxes.

7.0 Uncertainty Analysis

There are different components of uncertainty in the temperatures, radiative heat flux, convective heat flux, conductive properties of the materials, and positioning of the sensors reported here. Uncertainties are grouped into two categories according to the method used to estimate them. Type A uncertainties are those which are evaluated by statistical methods, and Type B are those which are evaluated by other means (16). Type B evaluation of standard uncertainty is usually based on scientific judgment using all the relevant information available, which may include previous measurement data, experience with or general knowledge of the materials or instruments, manufactures specifications, calibration data, and uncertainties assigned to reference data from handbooks.

Table 6 lists the uncertainties in measurements, obtained from manufacturer's literature associated with each sensor. Actual uncertainty will exceed these values. Information on thermal properties of sensors and materials, Table 3 to Table 5, came from manufacturers, handbooks, and reports. However, these data did not have uncertainties associated with them.

Each sensor was carefully positioned before the start of an experiment. When in the "exposed" and "substrate" configurations the distance from the radiant panel was dictated by the desired heat flux. At the 1.2 kW/m^2 setting, the distance between the sensors and the radiant panel is 1.21 m (47.5 in). A difference of ±0.2 cm (0.1 in) in the placement of the sensor would translate into approximately ± 0.3 % in the incident heat flux on the sensor. At the 5.0 kW/m^2 setting the distance between the sensor and the radiant panel is 0.57 m (22.5 in). Here a difference of ±0.2 cm (0.1 in) in the placement of the sensor would translate into approximately ±0.6 % in the incident heat flux on the sensor.

When the sensors are placed behind the protective clothing the protective clothing is positioned such that one of the three desired heat fluxes is imposed on the front face of the protective clothing, Figure 11 through Figure 14. The sensor is placed 6 mm (0.25 in) behind the protective clothing. The protective clothing has now become the radiator or source of heat flux for the sensor. Since the sensor is very close to the back side of the protective clothing even a difference of ± 0.2 cm would only cause a difference of ± 0.06 % in the incident heat flux on the sensor.

When placing the sensors such that they were touching the protective clothing, whether exposed or on the substrate, it was difficult to determine how firmly the sensor was touching the protective clothing. Variances in the pressure exerted by a sensor on the protective clothing could change the contact area between the sensor and protective clothing and therefore change the heat transfer characteristics. This change is caused by what is known as thermal contact resistance. The existence of a contact resistance is due principally to surface roughness effects. Contact spots between the sensor and the fabric are interspersed with gaps that are, in most instances, air filled. Heat transfer is therefore due to conduction across the actual contact area and to conduction and or radiation across the gaps.

8.0 Discussion

It is interesting to note that the thermocouples when exposed and placed behind the protective clothing ("fabric-exposed-space" configuration) all reported a higher temperature after the 10 min exposure than when the thermocouples were in the "exposed" only configuration. This is partly due to a convective boundary layer that is formed on the backside of the fabric as it is heated. For a vertical surface in a quiescent environment the thickness of this boundary layer can by calculated [15]. Given an ambient temperature of 22 °C (72 °F), and a surface temperature of 27 °C (81 °F) on the backside of the protective clothing, a convective boundary layer would be created that is approximately 35 mm (1.4 in) thick at the sensor. For a surface temperature of 125° C (237 °F) on the backside of the protective clothing this boundary layer thickness is 23 mm (0.9 in). Since the thermocouples are only 6 mm (0.25 in) from the back surface of the fabric they are within this boundary layer.

When the thermocouples are in the "substrate" configuration, their response is quite similar to both of the copper disks and the encapsulated thermocouple in the "exposed" configuration. At

the 5.0 kW/m^2 exposure the 0.13 mm (0.005 in) thermocouples on a substrate reported a temperature increase of between 106 °C and 112 °C (223 °F and 234 °F). Both copper disks and the encapsulated thermocouple reported a temperature increase of 102 °C to 106 °C (216 °F and 223 °F) when in the "exposed" configuration. Close agreement is also realized at the 1.2 kW/m^2 and 2.5 kW/m^2 exposures for the smaller thermocouple wire. This agreement in temperature increase is expected since the copper disk with either one or four type J thermocouples attached to it has a similar geometry as the thermocouples mounted on a substrate. In this case the copper disk is the substrate. In addition, the 0.26 mm (0.010 in) type J thermocouples are used with the copper disks. For the encapsulated thermocouple, the substrate is the cast resin plug that the type T thermocouple is embedded in. As the size of the thermocouple wire diameter increases the reported temperature rise decreases. Again this is most notable in the type T thermocouple. The 0.81 mm (0.032 in) type T thermocouple reported a temperature increase of 68 °C (154 °F) as compared to the 106 °C (223 °F) temperature increase of the smaller 0.13 mm (0.005 in) type T thermocouple.

Using Equation 1 and the properties of the substrate material from Table 3, calculations were made to determine the surface temperature of the substrate at the point in time where the semi infinite slab assumption would cease to be appropriate. Of the thermocouples, in all cases the smallest thermocouple wire sizes came closest to these calculated values, with the type J and K thermocouples giving the best results. For all three heat flux levels the increase in temperatures recorded by the smallest type J and type K thermocouples came to within 67 % of the calculated increase in surface temperatures of the substrate. The type T thermocouple which has the highest thermal conductivity of the three thermocouple materials was slightly lower, measuring 62 % of the calculated temperature increase for all three heat flux levels. The copper disks came closest to the calculated temperature increase. Both of the copper disks had increases in temperature that came to within 83 % of the calculated value at 1.2kW/m^2, 79 % of the calculated value at 2.5 kW/m^2 and 76 % of the calculated value at 5.0 kW/m^2. The encapsulated thermocouple gave results of 73 % of the calculated values for all three heat flux levels.

When the sensors were placed behind and touching the protective clothing and exposed ("fabric-exposed-no-space" configuration) or on a substrate ("fabric-substrate-no-space" configuration) the thermal conductivity of the thermocouple wire again becomes a factor. For all the thermocouples the increase in temperature reported follows the ranking of their respective thermal conductivities. The type K thermocouples with the lowest thermal conductivity reported the highest temperature increase while the type T thermocouple with the highest thermal conductivity reported the least temperature increase. The temperature increase of the copper disk, which has a high thermal conductivity has the highest temperature increase which appears inconsistent with what was described above. However, in this configuration the copper disk is acting as a heat collecting pad or heat sink to which thermocouple wires with low thermal conductivities are attached. This use of a heat sink or thermal pad made of a material with a high thermal conductivity is recommended [17] when trying to measure the surface temperature of a material with a low thermal conductivity, such as protective clothing. Some typical values for thermal conductivity of materials used in fire fighter protective clothing can be found in reference [18]. The thermal conductivity of the thermal lining material used in this experimental series is 0.035 $W/m \cdot K$.

There is no easy method of attaching a thermocouple or any alternate transducer to a surface so that it can be guaranteed to indicate the true surface temperature. To do this it would be necessary to mount the measuring device so that it could attain, but not affect the surface temperature. In most cases, the presence of the thermocouple or any other measuring device will cause a perturbation of the temperature distribution at the point of attachment, and thus it only will indicate the perturbed temperature. An additional consideration when trying to measure the surface temperature of a fabric is the surface contact between the sensor and the fabric. Variances in the pressure exerted by a sensor on the protective clothing could change the contact resistance between the sensor and protective clothing and therefore change the heat transfer characteristics. As discussed earlier this change is caused by what is known as thermal contact resistance which is due principally to surface roughness effects. There are many methods described in the literature that can be used to attach sensors to materials. However, these often describe methods of attaching sensors to metal objects by welding, brazing, clamping, etc. Stoll and Hardy [19] investigated several devices used for the measurement of a material's surface temperature. They attempted to measure the surface temperature of an oak tanned leather material and noted the difficulty of quantifying the contact pressure of the sensor on the material. Lawson and Twilley [11] describe a method of attaching thermocouples to a fabric for the purpose of measuring surface temperature.

When placed behind the protective clothing and with a space of 6 mm (0.25 in) between the sensors and the protective clothing ("fabric-exposed-space" configuration or "fabric-substrate-space" configuration) all except one sensor measured higher temperatures when on the substrate. This one was the copper disk with 4 thermocouples attached and only at the 5.0 kW/m^2 exposure. In this configuration there is a convective flow that is due to the back of the fabric heating and a convective flow that is caused by the substrate itself.

The use of thermocouples presents challenges including the ambiguities involved in heat flux calculations and skin burn injury estimations. For the purpose of measuring the surface temperature of a fabric with a low thermal conductivity, a thermocouple mounted to a heat sink that is then attached to the fabric appears to give the best or most representative results. Although not specifically designed for this purpose, the copper disk used in these experiments emulates this configuration. The copper disk which is a material with a high thermal conductivity is placed against the protective clothing and acts as a heat sink. Attached to the copper disk are 0.26 mm (0.010 in) type J thermocouples which are measuring the temperature of the copper disk. Data from the "Fabric exposed no space" configuration indicates that the copper disk reported a greater temperature increase than any of the thermocouples. For an imposed heat flux on the front surface of the protective clothing of 5 kW/m^2 the copper disk recorded a temperature increase of 91 °C (194 °F). For this same heat flux the 0.26 mm (0.010 in) type J thermocouple when placed directly on the protective clothing recorded a temperature increase of 46 °C (83 °F). Reference 17 suggests that the thermocouple attached to the heat sink be made from wires that have as low a thermal conductivity as possible. Of the three thermocouple materials used in these experiments the type K thermocouple has the lowest thermal conductivity. This suggests that if type K thermocouples had been attached to the copper disk that the recorded temperature may have been higher. From the thermocouples tested in this experimental series the 0.13 mm (0.005 in) type K thermocouple would give the most

accurate results. The use of a thermocouple made of such a small diameter wire does not pose a problem in small scale laboratory work. However, for large scale testing or field work where these thermal pads would be subject to movement the small diameter lead wires may be easily broken. In this case a compromise would need to be made between accuracy and ruggedness of the measuring device.

The use of copper disks to determine heat flux by measuring the initial temperature rise of the copper disk is a practice that is in use [20]. The following expression may be used to calculate the incident heat flux on the copper disk surface.

$$\dot{q}_c = \rho C_p l\left(\frac{\Delta T}{\Delta t}\right)=\left(\frac{MC_p}{A}\right)\left(\frac{\Delta T}{\Delta t}\right)$$

Equation 4

Where: $\dot{q}_c$ = incident heat flux kW/m^2

ρ = density of copper kg/m^3

C_p = specific heat of copper $kJ/kg \cdot k$

l = thickness of copper disk m

ΔT = copper disk temperature rise during exposure to radiant panel, initial linear temperature rise k

Δt = time period corresponding to ΔT temperature rise s

M = mass of copper disk kg

A = cross sectional area of copper disk m^2

The use of Equation 4 is limited to the initial linear portion of the time-temperature curve that is obtained during the copper disk's exposure to the heat source [20]. Analysis of the data at the 1.2 kW/m^2 exposure indicates that after 30 s the time-temperature curve is no longer linear. However, within this time frame and after the initial temperature transient effects were eliminated the calculated heat flux by use of Equation 4 was 1.15 kW/ m^2. At 2.5 kW/m^2 and 5.0 kW/m^2 the initial linear portion of the time-temperature curve is over a period of approximately 20 s and 15 s, respectively. At exposures to higher heat fluxes the period over which this time-temperature curve would be linear becomes smaller. Therefore, for exposures and time periods of interest to this experimental series the use of copper disk calorimeter is not recommended.

The manufacturer of the encapsulated thermocouple claims that heat flux can be calculated through the temperature rise of the encapsulated thermocouple by use of a proprietary method. We did not investigate this capability.

9.0 Conclusions

A series of experiments was conducted to investigate the response of different thermal sensors to three different heat fluxes and in six different configurations. It has been shown that the sensor configuration, thermal properties of the sensor itself, and the incident radiant flux all affected the final temperature increases or heat flux measurements.

For measuring the heat flux incident on a surface the water cooled Schmidt-Boelter total heat flux gauge yields values closest to what is predicted. The sapphire window radiometer with its spectral range on 0.15 μm to 5.5 μm only measured a portion of the radiant heat flux. Both the sapphire and zinc selenide window radiometers do not measure the convective portion of heat energy that may be present. The copper disk measurement of temperature can be converted into a heat flux by use of Equation 4. However this method is only appropriate during the initial linear temperature rise of the copper disk. The lowest heat flux of 1.2 kW/m^2 the temperature rise of the copper disk was linear for only the first 30 s. Therefore for the purpose of a 10 min exposure even at the lowest heat fluxes used in these experiments, the copper disk would be inappropriate. Logistically, the water cooled Schmidt-Boelter gauge may be difficult to implement when dozens of measurements are required in the field with an instrumented mannequin or actual fire fighter.

For temperature measurements, it has been shown that there is a wide variation in reported measurements among sensors, even those made of the same material. For measuring the surface temperature of a fabric, it appears that the use of a thermal pad made of a material with a high thermal conductivity to which is attached a thermocouple with lead wires made of a material with a low thermal conductivity, may be the most appropriate. In this experimental series the copper disk emulated this arrangement. The use of small thermal pads for temperature measurements should not impose any more difficulty in field use than thermocouples. Regardless of the method used for determining surface temperature, a methodology needs to be developed that can take this temperature and translate it to potential burn injury. This would be a subject for further research.

10.0 Acknowledgements

This work was funded by the National Institute of Occupational Safety and Health, Center for Disease Control, U.S. Department of Health and Human Services. Appreciation is extended to Tim Pizatella and Thomas Hodous of NIOSH for their support. To Daniel Madrzykowski and David Stroup for providing guidance in the experimental set up and sensor selection. Finally to William Twilley who constructed the experimental apparatus up and performed all of the experiments.

Table 1. Description of sensors.

Omega Engineering type J (Iron versus Copper Nickel) thermocouple – 0.81 mm (0.032 in) wire diameter. Thermocouple bead coated with a paint with an emissivity of 0.96.
Omega Engineering type J (Iron versus Copper Nickel) thermocouple – 0.51 mm (0.020 in) wire diameter. Thermocouple bead coated with a paint with an emissivity of 0.96.
Omega Engineering type J (Iron versus Copper Nickel) thermocouple – 0.26 mm (0.010 in) wire diameter. Thermocouple bead coated with a paint with an emissivity of 0.96.
Omega Engineering type J (Iron versus Copper Nickel) thermocouple – 0.13 mm (0.005 in) wire diameter. Thermocouple bead coated with a paint with an emissivity of 0.96.
Omega Engineering type K (Nickel-Chromium versus Nickel-Aluminum) thermocouple – 0.81 mm (0.032 in) wire diameter. Thermocouple bead coated with a paint with an emissivity of 0.96.
Omega Engineering type K (Nickel-Chromium versus Nickel-Aluminum) thermocouple – 0.51 mm (0.020 in) wire diameter. Thermocouple bead coated with a paint with an emissivity of 0.96.
Omega Engineering type K (Nickel-Chromium versus Nickel-Aluminum) thermocouple – 0.26 mm (0.010 in) wire diameter. Thermocouple bead coated with a paint with an emissivity of 0.96.
Omega Engineering type K (Nickel-Chromium versus Nickel-Aluminum) thermocouple – 0.13 mm (0.005 in) wire diameter. Thermocouple bead coated with a paint with an emissivity of 0.96.
Omega Engineering type T (Copper versus Copper Nickel) thermocouple – 0.81 mm (0.032 in) wire diameter. Thermocouple bead coated with a paint with an emissivity of 0.96.
Omega Engineering type T (Copper versus Copper Nickel) thermocouple – 0.51 mm (0.020 in) wire diameter. Thermocouple bead coated with a paint with an emissivity of 0.96.
Omega Engineering type T (Copper versus Copper Nickel) thermocouple – 0.26 mm (0.010 in) wire diameter. Thermocouple bead coated with a paint with an emissivity of 0.96.
Omega Engineering type T (Copper versus Copper Nickel) thermocouple – 0.13 mm (0.005 in) wire diameter. Thermocouple bead coated with a paint with an emissivity of 0.96.
Copper disk with 4 Omega Engineering type J (Iron versus Copper Nickel) thermocouples, 0.26 mm (0.010) wire diameter attached. Disk diameter 3.99 cm, Disk thickness 0.162 cm, Disk mass 0.0174 kg. Disk surface coated with a paint with an emissivity of 0.96.
Copper disk with 1 Omega Engineering type J (Iron versus Copper Nickel) thermocouple, 0.26 mm (0.010) wire diameter attached. Disk diameter 3.99 cm, Disk thickness 0.157 cm, Disk mass 0.0173 kg. Disk surface coated with a paint with an emissivity of 0.96.
E. I. Du Pont encapsulated type T (Copper versus Copper Nickel) thermocouple
Medtherm Corporation water cooled Schmidt-Boelter total heat flux transducer. Model number 64-1T-1R-20898. Nominal range of 0 kW/m^2 to 10 kW/m^2 with a corresponding voltage range of 0 mV to 9 mV. The time constant to reach 63 % of final value for this heat flux gauge is not more than 290 ms with a corresponding time to reach 95 % of the final output of not more than 1 s.

Medtherm Corporation water cooled sapphire window radiometer. Model number 64-10SB-20/SW-1C-150. Spectral transmittance of 0.15 μm to 5.0 μm. Nominal range of 0 kW/m^2 to 10 kW/m^2 with a corresponding voltage range of 0 to 7.5 mV. The time constant to reach 63 % of final value is not more than 290 ms with a corresponding time to reach 95 % of the final output of not more than 1 s.
Medtherm Corporation water cooled zinc selenide window radiometer. Model number 64-10SB-20/ZnSeW-1C-150. Spectral transmittance of 0.5 μm to 22 μm. Nominal range of 0 kW/m^2 to 100 kW/m^2 with a corresponding voltage range of 0 to 8.6 mV. The time constant to reach 63 % of final value is not more than 290 ms with a corresponding time to reach 95 % of the final output of not more than 1 s. View angle of 150 °.
Vatell Corporation thin film heat flux gauge. Model number B02. Dimensions 2.5 cm X 2.5 cm, 0.4 mm thick. Rise time 60 ms (10 % - 90 % of signal). Emissivity of 0.94.

Table 2. Experimental Configurations

Configuration	Description
1. Exposed	The sensor is exposed to the radiant panel.
2. Substrate	The sensor is mounted on a substrate such that the surface of the sensor is flush with the surface of the substrate and is exposed to the radiant panel.
3. Fabric-exposed-no space	A section of fire fighter protective clothing is placed between the sensor and the radiant panel. The sensor is not mounted on a substrate. The sensor is touching the back of the protective clothing material.
4. Fabric-exposed-space	A section of fire fighter protective clothing is placed between the sensor and the radiant panel. The sensor is not mounted on a substrate. There is an air gap between the sensor and the back of the protective clothing of 6 mm (0.25 in).
5. Fabric-substrate-no space	A section of fire fighter protective clothing is placed between the sensor and the radiant panel. The sensor is mounted on a substrate such that the surface of the sensor is flush with the surface of the substrate. The sensor is touching the back of the protective clothing material.
6. Fabric-substrate-space	A section of fire fighter protective clothing is placed between the sensor and the radiant panel. The sensor is mounted on a substrate such that the surface of the sensor is flush with the surface of the substrate. There is an air gap between the sensor and the back of the protective clothing of 6 mm (0.25 in).

Table 3. Thermal properties of "Bakelite" substrate material

Thermal conductivity $W/m \cdot K$	Density kg/m^3	Specific Heat $J/kg \cdot K$	Emissivity
0.24	1277	1465	.96

Table 4. Thermal properties of protective clothing

Material*	Thermal conductivity $W/m \cdot K$	Density kg/m^3	Specific Heat $J/kg \cdot K$
Outer shell- PBI™ Kevlar® Kombat™	0.048	321.8	N/A
Moisture barrier- Nomex® E-89 Crosstech®	0.035	143.1	N/A
Thermal liner- Aralite®	0.035	74.2	N/A

* PBI™ is a registered trademark of the Celanese Corporation.
Nomex® and Kevlar® are registered trademarks of E. I. Du Pont
Crosstech® is a registered trademark of W. L. Gore and Associates
Aralite® and Kombat™ are registered trademarks of Southern Mills

Table 5. Thermal conductivity of thermocouple materials

Thermocouple Type	Materials	Thermal Conductivity $W/m \cdot K$
J	Iron	75
	Copper Nickel	21
K	Nickel Chromium	19
	Nickel Aluminum	29
T	Copper	401
	Copper Nickel	21

Table 6. Measurement uncertainties of sensors

Sensor	Manufacturer's Stated Uncertainty (%)	Repeatability in Experiments (%)
Thermocouples	± 1	± 0.5
Schmidt-Boelter total heat flux gauge	± 3	± 8.6
Sapphire window radiometer	± 3	± 10.6
Zinc Selenide window radiometer	± 3	± 4.7
Copper disk	± 1	± 0.3
Encapsulated thermocouple	± 1	± 0.3
Thin Film heat flux gauge.	± 2.5	± 9.3

Table 7. Response of 0.13 mm (0.005 in) type J thermocouple after 10 min exposure.

Configuration	Temperature increase at 1.2 kW/m^2 exposure (°C)	Temperature increase at 2.5 kW/m^2 exposure (°C)	Temperature increase at 5.0 kW/m^2 exposure (°C)
Exposed	2.4 ± 1.1	4.1 ± 1.6	5.6 ± 1.2
Substrate	31.3 ± 1.1	60.0 ± 0.9	110.8 ± 3.1
Fabric-Exposed-No Space	19.5 ± 3.1	32.5 ± 4.4	59.1 ± 4.8
Fabric-Exposed-Space	2.6 ± 1.4	9.3 ± 5.1	13.6 ± 6.5
Fabric-Substrate-No Space	17.2 ± 0.6	29.1 ± 0.4	58.6 ± 2.1
Fabric-Substrate-Space	11.2 ± 0.6	18.2 ± 0.7	31.0 ± 0.9

Table 8. Response of 0.26 mm (0.010 in) type J thermocouple after 10 min exposure.

Configuration	Temperature increase at 1.2 kW/m^2 exposure (°C)	Temperature increase at 2.5 kW/m^2 exposure (°C)	Temperature increase at 5.0 kW/m^2 exposure (°C)
Exposed	2.2 ± 0.7	3.5 ± 0.8	6.0 ± 0.8
Substrate	29.7 ± 1.6	57.0 ± 0.9	106.0 ± 1.5
Fabric-Exposed-No Space	16.7 ± 2.1	27.1 ± 1.3	45.9 ± 3.0
Fabric-Exposed-Space	4.1 ± 1.6	9.0 ± 3.1	11.2 ± 3.4
Fabric-Substrate-No Space	18.6 ± 0.9	31.9 ± 0.5	59.1 ± 1.3
Fabric-Substrate-Space	11.4 ± 0.5	18.1 ± 0.6	25.4 ± 1.2

Table 9. Response of 0.51 mm (0.020 in) type J thermocouple after 10 min exposure.

Configuration	Temperature increase at 1.2 kW/m^2 exposure (°C)	Temperature increase at 2.5 kW/m^2 exposure (°C)	Temperature increase at 5.0 kW/m^2 exposure (°C)
Exposed	2.1 ± 0.6	3.5 ± 0.9	6.3 ± 0.8
Substrate	28.5 ± 1.8	54.5 ± 1.8	102.0 ± 2.2
Fabric-Exposed-No Space	11.5 ± 1.0	17.6 ± 1.1	32.6 ± 2.4
Fabric-Exposed-Space	3.7 ± 0.9	6.0 ± 1.3	10.7 ± 1.8
Fabric-Substrate-No Space	17.3 ± 0.8	29.8 ± 0.5	63.0 ± 1.4
Fabric-Substrate-Space	10.4 ± 0.5	16.3 ± 0.6	29.0 ± 1.2

Table 10. Response of 0.81 mm (0.032 in) type J thermocouple after 10 min exposure.

Configuration	Temperature increase at 1.2 kW/m^2 exposure (°C)	Temperature increase at 2.5 kW/m^2 exposure (°C)	Temperature increase at 5.0 kW/m^2 exposure (°C)
Exposed	2.2 ± 0.6	4.5 ± 0.7	9.0 ± 1.0
Substrate	25.4 ± 2.0	48.5 ± 3.0	91.0 ± 4.8
Fabric-Exposed-No Space	10.3 ± 0.7	16.3 ± 1.9	29.2 ± 2.3
Fabric-Exposed-Space	3.6 ± 1.2	6.3 ± 0.9	10.2 ± 1.6
Fabric-Substrate-No Space	16.4 ± 0.7	28.3 ± 0.5	N/A
Fabric-Substrate-Space	9.0 ± 0.8	13.5 ± 0.6	N/A

Table 11. Response of 0.13 mm (0.005 in) type K thermocouple after 10 min exposure.

Configuration	Temperature increase at 1.2 kW/m^2 exposure (°C)	Temperature increase at 2.5 kW/m^2 exposure (°C)	Temperature increase at 5.0 kW/m^2 exposure (°C)
Exposed	2.7 ± 0.8	4.7 ± 1.0	8.3 ± 1.1
Substrate	30.8 ± 1.5	59.5 ± 2.2	112.0 ± 4.6
Fabric-Exposed-No Space	23.7 ± 1.1	38.2 ± 2.3	69.5 ± 3.8
Fabric-Exposed-Space	3.3 ± 3.8	8.7 ± 6.5	20.2 ± 7.3
Fabric-Substrate-No Space	17.3 ± 0.8	29.8 ± 0.5	59.6 ± 1.1
Fabric-Substrate-Space	10.4 ± 0.9	15.3 ± 0.7	24.0 ± 1.5

Table 12. Response of 0.26 mm (0.010 in) type K thermocouple after 10 min exposure.

Configuration	Temperature increase at 1.2 kW/m^2 exposure (°C)	Temperature increase at 2.5 kW/m^2 exposure (°C)	Temperature increase at 5.0 kW/m^2 exposure (°C)
Exposed	2.1 ± 0.8	3.3 ± 0.8	5.5 ± 0.8
Substrate	29.2 ± 2.2	56.3 ± 2.0	105.3 ± 3.8
Fabric-Exposed-No Space	20.3 ± 1.4	31.5 ± 2.2	51.1 ± 3.6
Fabric-Exposed-Space	3.5 ± 2.2	5.8 ± 1.9	12.1 ± 4.8
Fabric-Substrate-No Space	20.6 ± 0.8	35.6 ± 0.5	71.0 ± 1.2
Fabric-Substrate-Space	12.0 ± 0.7	18.3 ± 1.0	27.5 ± 2.0

Table 13. Response of 0.51 mm (0.020 in) type K thermocouple after 10 min exposure.

Configuration	Temperature increase at 1.2 kW/m^2 exposure (°C)	Temperature increase at 2.5 kW/m^2 exposure (°C)	Temperature increase at 5.0 kW/m^2 exposure (°C)
Exposed	2.5 ± 0.6	4.3 ± 0.7	7.7 ± 0.6
Substrate	29.0 ± 1.2	56.0 ± 1.2	105.1 ± 1.2
Fabric-Exposed-No Space	14.4 ± 1.3	23.2 ± 1.7	35.6 ± 2.3
Fabric-Exposed-Space	3.9 ± 1.0	7.0 ± 1.7	11.0 ± 1.7
Fabric-Substrate-No Space	19.0 ± 0.8	32.6 ± 0.5	66.3 ± 1.1
Fabric-Substrate-Space	11.6 ± 0.6	18.2 ± 0.6	29.3 ± 1.2

Table 14. Response of 0.81 mm (0.032 in) type K thermocouple after 10 min exposure.

Configuration	Temperature increase at 1.2 kW/m^2 exposure (°C)	Temperature increase at 2.5 kW/m^2 exposure (°C)	Temperature increase at 5.0 kW/m^2 exposure (°C)
Exposed	2.5 ± 0.6	4.4 ± 0.8	8.3 ± 0.4
Substrate	27.6 ± 1.1	53.2 ± 1.4	99.1 ± 3.3
Fabric-Exposed-No Space	6.4 ± 5.6	6.0 ± 3.1	30.3 ± 2.7
Fabric-Exposed-Space	3.7 ± 1.1	3.7 ± 3.2	11.0 ± 2.1
Fabric-Substrate-No Space	18.0 ± 0.7	30.9 ± 0.5	61.1 ± 1.1
Fabric-Substrate-Space	10.9 ± 0.6	17.6 ± 0.6	29.3 ± 0.8

Table 15. Response of 0.13 mm (0.005 in) type T thermocouple after 10 min exposure.

Configuration	Temperature increase at 1.2 kW/m^2 exposure (°C)	Temperature increase at 2.5 kW/m^2 exposure (°C)	Temperature increase at 5.0 kW/m^2 exposure (°C)
Exposed	1.6 ± 0.6	2.9 ± 1.1	5.1 ± 1.4
Substrate	29.6 ± 1.1	57.1 ± 1.8	106.0 ± 3.4
Fabric-Exposed-No Space	17.1 ± 1.1	27.0 ± 3.1	42.6 ± 4.2
Fabric-Exposed-Space	3.2 ± 3.0	5.5 ± 3.0	11.0 ± 7.5
Fabric-Substrate-No Space	15.6 ± 0.5	26.8 ± 0.4	55.7 ± 1.3
Fabric-Substrate-Space	10.4 ± 0.6	16.9 ± 0.5	28.3 ± 0.7

Table 16. Response of 0.26 mm (0.010 in) type T thermocouple after 10 min exposure.

Configuration	Temperature increase at 1.2 kW/m^2 exposure (°C)	Temperature increase at 2.5 kW/m^2 exposure (°C)	Temperature increase at 5.0 kW/m^2 exposure (°C)
Exposed	1.7 ± 0.6	2.8 ± 1.2	4.2 ± 1.0
Substrate	25.7 ± 1.1	49.9 ± 1.0	93.9 ± 2.5
Fabric-Exposed-No Space	9.9 ± 1.8	14.9 ± 1.6	29.0 ± 2.0
Fabric-Exposed-Space	3.0 ± 1.2	5.0 ± 1.5	9.5 ± 2.7
Fabric-Substrate-No Space	14.6 ± 0.5	25.2 ± 0.4	51.4 ± 1.0
Fabric-Substrate-Space	9.6 ± 0.6	15.0 ± 0.7	24.2 ± 0.7

Table 17. Response of 0.51 mm (0.020 in) type T thermocouple after 10 min exposure.

Configuration	Temperature increase at 1.2 kW/m^2 exposure (°C)	Temperature increase at 2.5 kW/m^2 exposure (°C)	Temperature increase at 5.0 kW/m^2 exposure (°C)
Exposed	1.8 ± 0.6	2.9 ± 0.7	5.6 ± 0.6
Substrate	21.0 ± 0.8	40.7 ± 1.3	77.6 ± 3.4
Fabric-Exposed-No Space	7.6 ± 1.0	12.0 ± 0.9	22.1 ± 1.9
Fabric-Exposed-Space	3.0 ± 0.9	5.3 ± 1.0	8.6 ± 1.6
Fabric-Substrate-No Space	13.0 ± 0.5	22.0 ± 0.3	44.6 ± 1.1
Fabric-Substrate-Space	8.1 ± 0.6	12.1 ± 0.7	19.0 ± 0.6

Table 18. Response of 0.81 mm (0.032 in) type T thermocouple after 10 min exposure.

Configuration	Temperature increase at 1.2 kW/m^2 exposure (°C)	Temperature increase at 2.5 kW/m^2 exposure (°C)	Temperature increase at 5.0 kW/m^2 exposure (°C)
Exposed	2.0 ± 0.7	3.2 ± 0.9	6.5 ± 0.8
Substrate	18.6 ± 1.0	35.7 ± 1.9	68.0 ± 4.4
Fabric-Exposed-No Space	6.0 ± 0.7	10.0 ± 1.0	17.1 ± 1.5
Fabric-Exposed-Space	2.5 ± 0.6	5.0 ± 0.8	8.2 ± 1.2
Fabric-Substrate-No Space	12.1 ± 0.6	20.2 ± 0.3	41.2 ± 1.2
Fabric-Substrate-Space	7.1 ± 0.9	10.0 ± 0.6	15.7 ± 0.6

Table 19. Response of encapsulated thermocouple after 10 min exposure.

Configuration	Temperature increase at 1.2 kW/m^2 exposure (°C)	Temperature increase at 2.5 kW/m^2 exposure (°C)	Temperature increase at 5.0 kW/m^2 exposure (°C)
Exposed	28.7 ± 1.1	55.7 ± 1.8	105.6 ± 0.9
Substrate	34.2 ± 0.7	64.5 ± 1.3	118.5 ± 1.6
Fabric-Exposed-No Space	23.1 ± 0.9	39.9 ± 0.8	80.7 ± 1.4
Fabric-Exposed-Space	8.0 ± 0.8	13.0 ± 0.5	25.3 ± 1.1
Fabric-Substrate-No Space	17.1 ± 0.3	31.7 ± 0.6	64.2 ± 0.7
Fabric-Substrate-Space	9.0 ± 0.7	15.3 ± 0.5	31.3 ± 1.4

Table 20. Response of copper disk with one thermocouple attached after 10 min exposure.

Configuration	Temperature increase at 1.2 kW/m^2 exposure (°C)	Temperature increase at 2.5 kW/m^2 exposure (°C)	Temperature increase at 5.0 kW/m^2 exposure (°C)
Exposed	31.6 ± 0.8	57.9 ± 1.0	105.3 ± 1.5
Substrate	39.1 ± 0.7	72.1 ± 0.7	129.8 ± 1.2
Fabric-Exposed-No Space	N/A	N/A	N/A
Fabric-Exposed-Space	N/A	N/A	N/A
Fabric-Substrate-No Space	N/A	N/A	N/A
Fabric-Substrate-Space	N/A	N/A	N/A

Table 21. Response of copper disk with four thermocouples attached after 10 min exposure.

Configuration	Temperature increase at 1.2 kW/m^2 exposure (°C)	Temperature increase at 2.5 kW/m^2 exposure (°C)	Temperature increase at 5.0 kW/m^2 exposure (°C)
Exposed	30.8 ± 1.1	56.0 ± 1.2	101.8 ± 2.5
Substrate	38.6 ± 0.6	72.1 ± 1.1	131.5 ± 1.4
Fabric-Exposed-No Space	25.5 ± 0.5	48.4 ± 1.2	91.3 ± 4.0
Fabric-Exposed-Space	8.6 ± 0.4	14.8 ± 1.1	37.2 ± 2.3
Fabric-Substrate-No Space	20.6 ± 0.7	36.0 ± 0.6	69.2 ± 0.8
Fabric-Substrate-Space	12.4 ± 0.5	20.0 ± 0.8	33.0 ± 1.1

Table 22. Response of thin film heat flux sensor after 10 min exposure

Configuration	Measured heat flux at 1.2 kW/m^2 exposure (kW/m^2)	Measured heat flux at 2.5 kW/m^2 exposure (kW/m^2)	Measured heat flux at 5.0 kW/m^2 exposure (kW/m^2)
Exposed	0.74 ± 0.07	1.58 ± 0.16	3.32 ± 0.40
Substrate	0.78 ± 0.08	1.65 ± 0.11	3.14 ± 0.23
Fabric-Exposed-No Space	0.40 ± 0.02	0.85 ± 0.07	1.81 ± 0.06
Fabric-Exposed-Space	0.16 ± 0.03	0.29 ± 0.08	0.54 ± 0.07
Fabric-Substrate-No Space	0.45 ± 0.01	0.85 ± 0.01	1.82 ± 0.03
Fabric-Substrate-Space	0.27 ± 0.02	0.44 ± 0.04	0.75 ± 0.11

Table 23. Response of Sapphire window radiometer after 10 min exposure.

Configuration	Measured heat flux at 1.2 kW/m^2 exposure (kW/m^2)	Measured heat flux at 2.5 kW/m^2 exposure (kW/m^2)	Measured heat flux at 5.0 kW/m^2 exposure (kW/m^2)
Exposed	0.90 ± 0.03	1.82 ± 0.03	3.80 ± 0.10
Substrate	N/A	N/A	N/A
Fabric-Exposed-No Space	0.06 ± 0.01	0.11 ± 0.01	N/A
Fabric-Exposed-Space	0.05 ± 0.01	0.11 ± 0.01	N/A
Fabric-Substrate-No Space	0.05 ± 0.01	0.10 ± 0.01	N/A
Fabric-Substrate-Space	0.06 ± 0.01	0.13 ± 0.01	N/A

Table 24. Response of Schmidt-Boelter Total Heat Flux Gauge after 10 min exposure.

Configuration	Measured heat flux at 1.2 kW/m^2 exposure (kW/m^2)	Measured heat flux at 2.5 kW/m^2 exposure (kW/m^2)	Measured heat flux at 5.0 kW/m^2 exposure (kW/m^2)
Exposed	1.27 ± 0.03	2.52 ± 0.11	5.0 ± 0.09
Substrate	N/A	N/A	N/A
Fabric-Exposed-No Space	0.63 ± 0.01	1.17 ± 0.02	N/A
Fabric-Exposed-Space	0.22 ± 0.07	0.57 ± 0.08	N/A
Fabric-Substrate-No Space	0.55 ± 0.11	1.03 ± 0.02	N/A
Fabric-Substrate-Space	0.33 ± 0.03	0.74 ± 0.04	N/A

Table 25. Response of Zinc Selenide radiometer after 10 min exposure.

Configuration	Measured heat flux at 1.2 kW/m^2 exposure (kW/m^2)	Measured heat flux at 2.5 kW/m^2 exposure (kW/m^2)	Measured heat flux at 5.0 kW/m^2 exposure (kW/m^2)
Exposed	1.18 ±0.05	2.40±0.03	4.84±0.42
Substrate	N/A	N/A	N/A
Fabric-Exposed-No Space	N/A	N/A	N/A
Fabric-Exposed-Space	N/A	N/A	N/A
Fabric-Substrate-No Space	N/A	N/A	N/A
Fabric-Substrate-Space	N/A	N/A	N/A

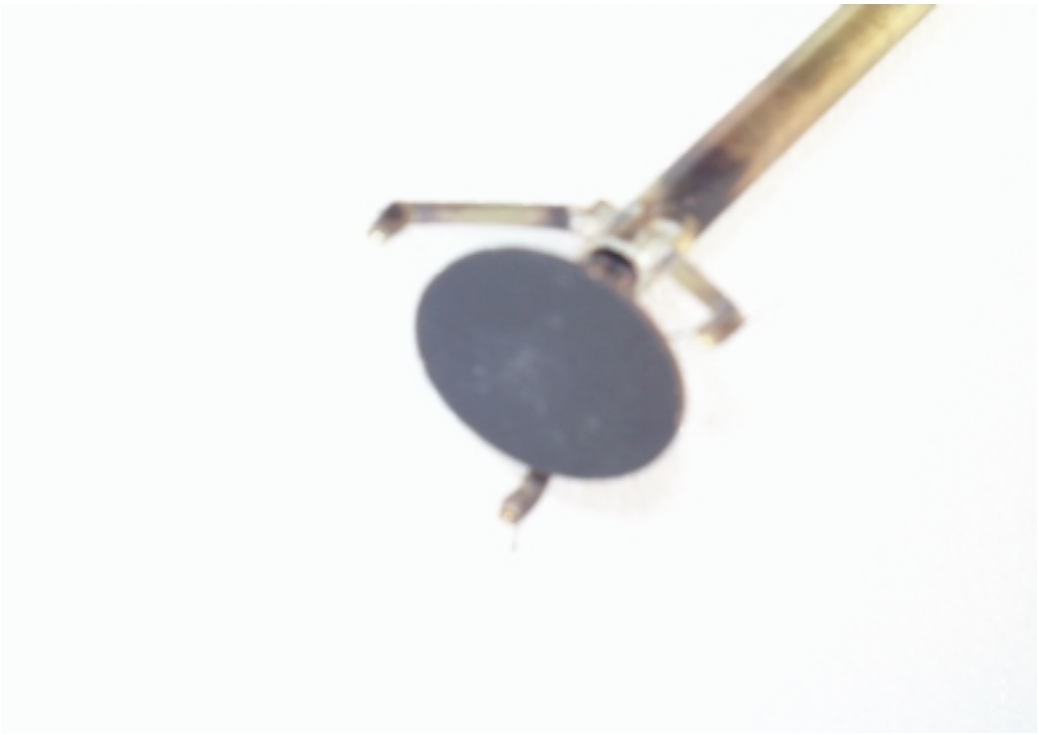

Figure 1. Copper disk in the exposed position, no substrate.

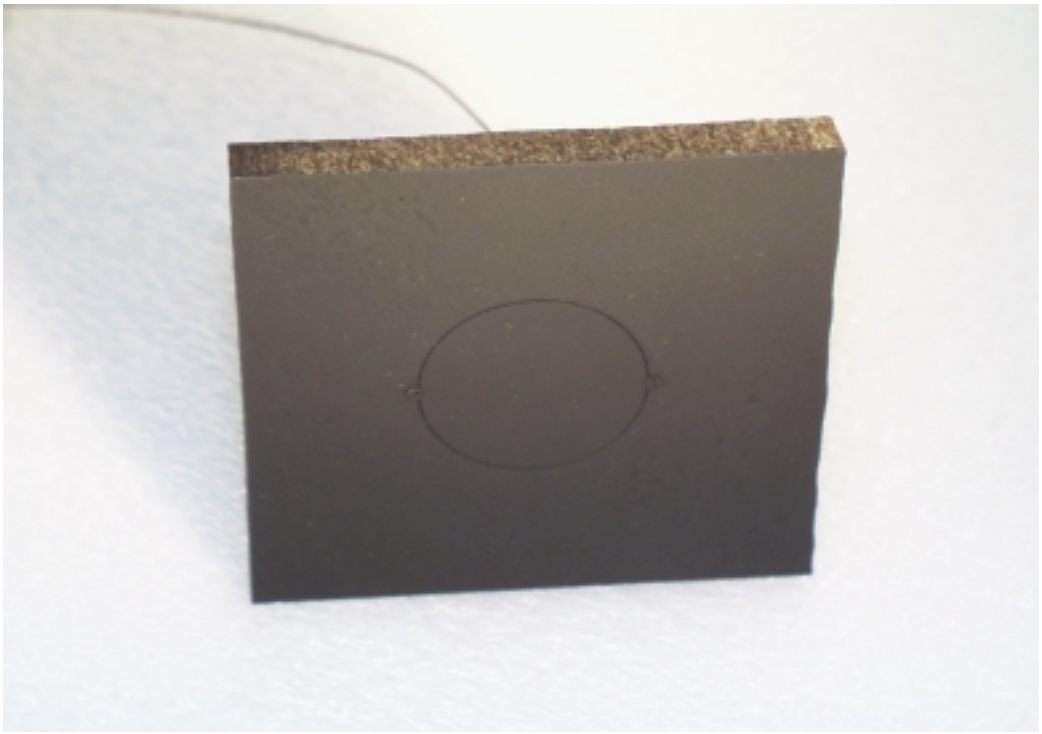

Figure 2. Copper disk in substrate.

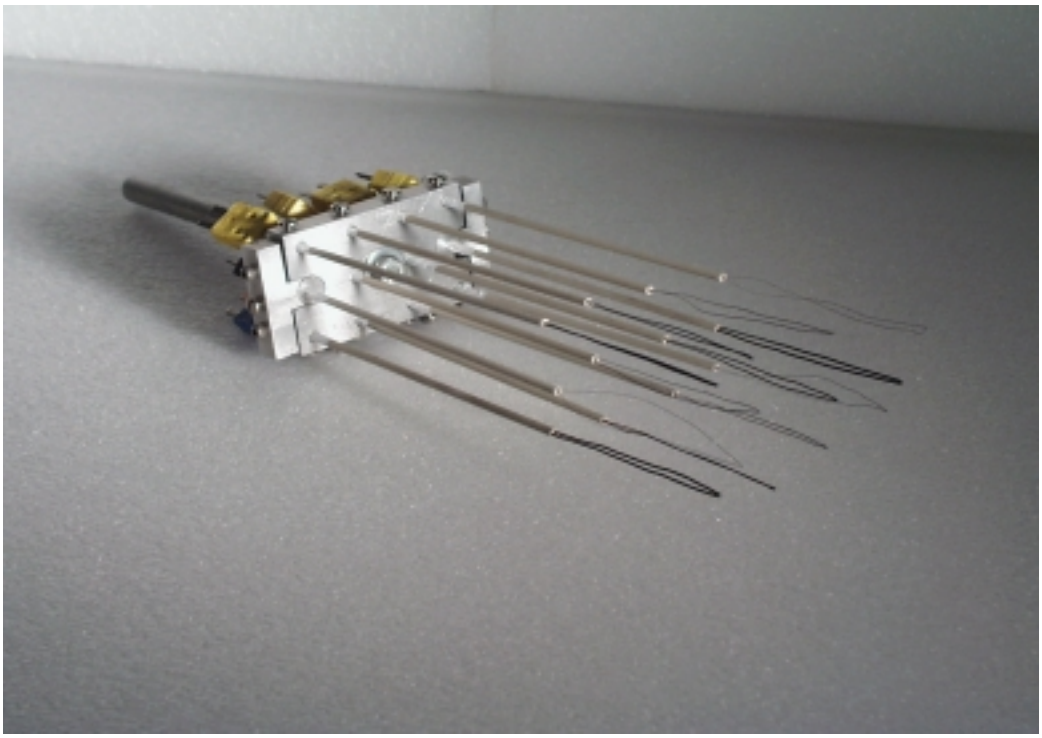

Figure 3. 12 thermocouples exposed.

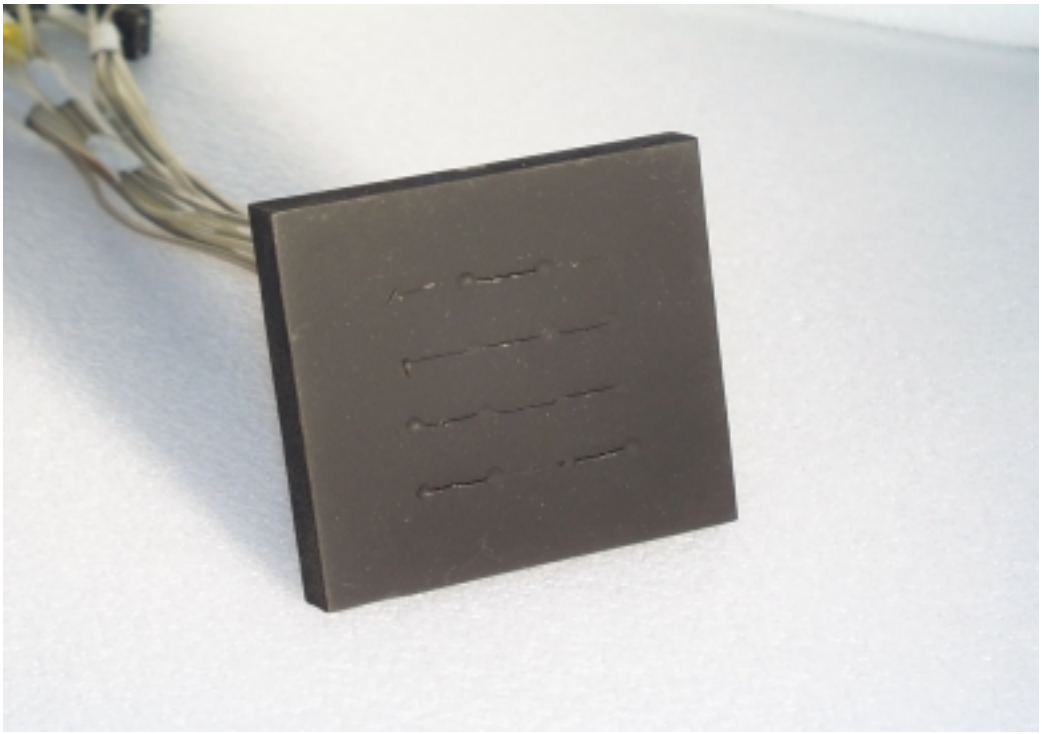

Figure 4. 12 thermocouples mounted on substrate.

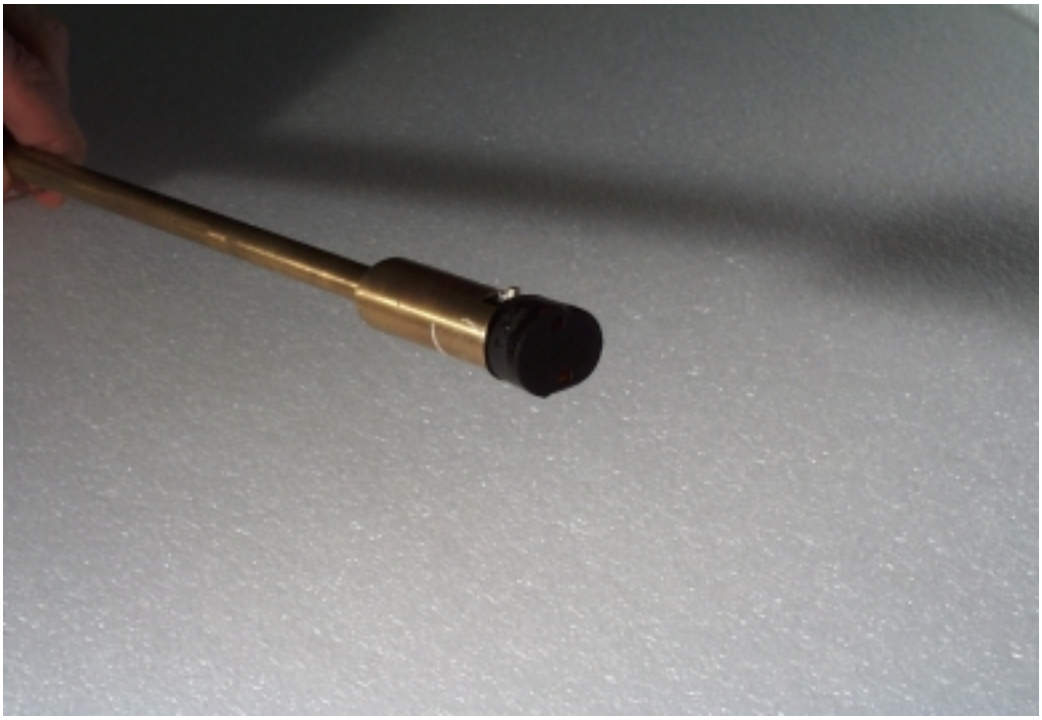

Figure 5. Encapsulated type T (Copper versus Copper Nickel) thermocouple exposed.

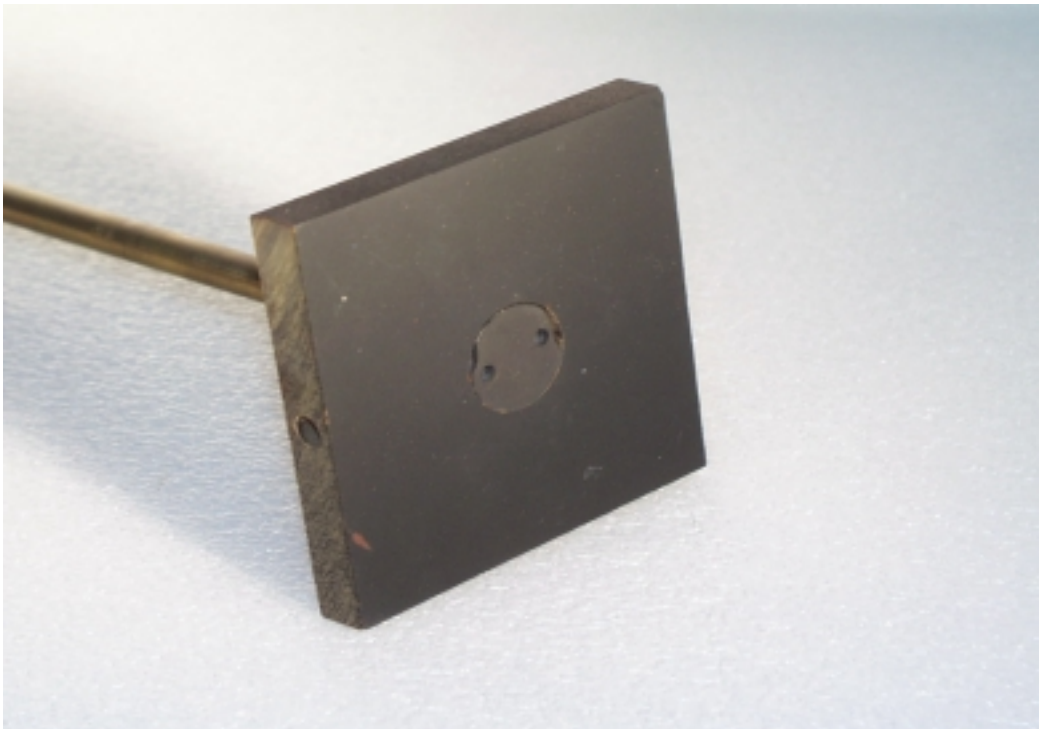

Figure 6. Encapsulated type T (Copper versus Copper Nickel) thermocouple mounted in substrate.

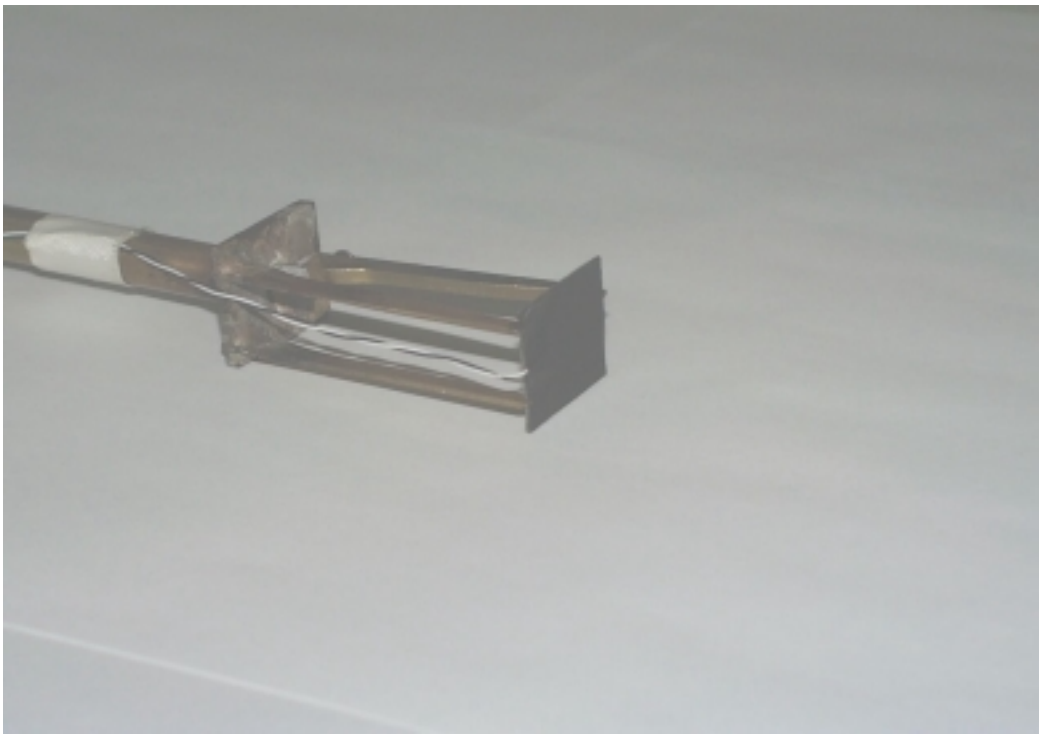

Figure 7. Thin film sensor in the exposed position.

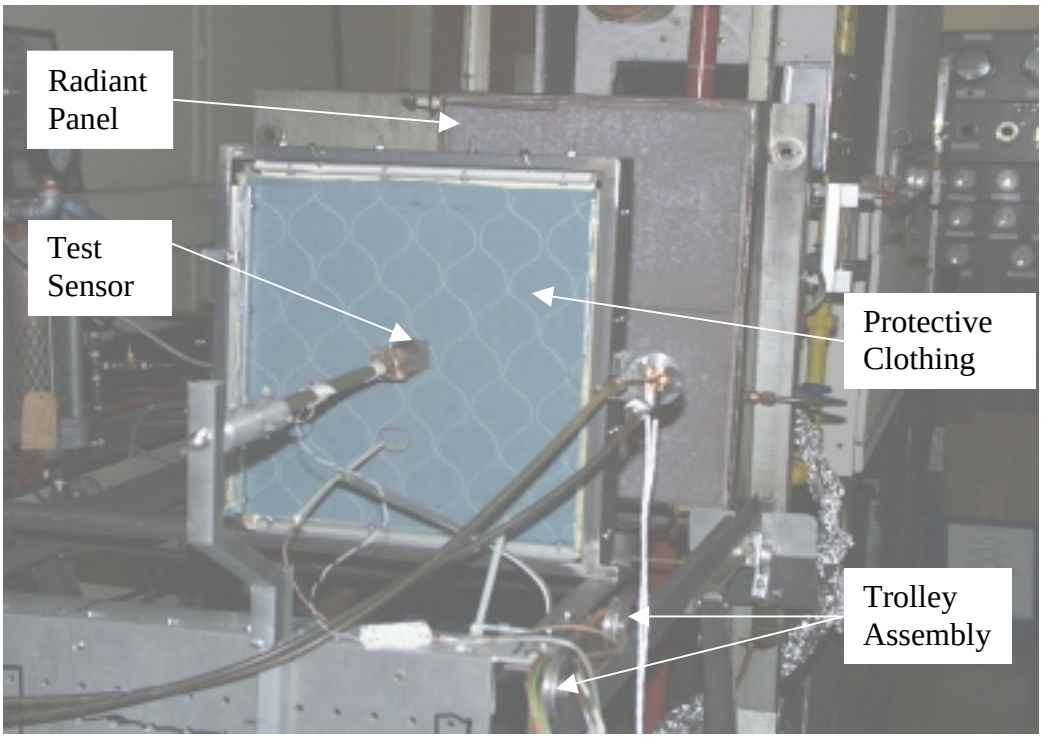

Figure 8. Test apparatus. This figure show the protective clothing set between the radiant panel and the sensor.

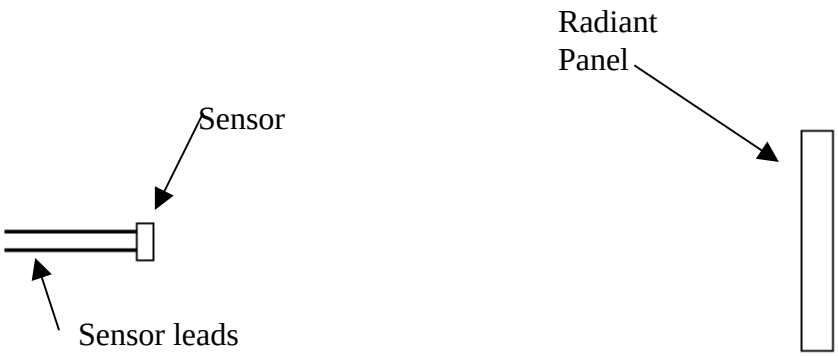

Figure 9. Experimental set up for “Exposed” configuration. Drawing not to scale.

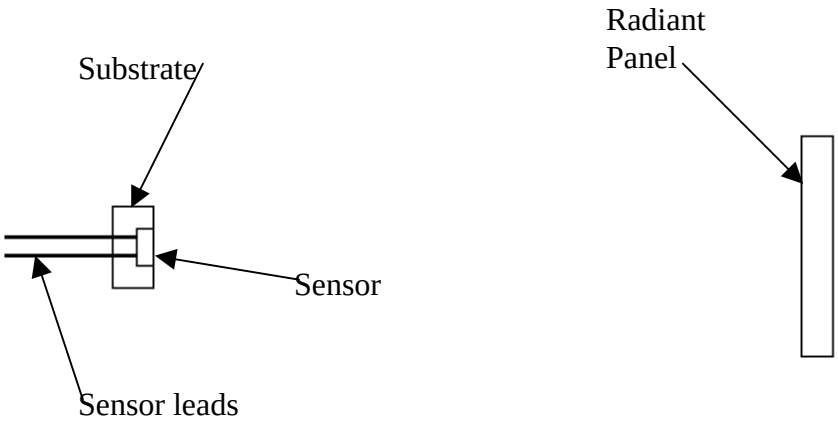

Figure 10. Experimental set up for “Substrate” configuration. Sensor is mounted in the substrate such that its surface is flush with the substrate surface. Drawing not to scale.

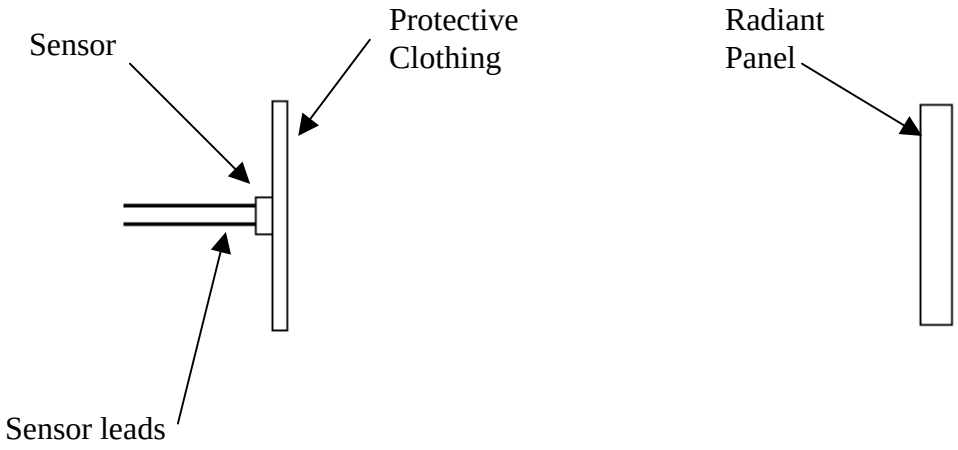

Figure 11. Experimental set up for " Fabric-Exposed-No Space" configuration. Sensor is touching the back of the protective clothing. Drawing not to scale.

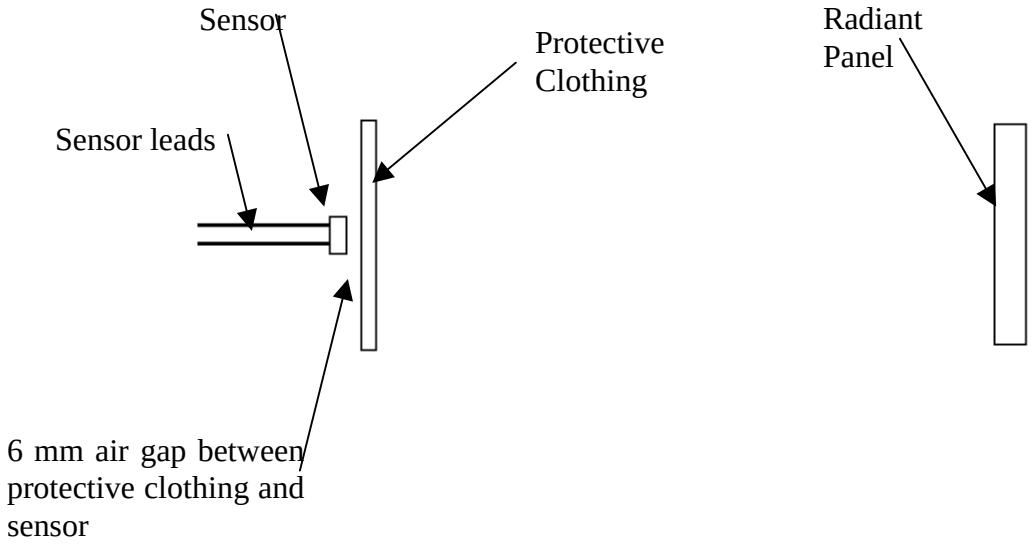

Figure 12. Experimental set up for "Fabric-Exposed-Space" configuration. There is an air gap of 6mm (0.25 in) between the sensor and the protective clothing. Drawing not to scale.

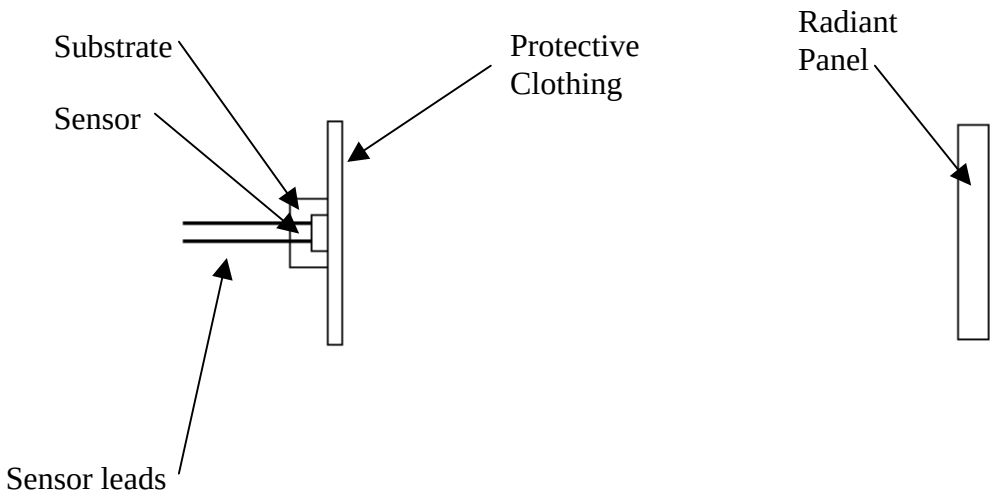

Figure 13. Experimental set up for "Fabric-Substrate-No Space" configuration. Sensor is mounted in substrate and surface of sensor and substrate are touching protective clothing. Drawing not to scale.

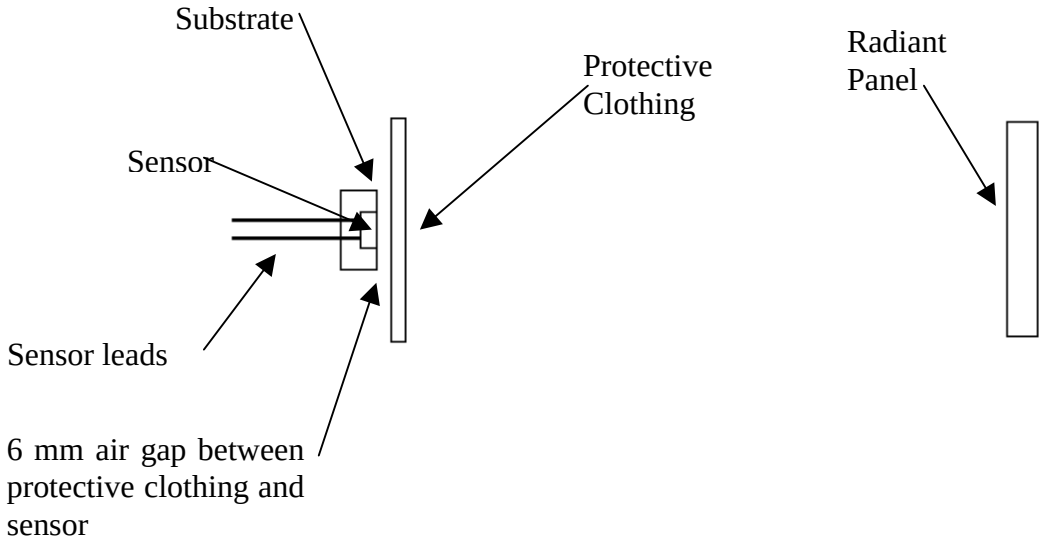

Figure 14. Experimental set up for "Fabric-Substrate-Space" configuration. Sensor is mounted in substrate and there is a 6 mm (0.25 in) air gap between the protective clothing and the sensor. Drawing not to scale.

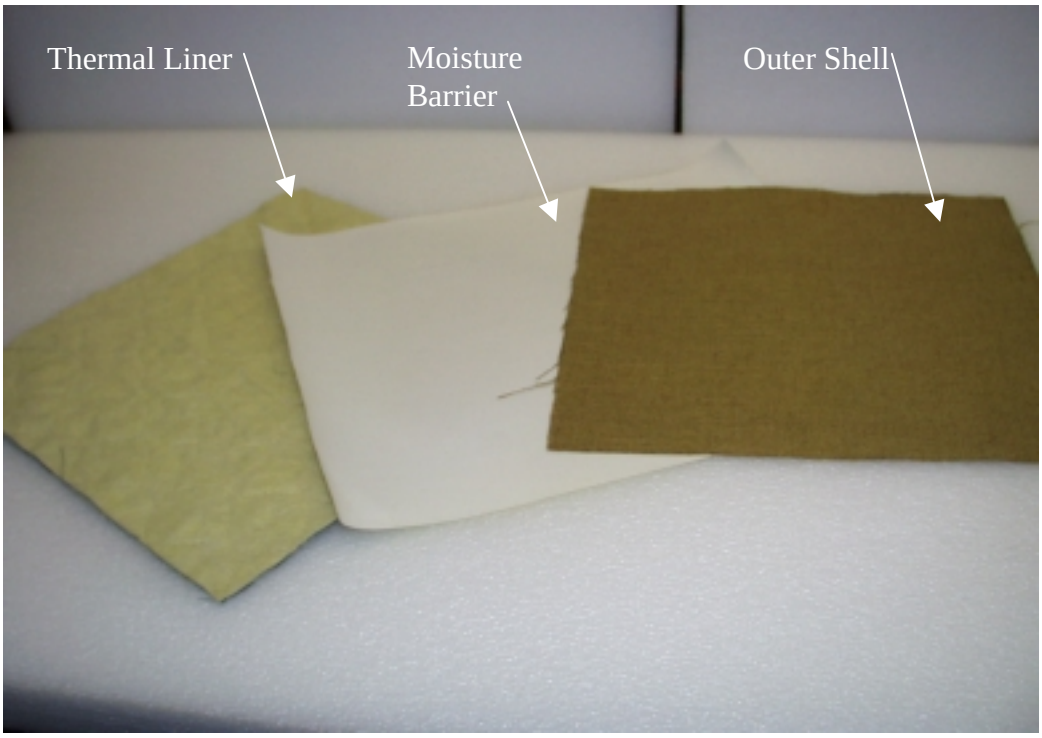

Figure 15. Three layers that make up typical fire fighter protective clothing.

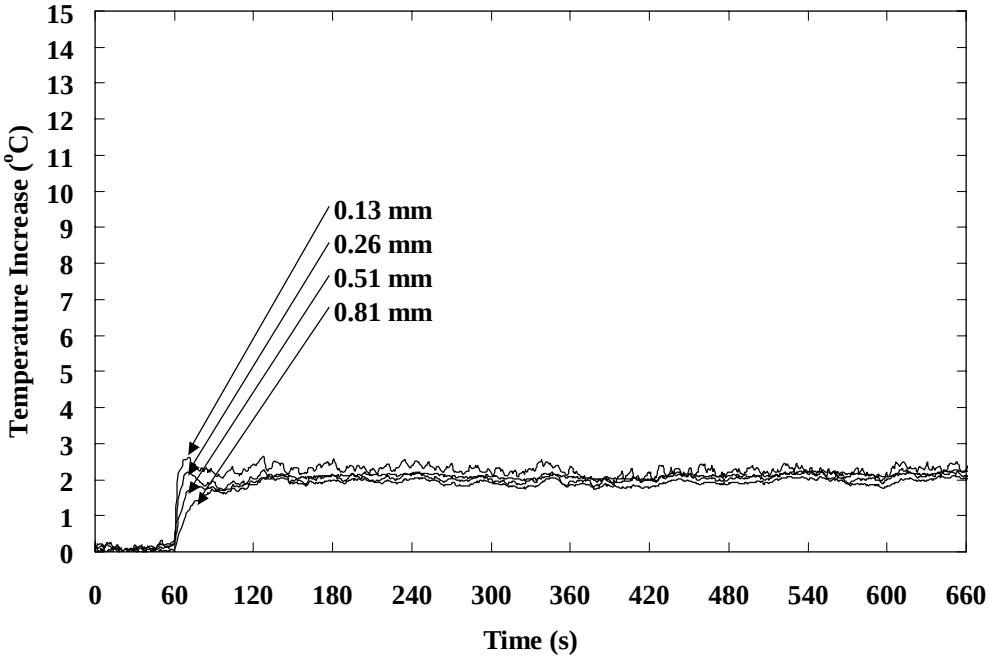

Figure 16. Response of all type J thermocouples, exposed, 1.2 kW/m^2.

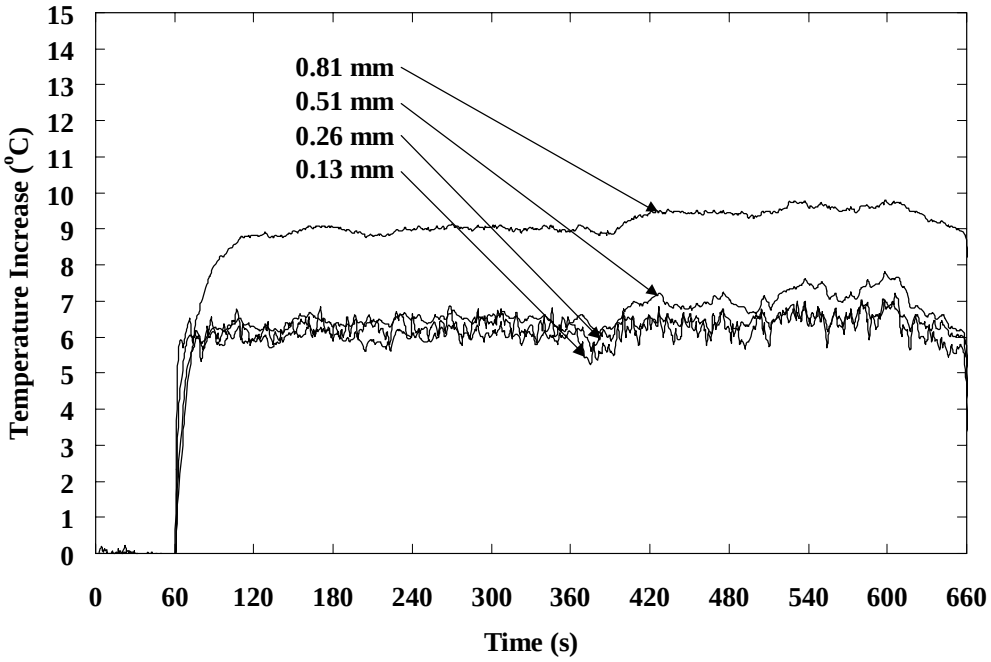

Figure 17. Response of all type J thermocouples, exposed, 5.0 kW/m^2.

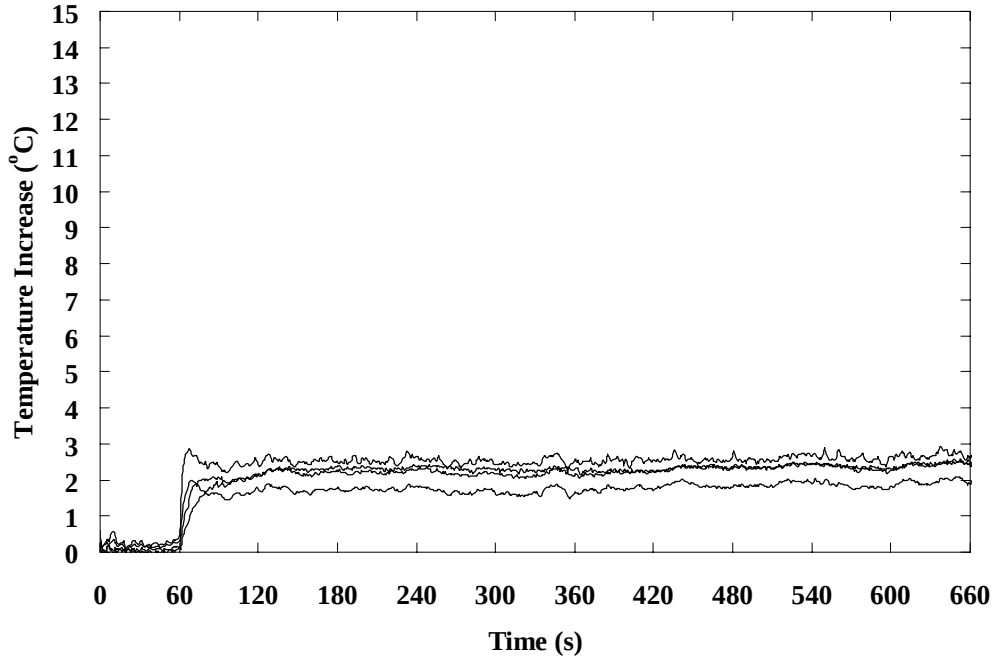

Figure 18. Response of all type K thermocouples, exposed, 1.2 kW/m^2.

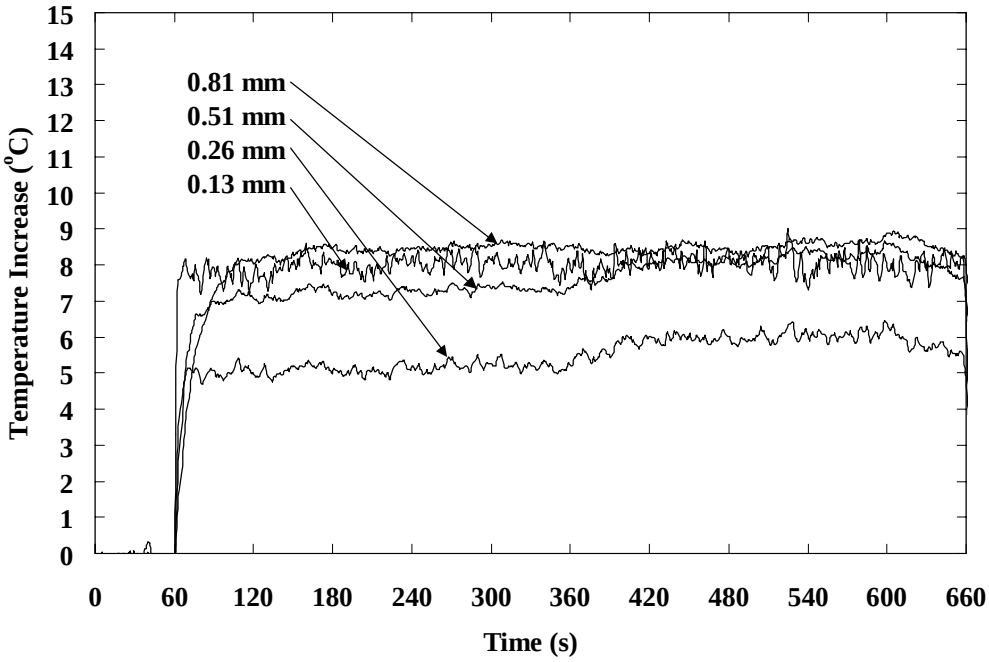

Figure 19. Response of all type K thermocouples, exposed, 5.0 kW/m^2.

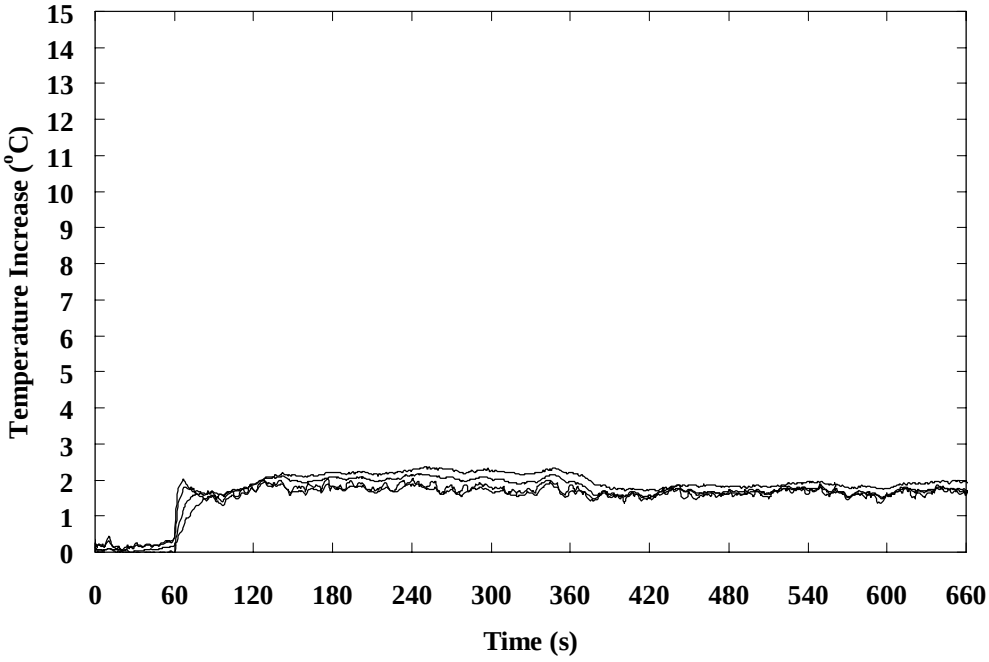

Figure 20. Response of all type T thermocouples, exposed, 1.2 kW/m^2.

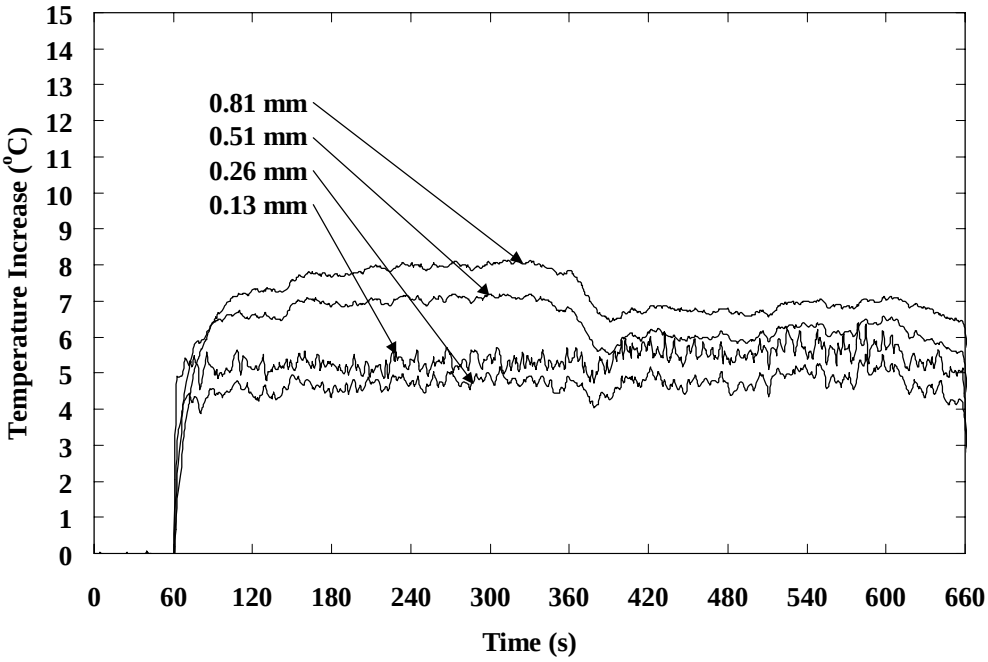

Figure 21. Response of all type T thermocouples, exposed, 5.0 kW/m^2.

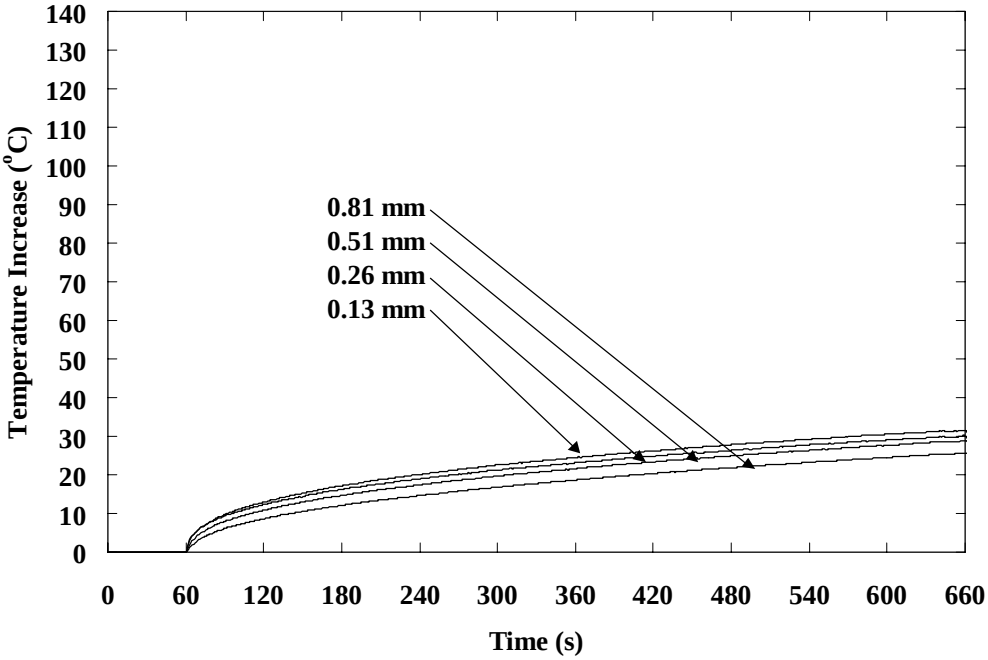

Figure 22. Response of all type J thermocouples, substrate, 1.2 kW/m^2.

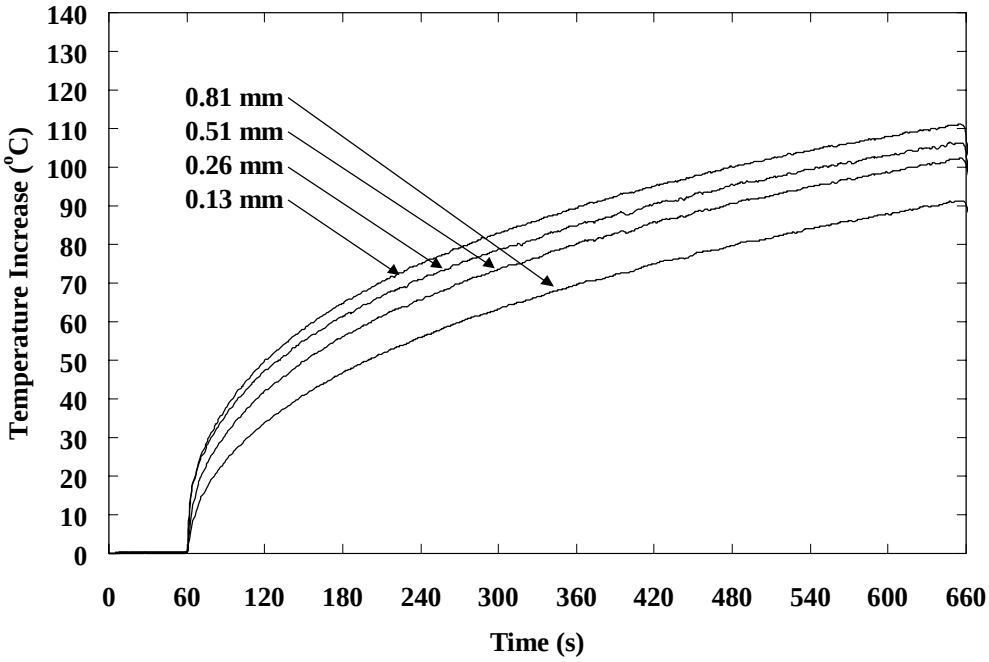

Figure 23. Response of all type J thermocouples, substrate, 5.0 kW/m^2.

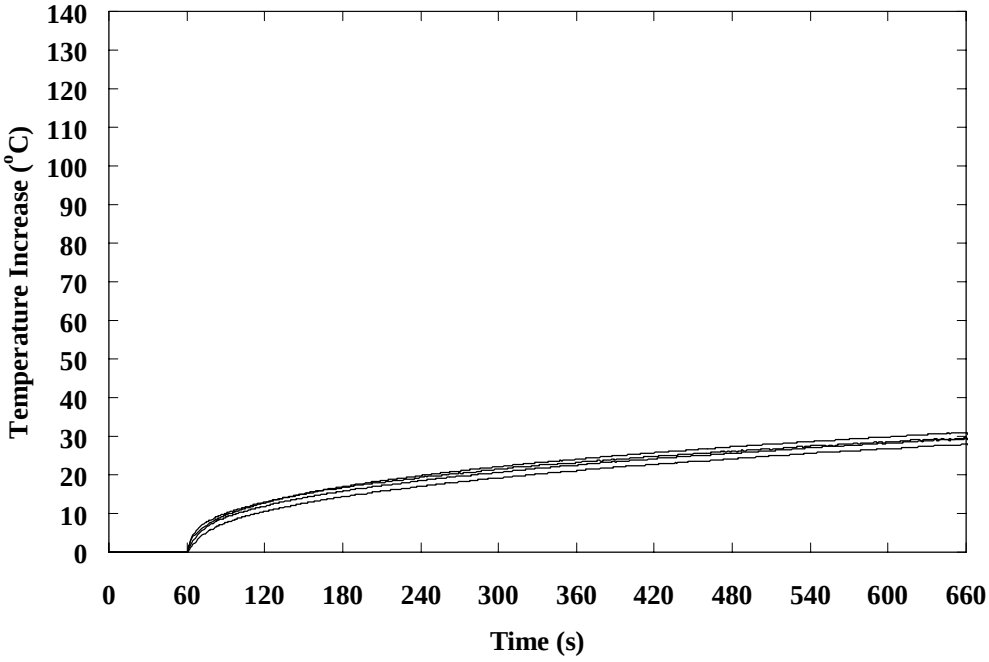

Figure 24. Response of all type K thermocouples, substrate, 1.2 kW/m^2.

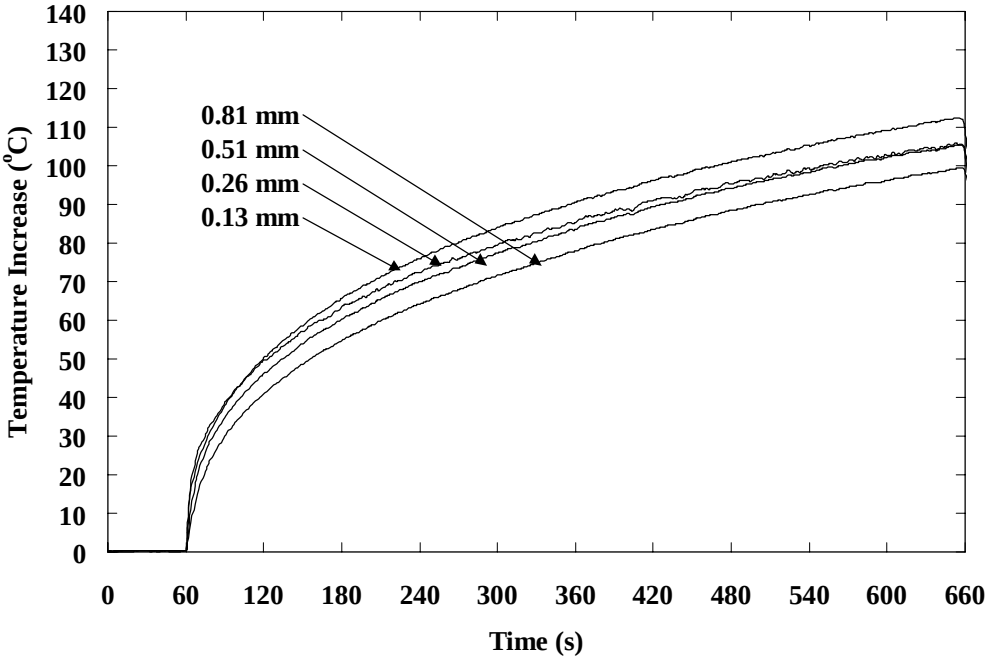

Figure 25. Response of all type K thermocouples, substrate, 5.0 kW/m^2.

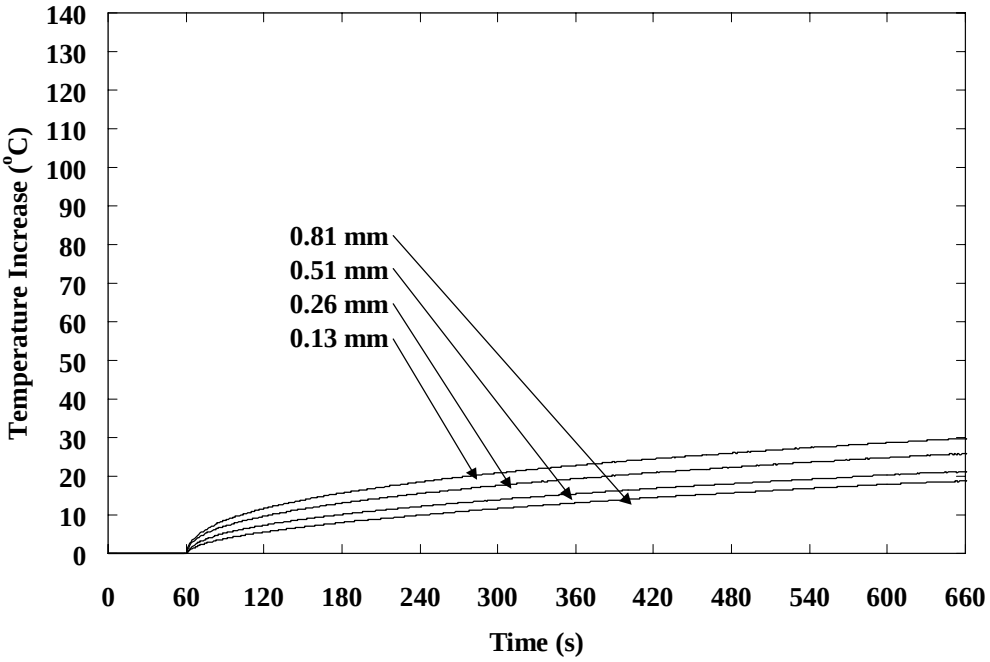

Figure 26. Response of all type T thermocouples, substrate, 1.2 kW/m^2.

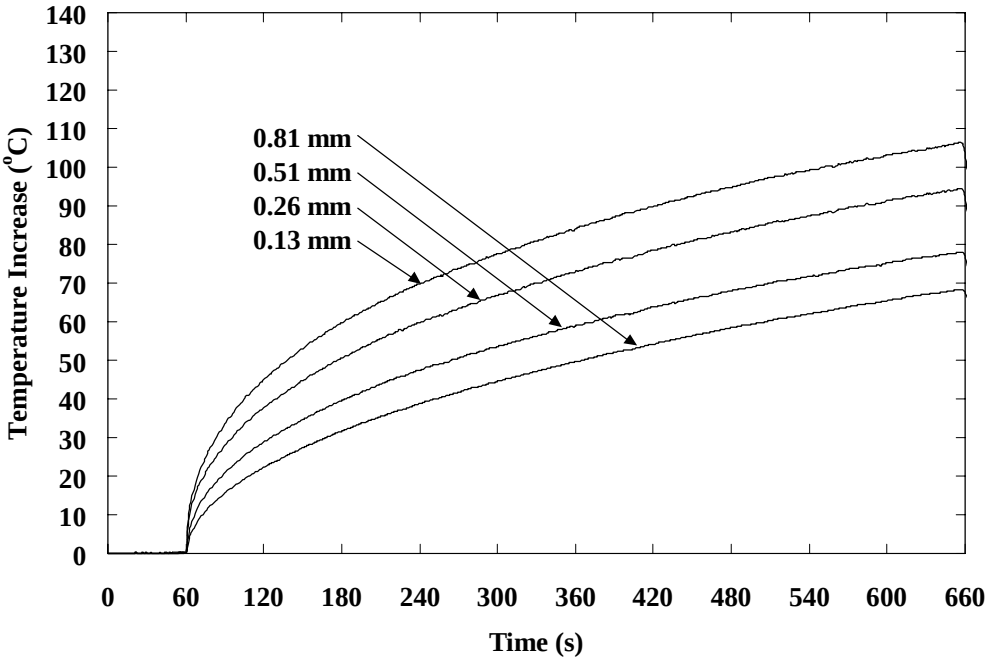

Figure 27. Response of all type T thermocouples, substrate, 5.0 kW/m^2.

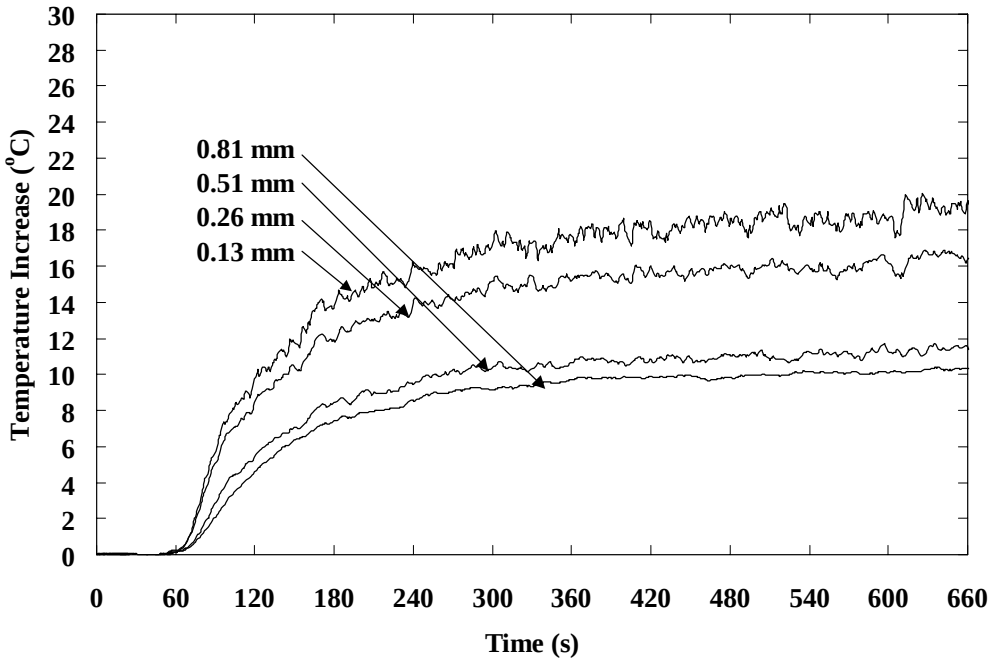

Figure 28. Response of all type J thermocouples, fabric-exposed-no space, 1.2 kW/m^2.

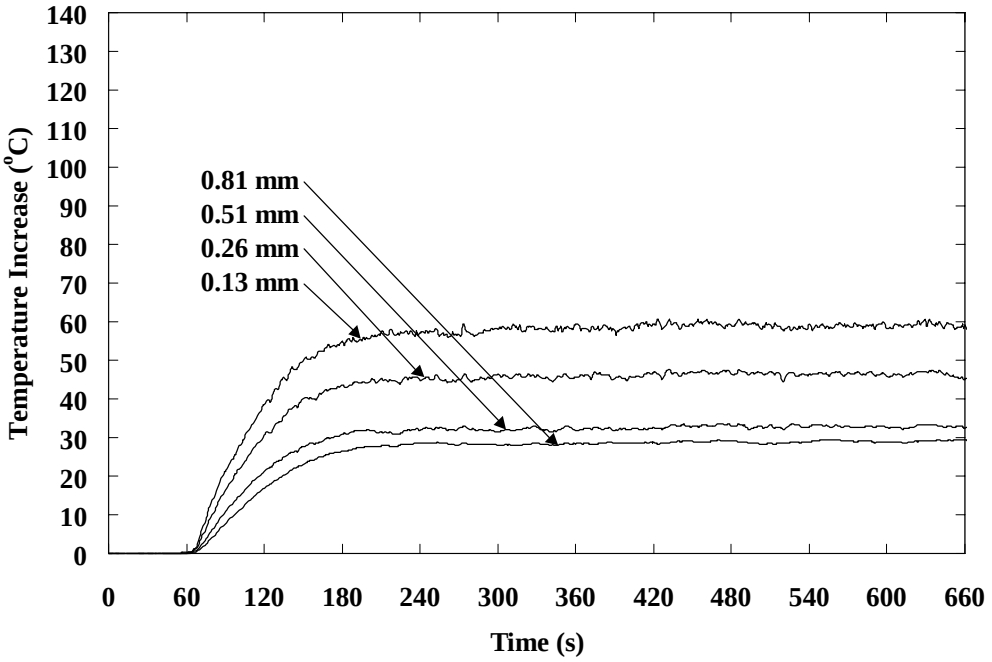

Figure 29. Response of all type J thermocouples, fabric-exposed-no space 5.0 kW/m^2.

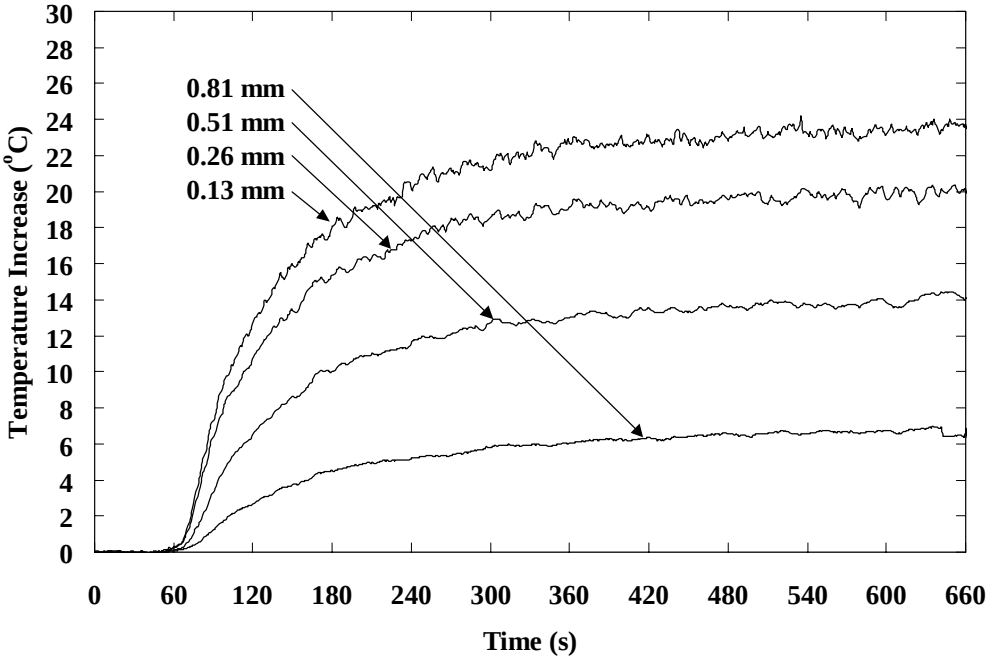

Figure 30. Response of all type K thermocouples, fabric-exposed-no space, 1.2 kW/m^2.

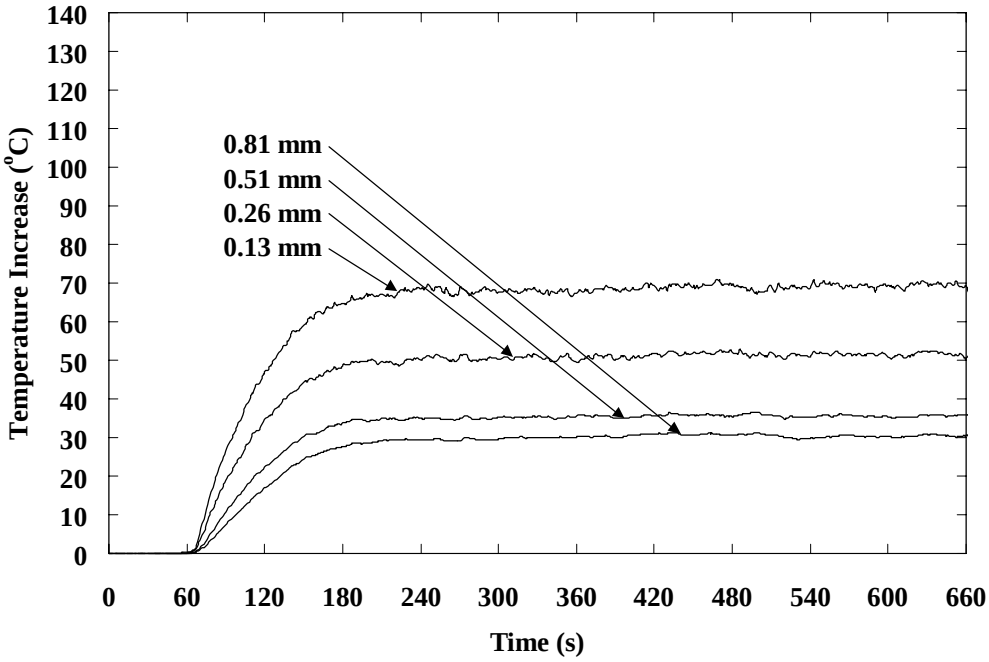

Figure 31. Response of all type K thermocouples, fabric-exposed-no space, 5.0 kW/m^2.

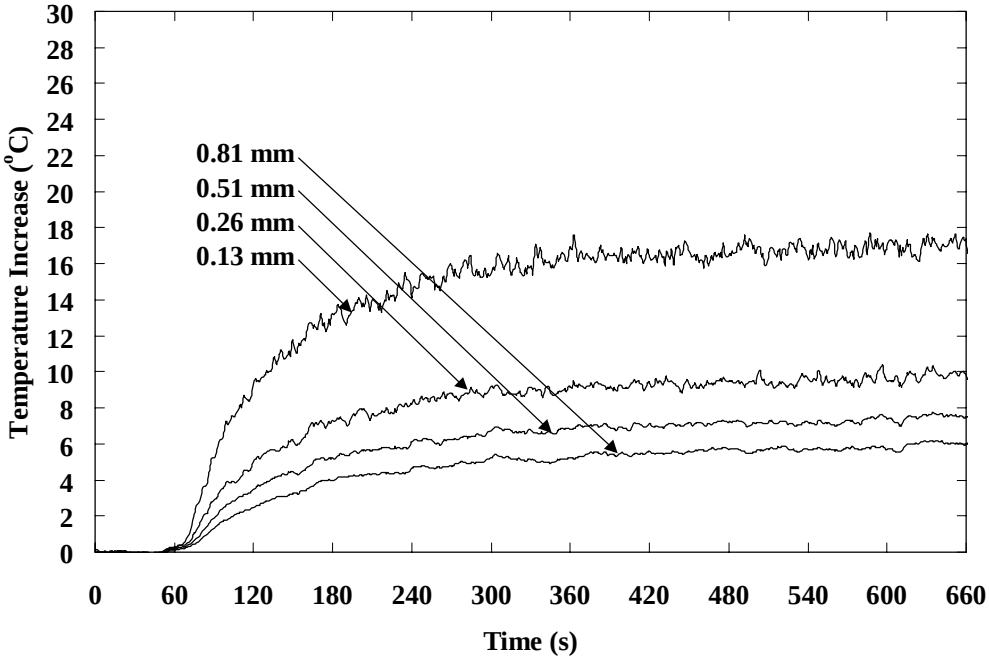

Figure 32. Response of all type T thermocouples, fabric-exposed-no space, 1.2 kW/m^2.

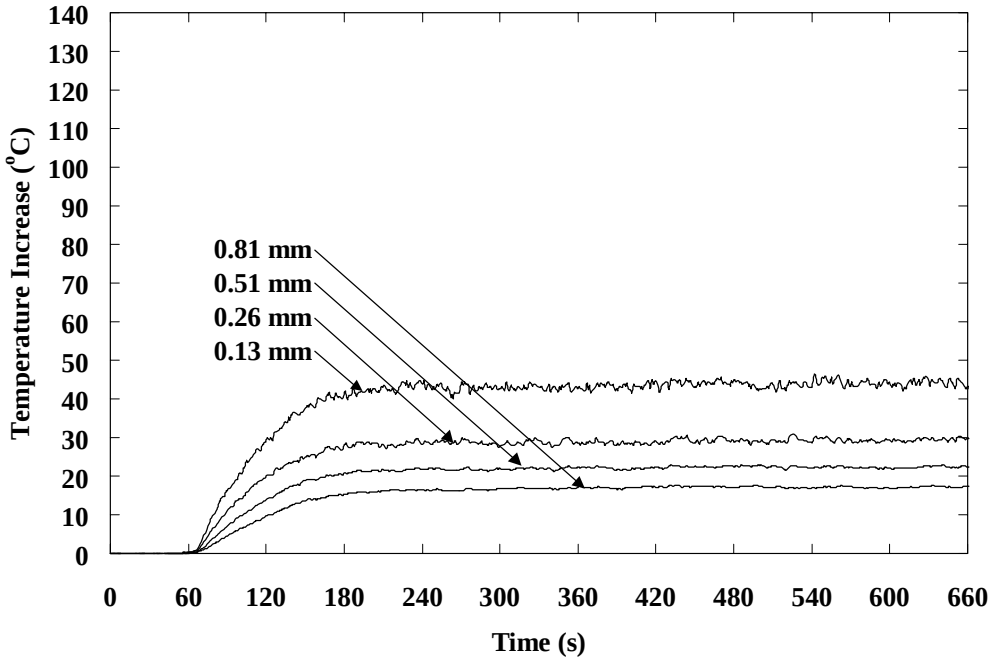

Figure 33. Response of all type T thermocouples, fabric-exposed-no space, 5.0 kW/m^2.

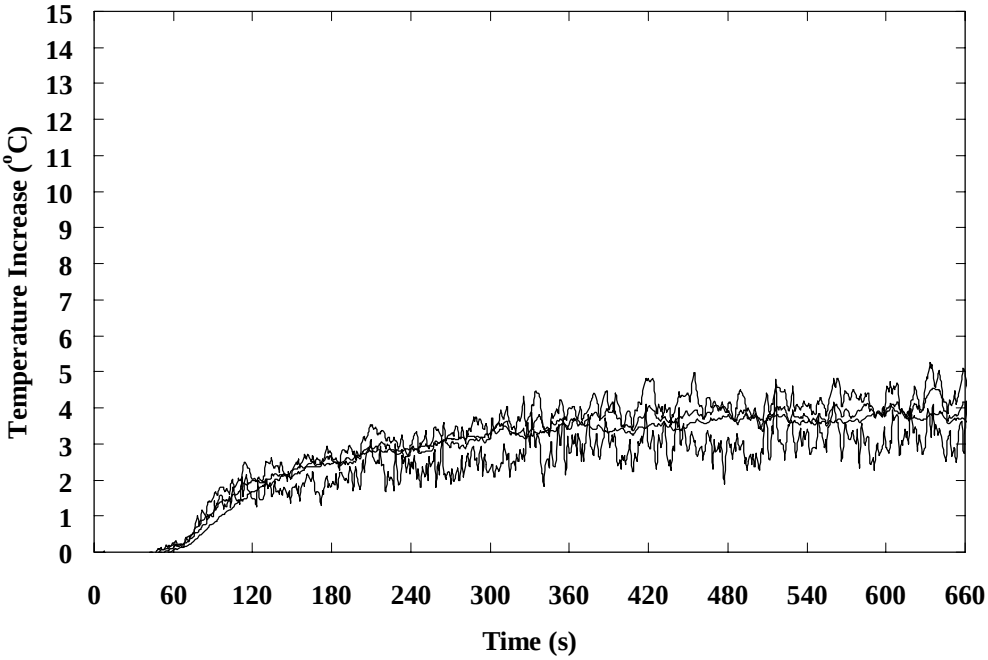

Figure 34. Response of all type J thermocouples, fabric-exposed-space, 1.2 kW/m^2.

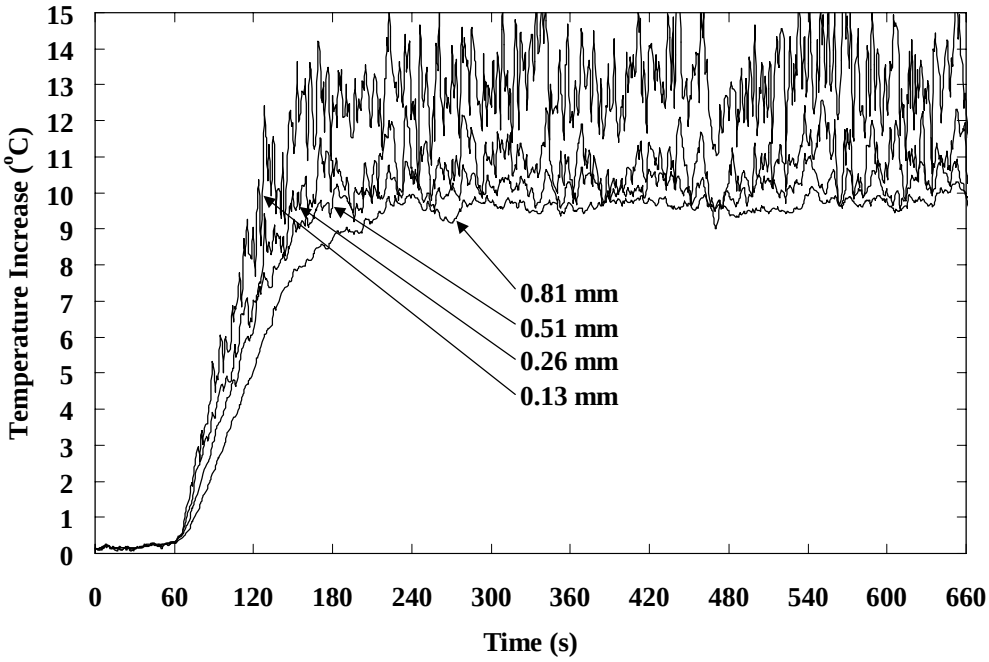

Figure 35. Response of all type J thermocouples, fabric-exposed-space, 5.0 kW/m^2.

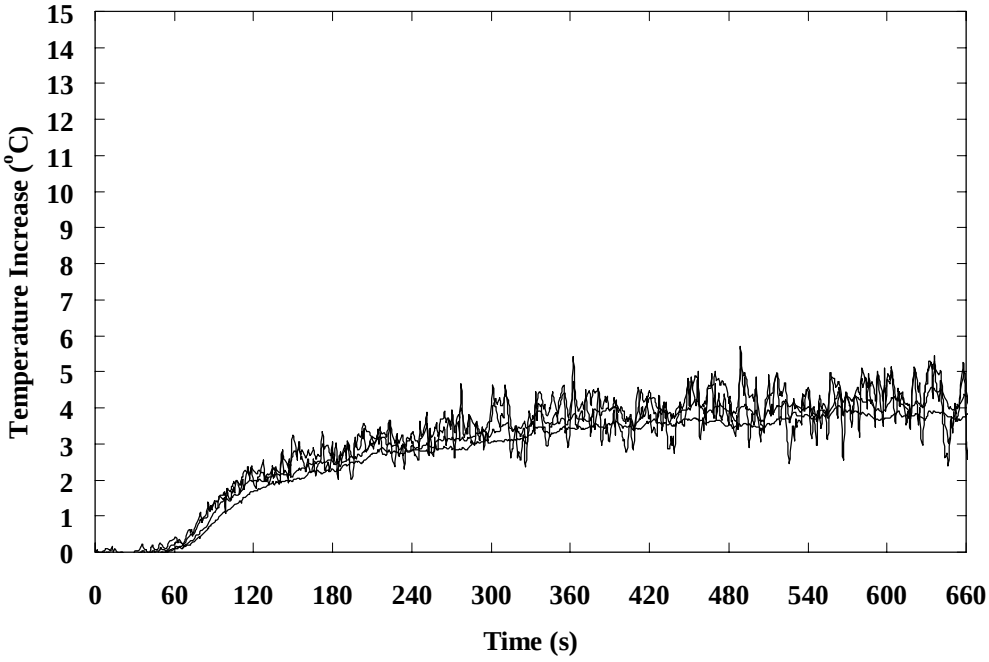

Figure 36. Response of all type K thermocouples, fabric-exposed-space, 1.2 kW/m^2.

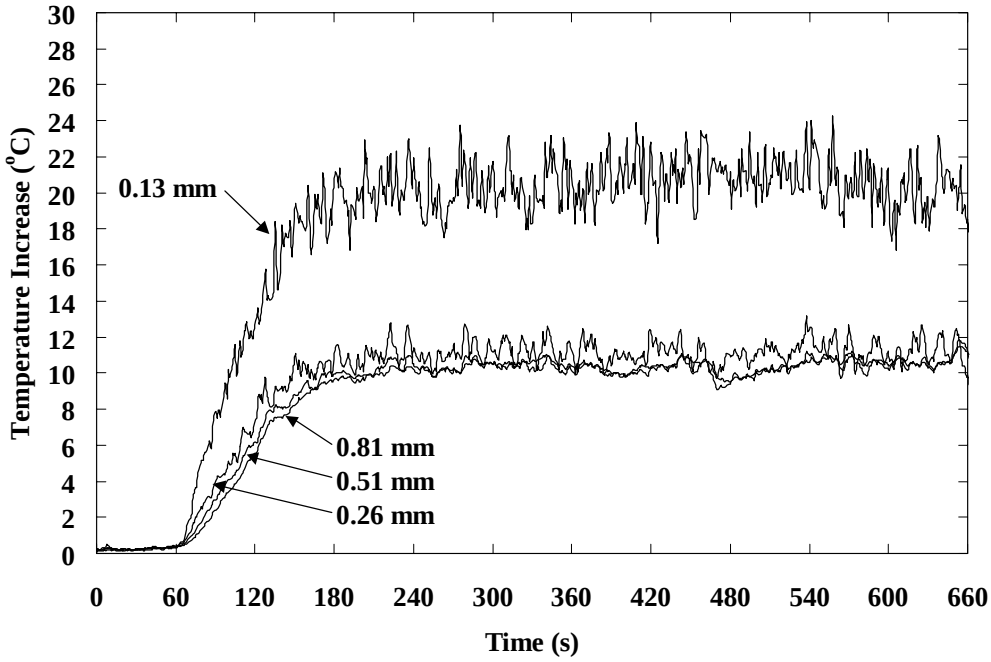

Figure 37. Response of all type K thermocouples, fabric-exposed-space, 5.0 kW/m^2.

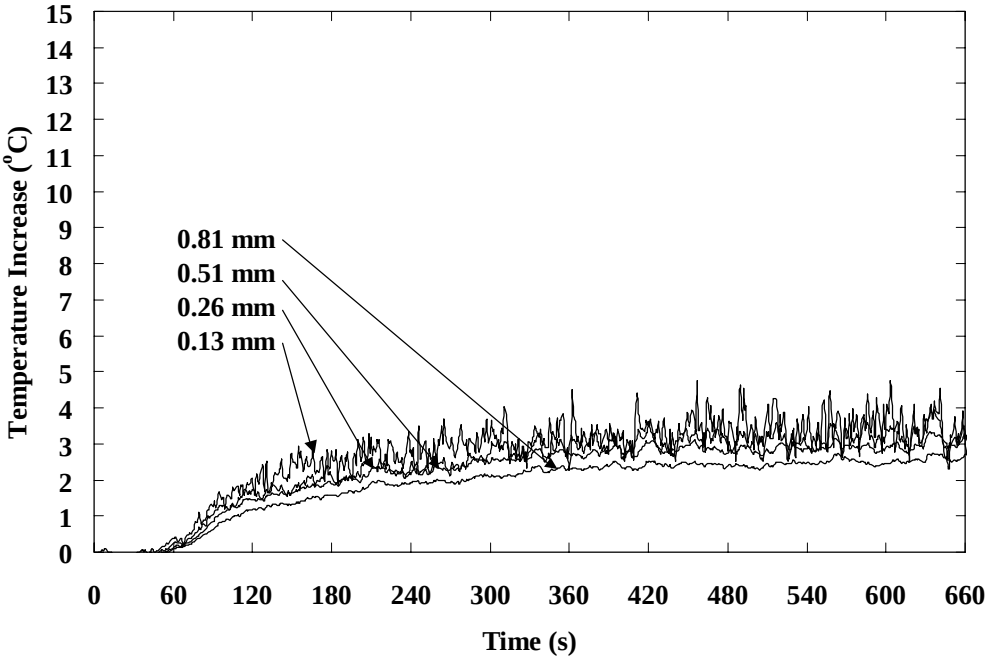

Figure 38. Response of all type T thermocouples, fabric-exposed-space, 1.2 kW/m^2.

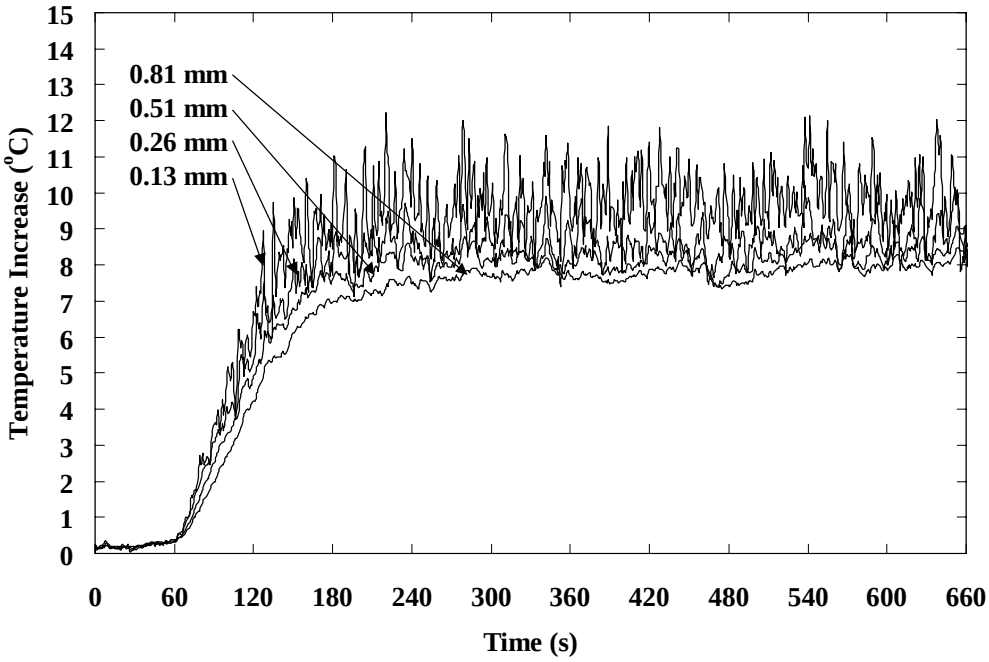

Figure 39. Response of all type T thermocouples, fabric-exposed-space, 5.0 kW/m^2.

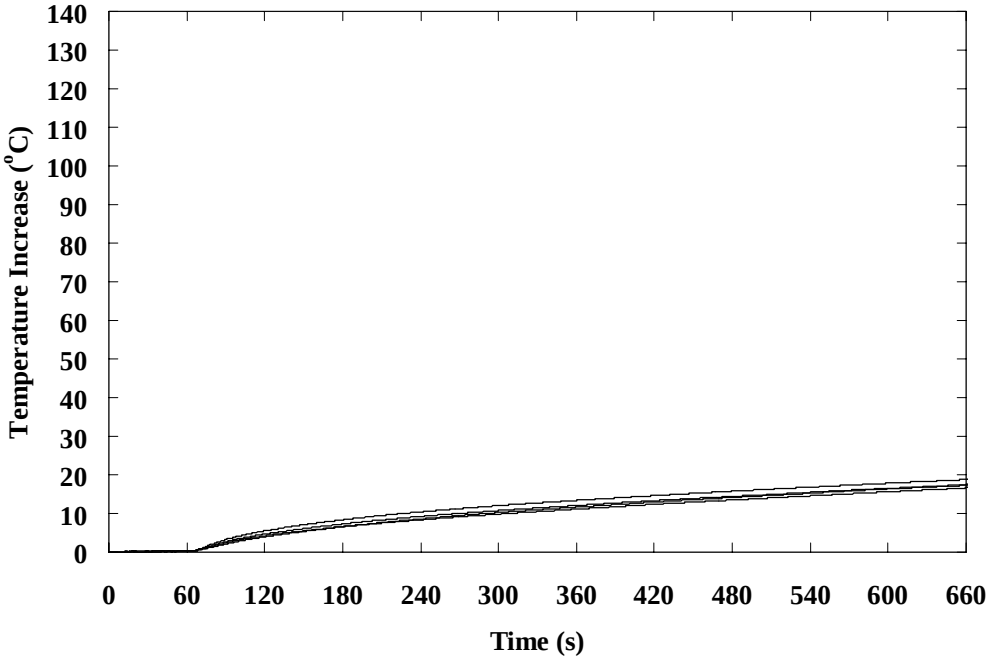

Figure 40. Response of all type J thermocouples, fabric-substrate-no space, 1.2 kW/m^2.

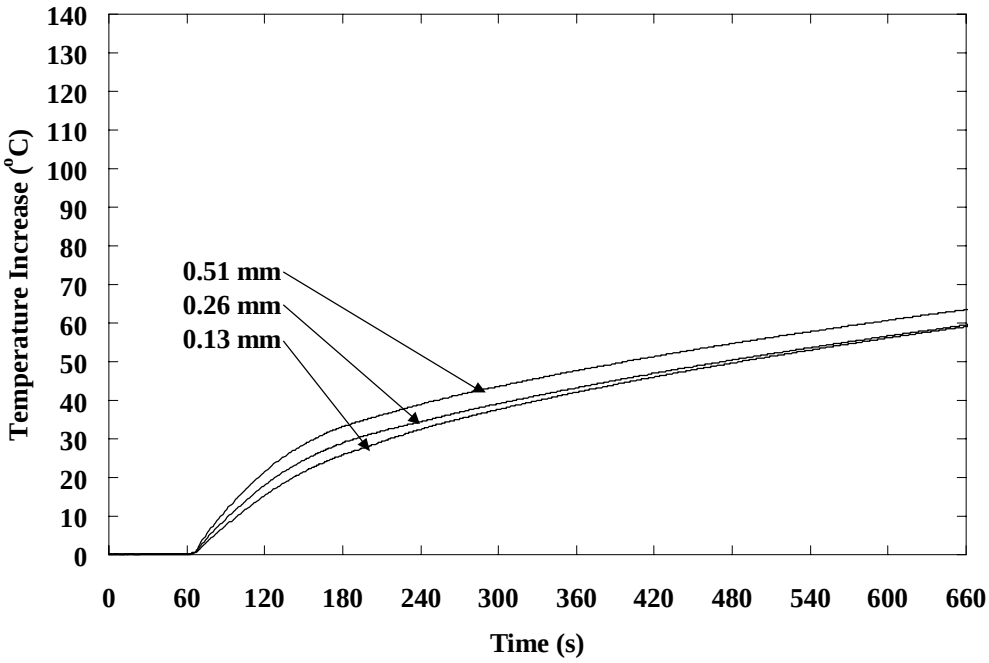

Figure 41. Response of 0.13 mm, 0.26 mm, and 0.51 mm type J thermocouples, fabric-substrate-no space, 5.0 kW/m^2. No data for 0.81 mm type J thermocouple.

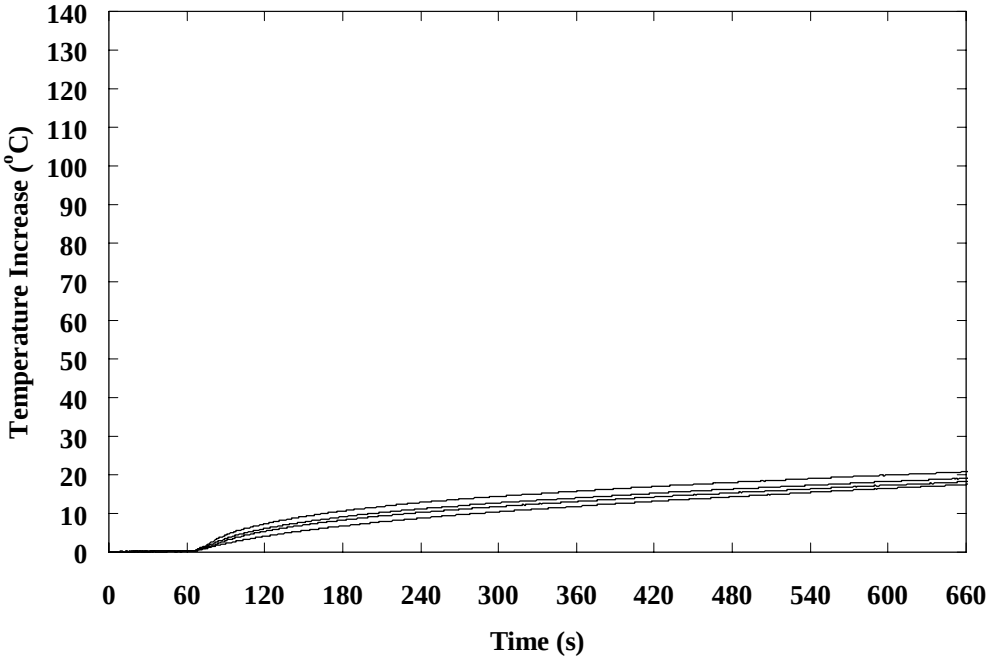

Figure 42. Response of all type K thermocouples, fabric-substrate-no space, 1.2 kW/m^2.

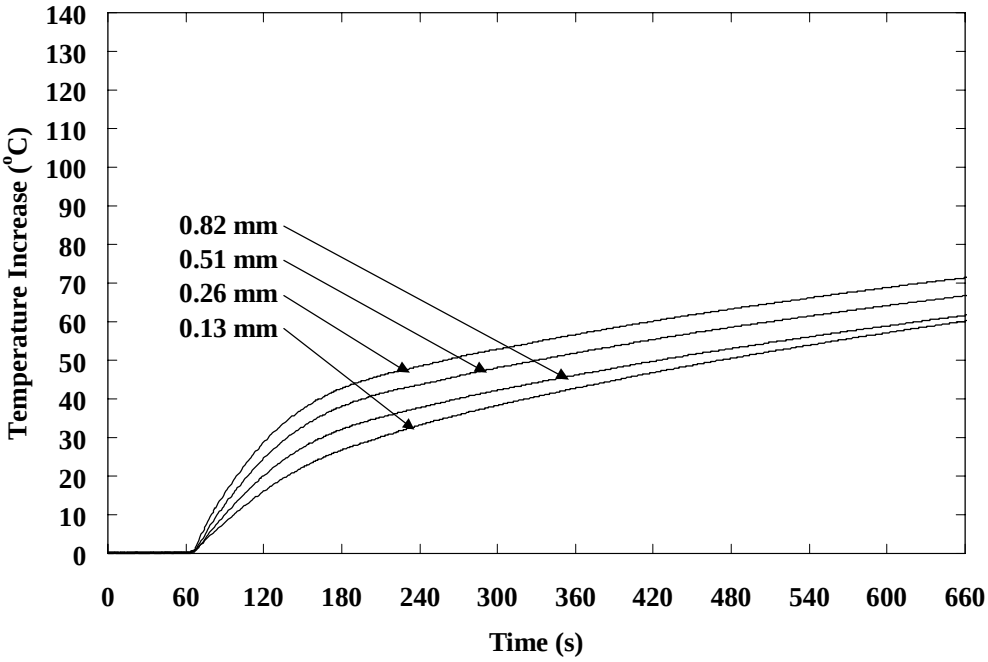

Figure 43. Response of all type K thermocouples, fabric-substrate-no space, 5.0 kW/m^2.

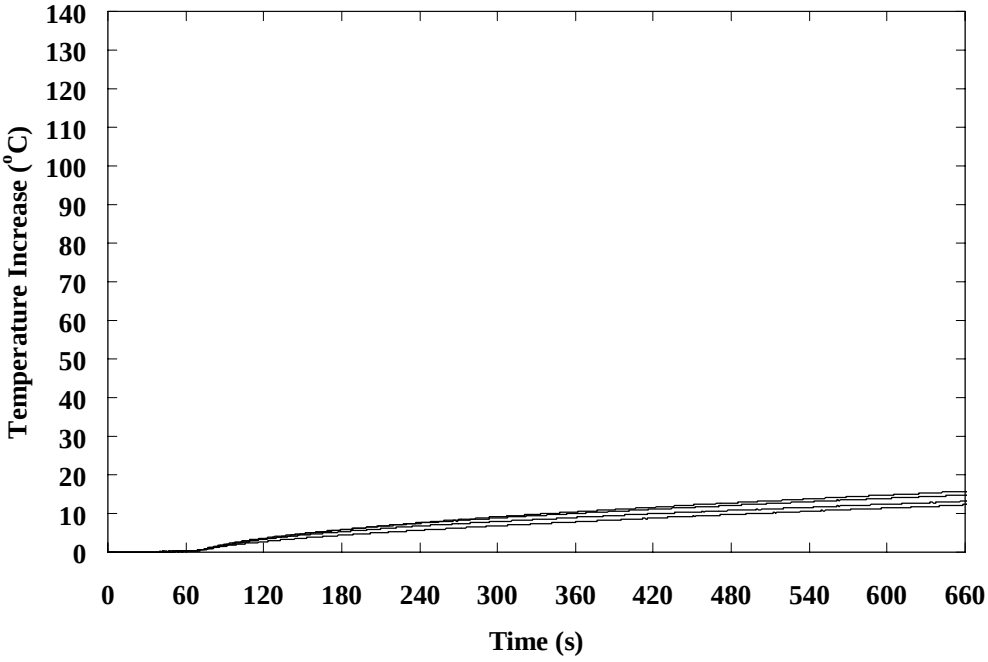

Figure 44. Response of all type T thermocouples, fabric-substrate-no space, 1.2 kW/m^2.

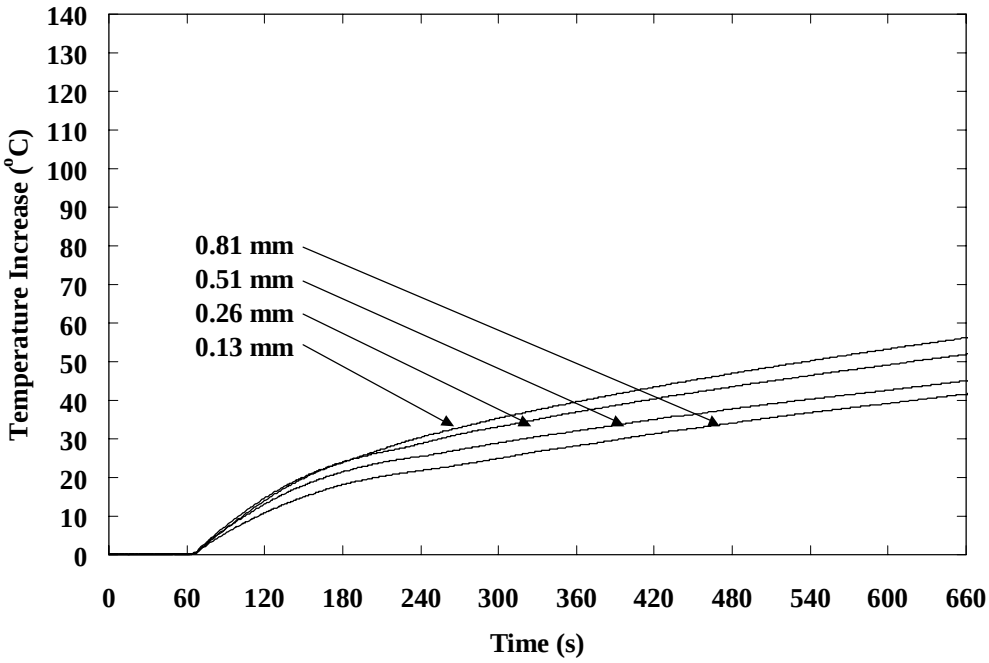

Figure 45. Response of all type T thermocouples, fabric-substrate-no space, 5.0 kW/m^2.

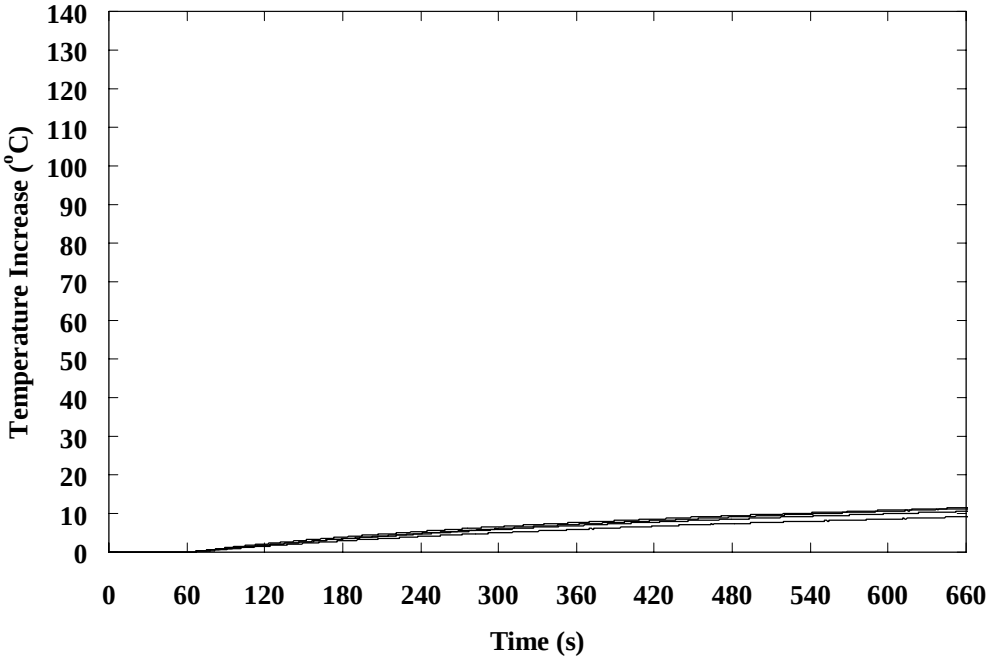

Figure 46. Response of all type J thermocouples, fabric-substrate-space, 1.2 kW/m^2.

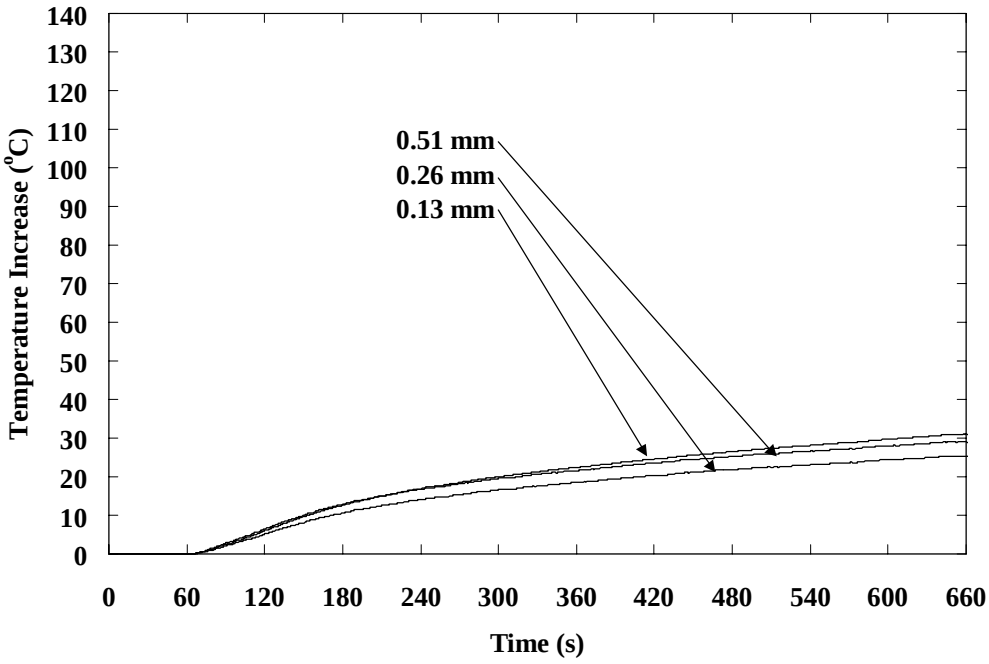

Figure 47. Response of 0.13 mm, 0.26 mm, and 0.51 mm type J thermocouples, fabric-substrate-space, 5.0 kW/m^2. No data for 0.81 mm type J thermocouple.

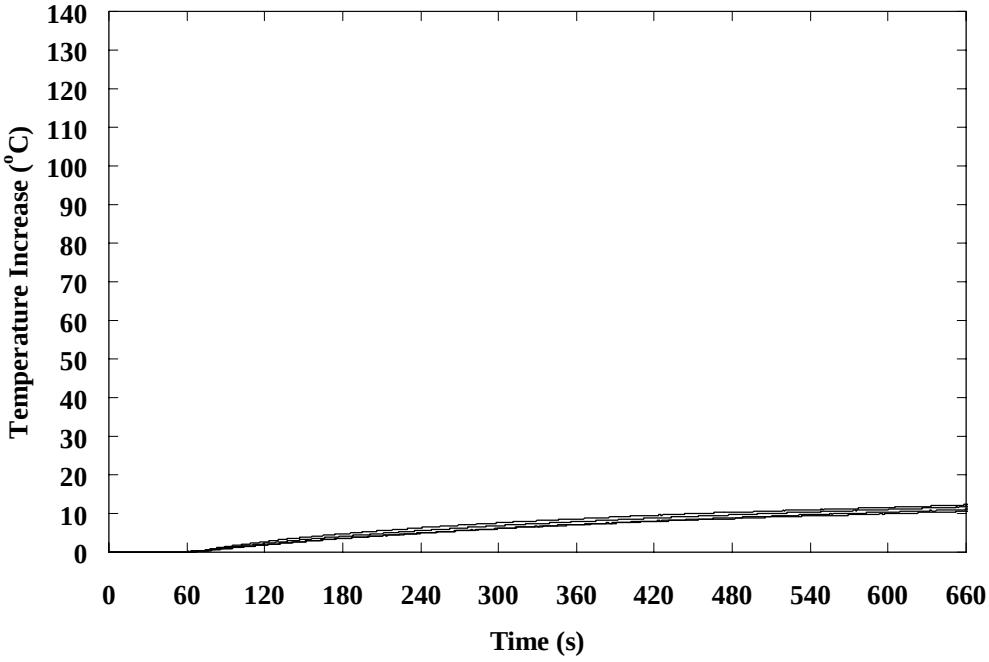

Figure 48. Response of all type K thermocouples, fabric-substrate-space, 1.2 kW/m^2.

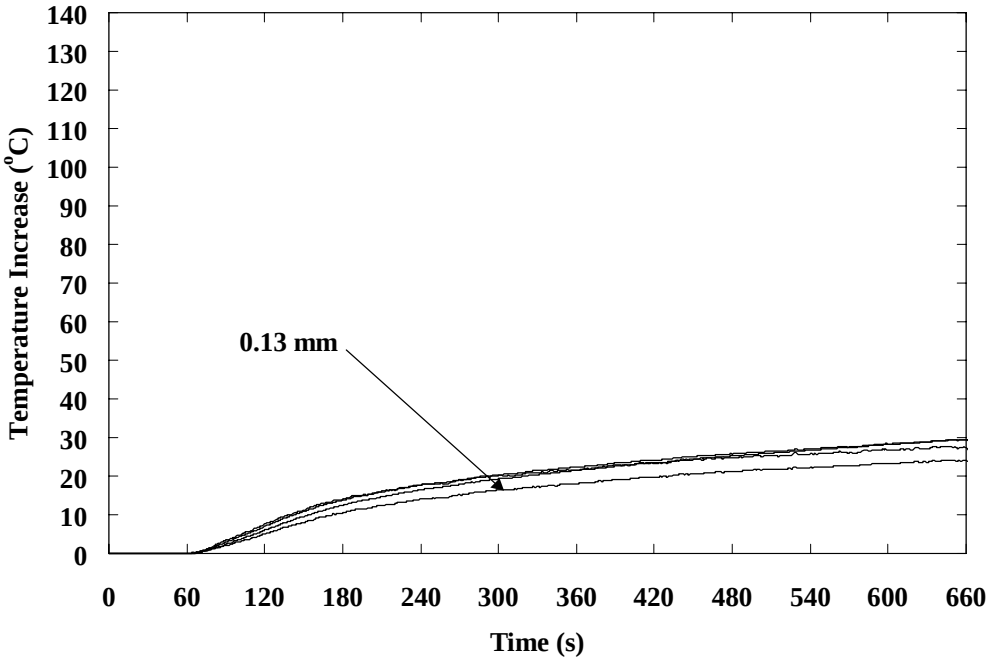

Figure 49. Response of all type K thermocouples, fabric-substrate-space, 5.0 kW/m^2.

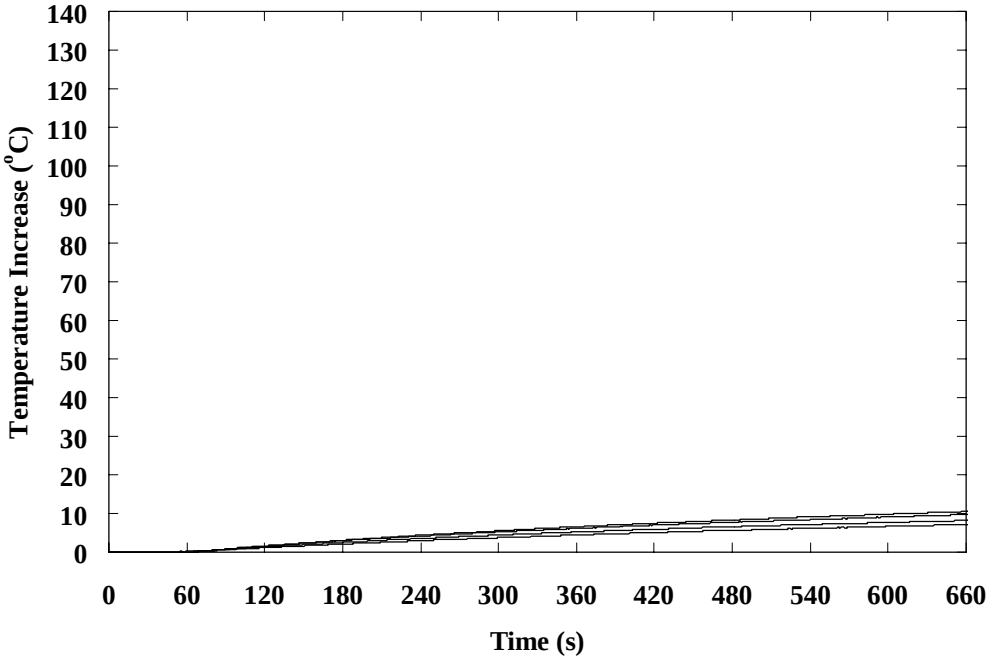

Figure 50. Response of all type T thermocouples, fabric-substrate-space, 1.2 kW/m^2.

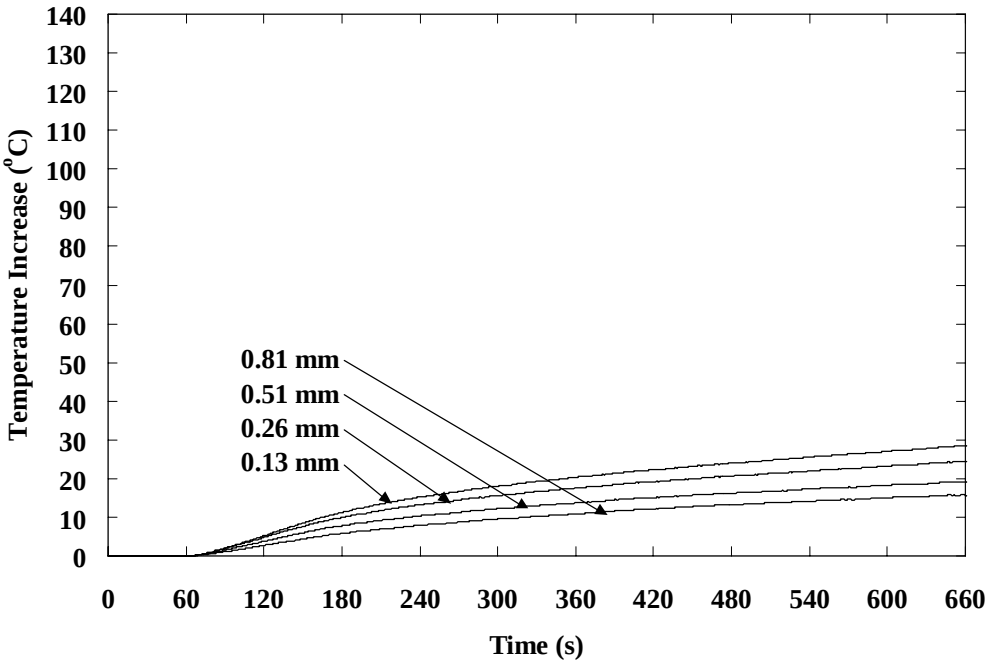

Figure 51. Response of all type T thermocouples, fabric-substrate-space, 5.0 kW/m^2.

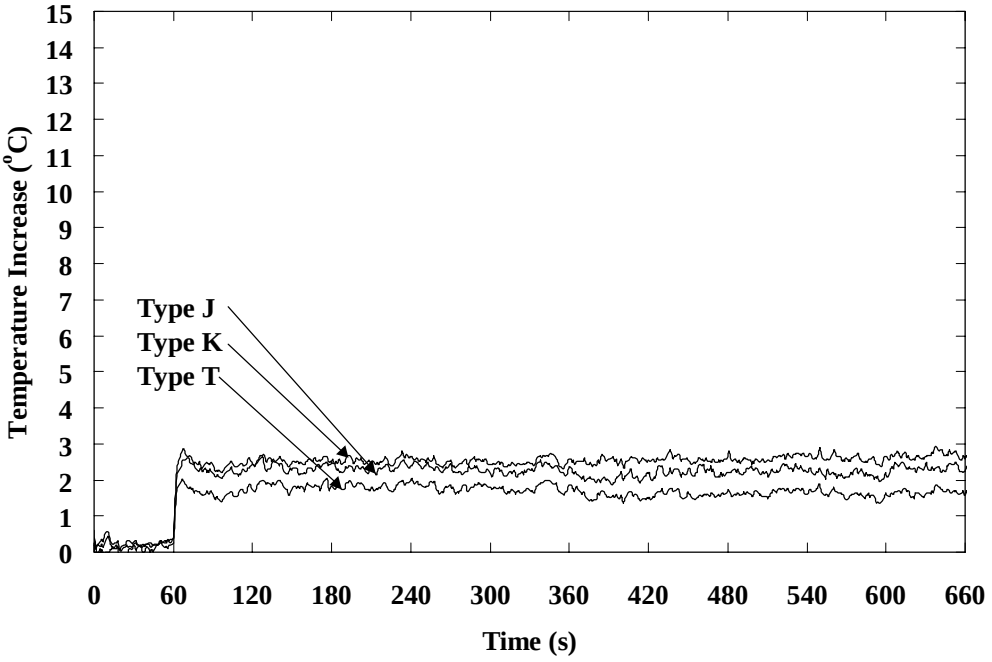

Figure 52. Response of type J, K, and T thermocouples, 0.13 mm wire diameter, exposed, 1.2 kW/m^2.

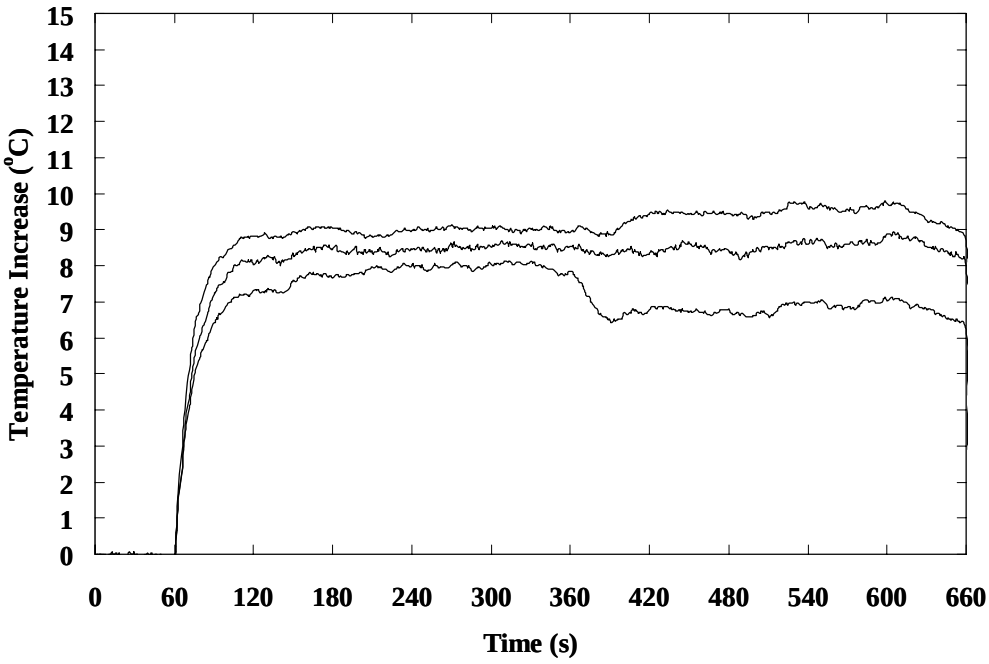

Figure 53. Response of type J, K, and T thermocouples, 0.13 mm wire diameter, exposed, 5.0 kW/m^2.

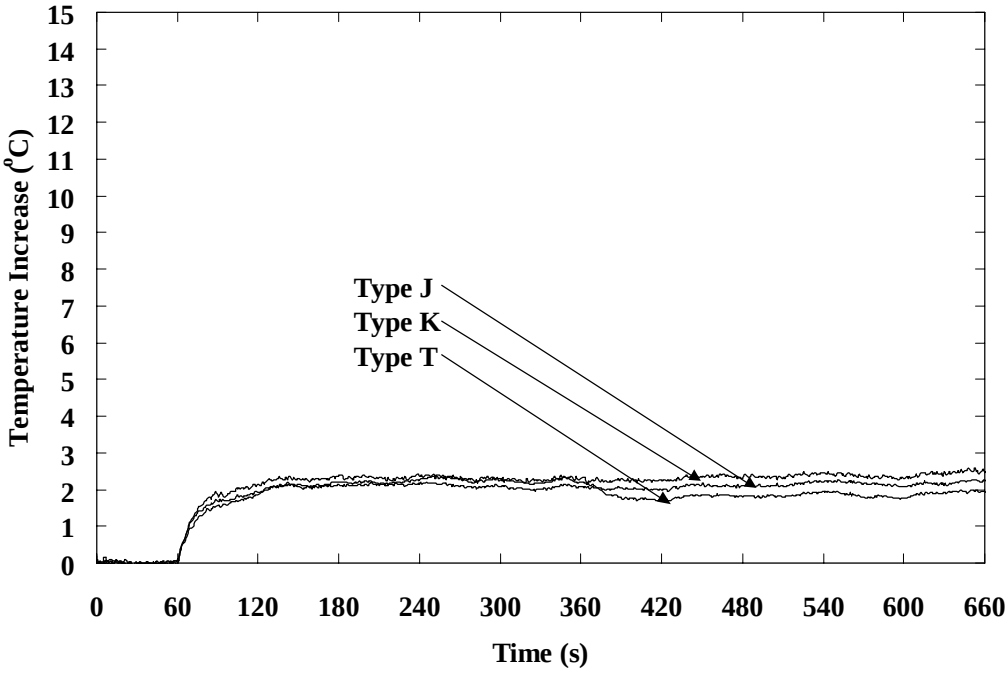

Figure 54. Response of type J, K, and T thermocouples, 0.81 mm wire diameter, exposed, 1.2 kW/m^2.

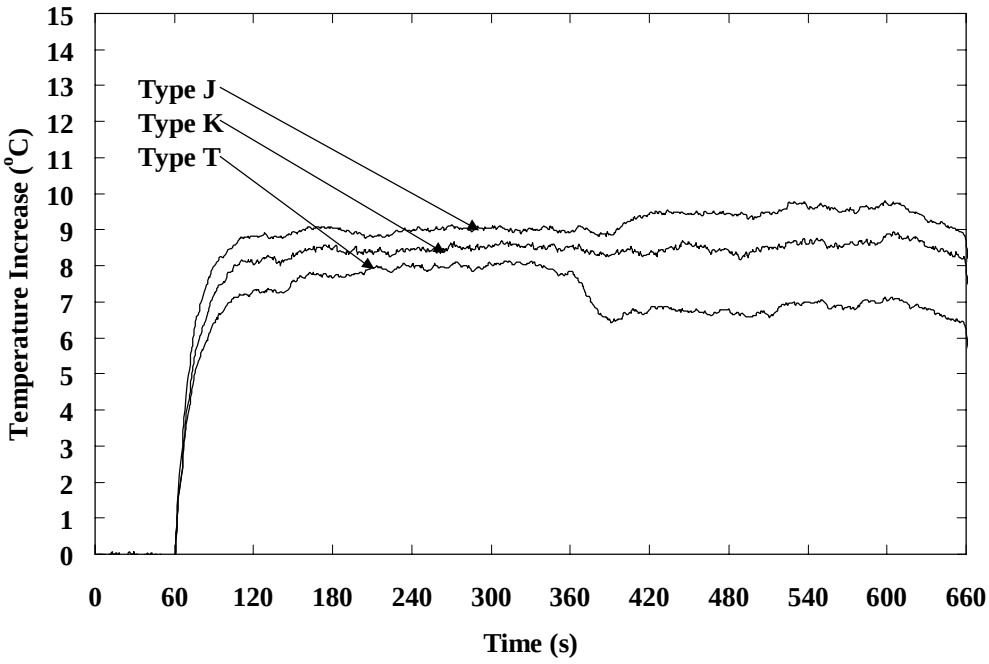

Figure 55. Response of type J, K, and T thermocouples, 0.81 mm wire diameter, exposed, 5.0 kW/m^2.

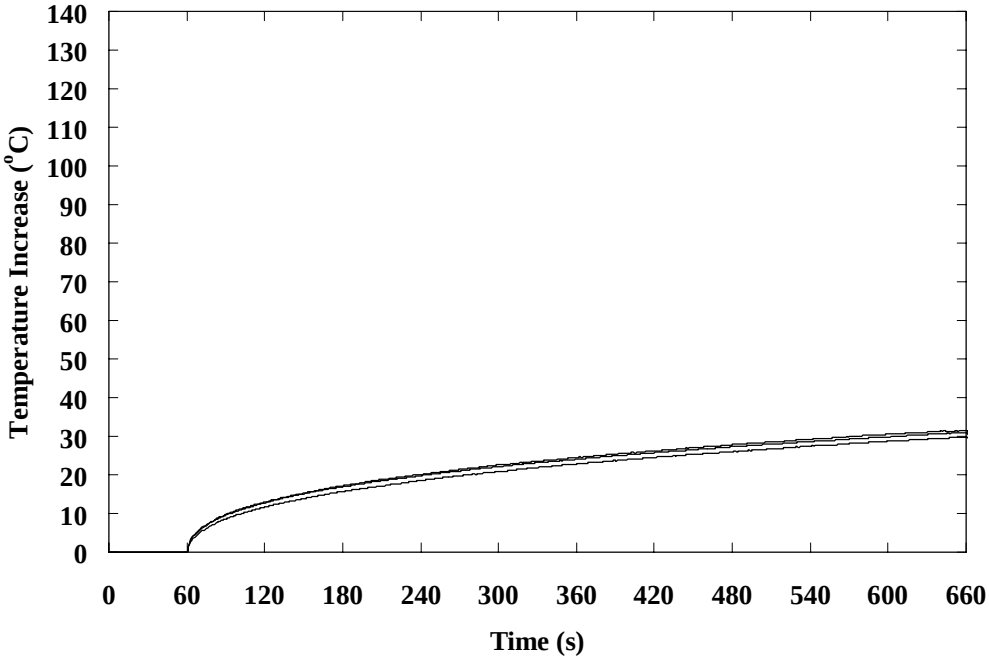

Figure 56. Response of type J, K, and T thermocouples, 0.13 mm wire diameter, substrate, 1.2 kW/m^2.

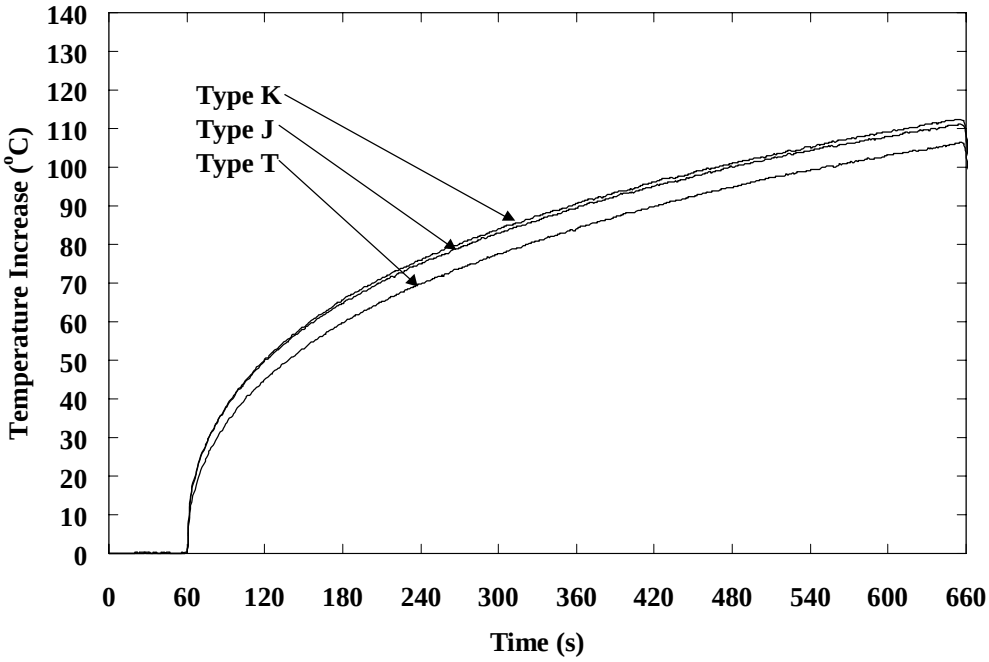

Figure 57. Response of type J, K, and T thermocouples, 0.13 mm wire diameter, substrate, 5.0 kW/m^2.

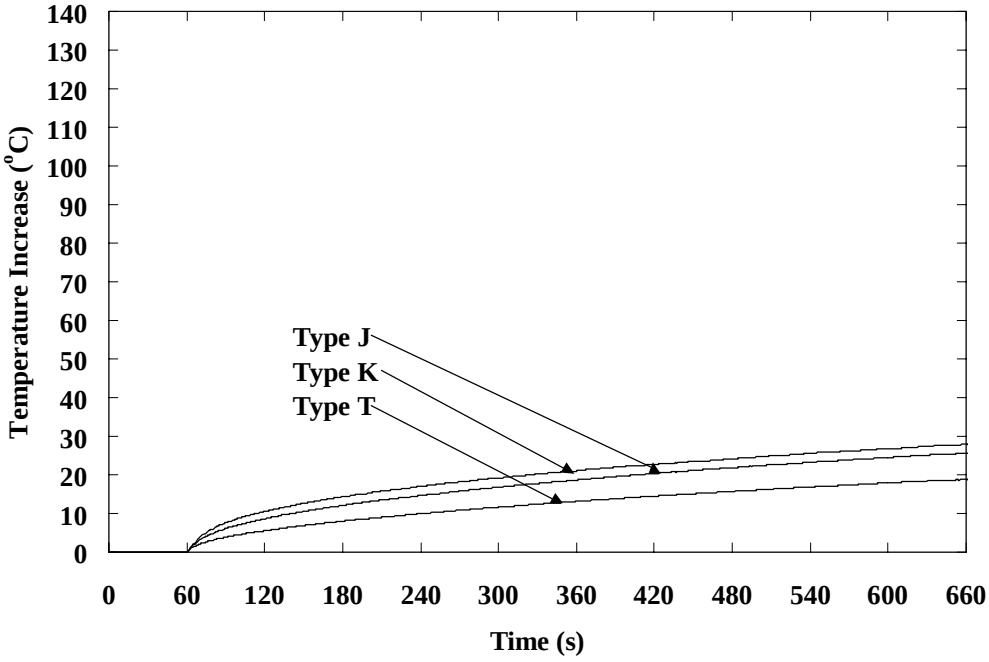

Figure 58. Response of type J, K, and T thermocouples, 0.81 mm wire diameter, substrate, 1.2 kW/m^2.

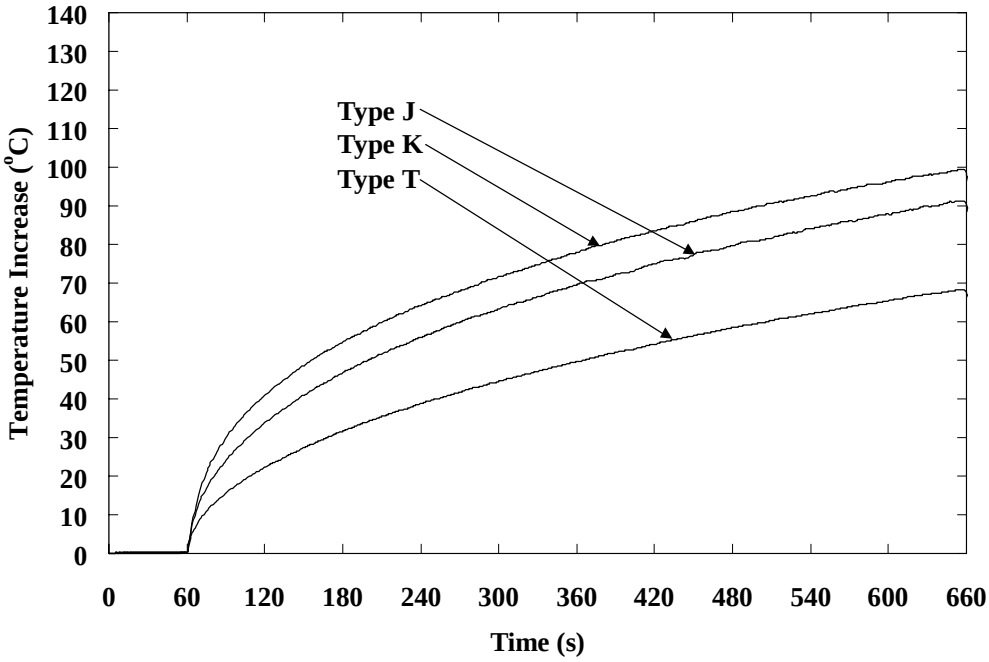

Figure 59. Response of type J, K, and T thermocouples, 0.81 mm wire diameter, substrate 5.0 kW/m^2.

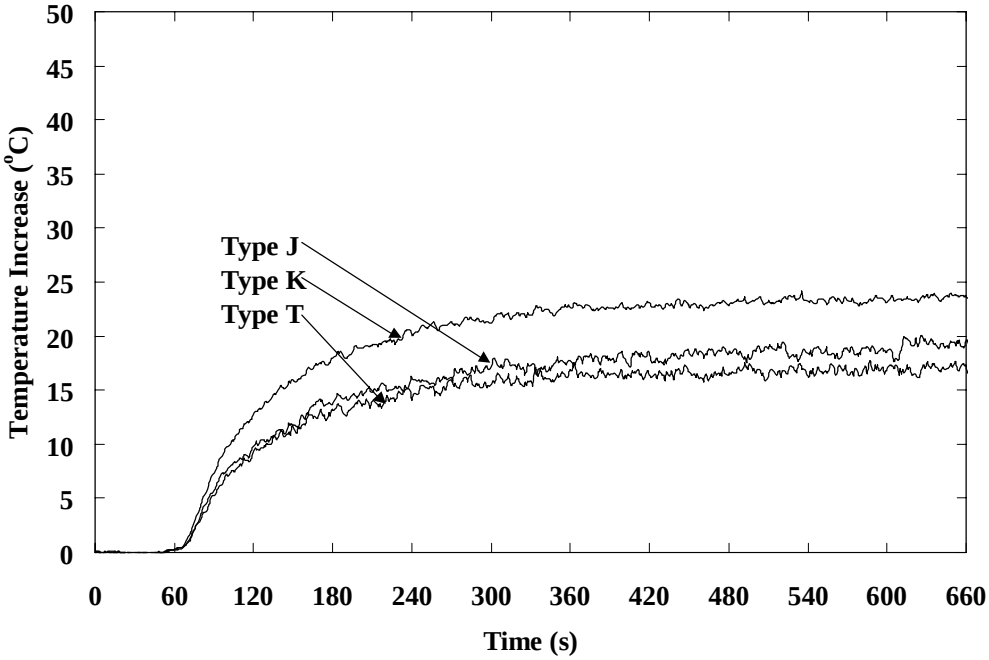

Figure 60. Response of type J, K, and T thermocouples, 0.13 mm wire diameter, fabric-exposed-no space, 1.2 kW/m^2.

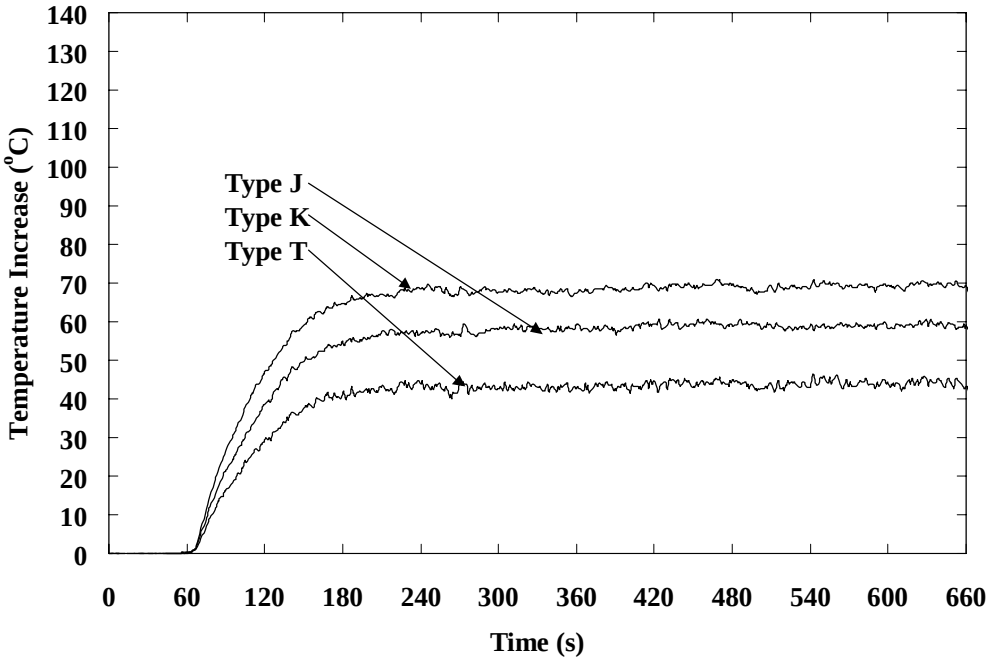

Figure 61. Response of type J, K, and T thermocouples, 0.13 mm wire diameter, fabric-exposed-no space, 5.0 kW/m^2.

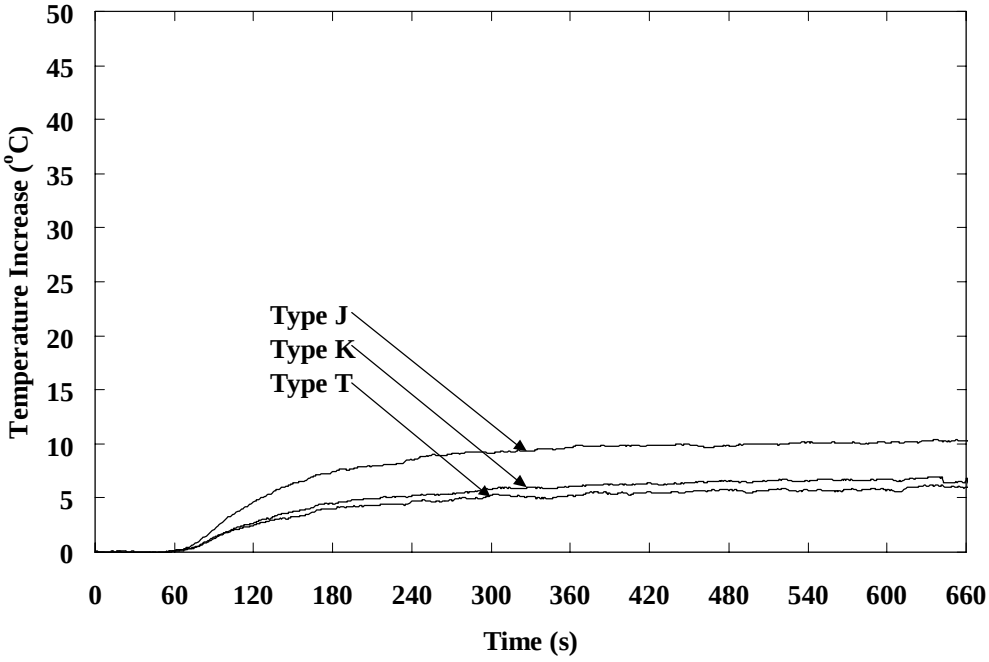

Figure 62. Response of type J, K, and T thermocouples, 0.81 mm wire diameter, fabric-exposed-no space, 1.2 kW/m^2.

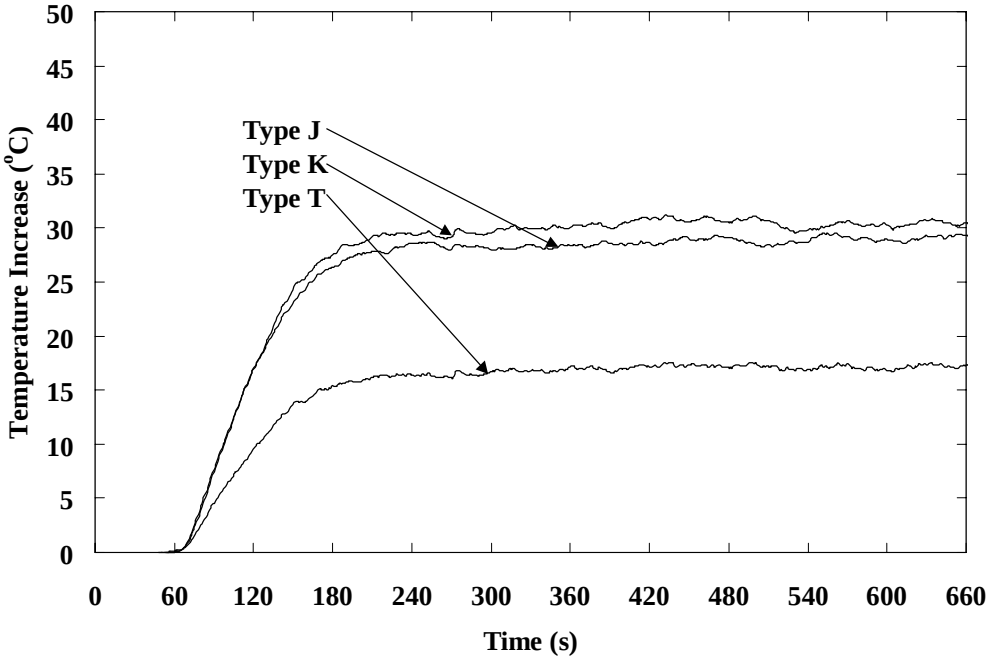

Figure 63. Response of type J, K, and T thermocouples, 0.81 mm wire diameter, fabric-exposed-no space, 5.0 kW/m^2.

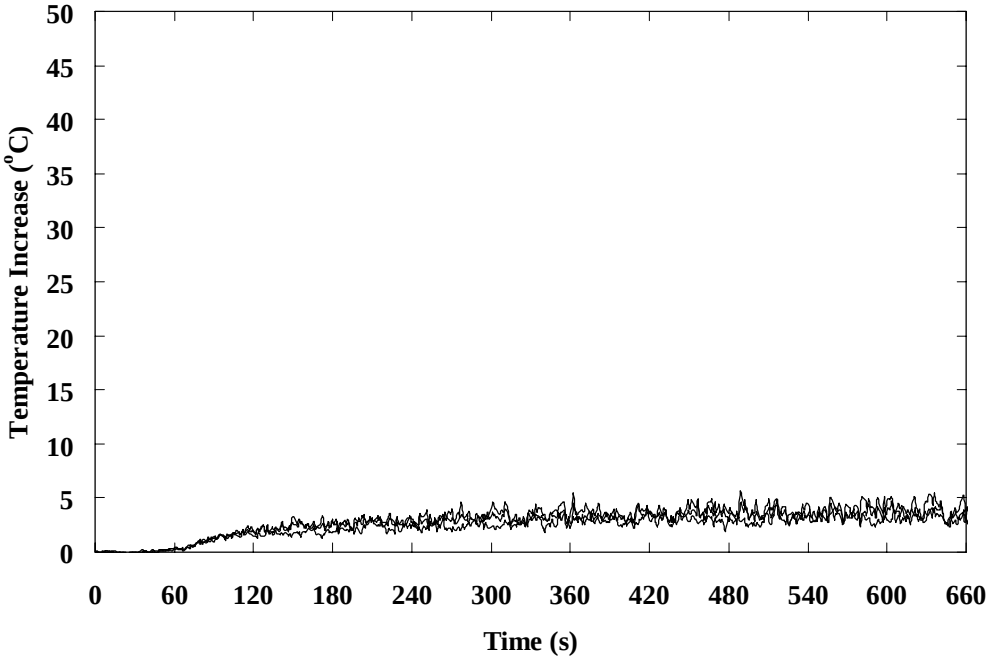

Figure 64. Response of type J, K, and T thermocouples, 0.13 mm wire diameter, fabric-exposed-space, 1.2 kW/m^2.

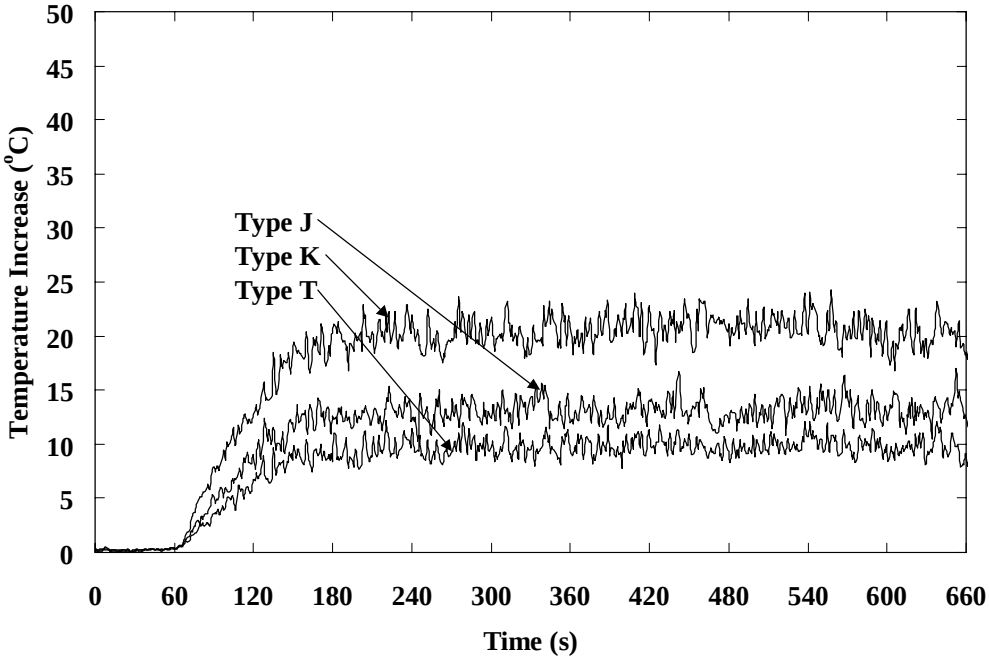

Figure 65. Response of type J, K, and T thermocouples, 0.13 mm wire diameter, fabric-exposed-space, 5.0 kW/m^2.

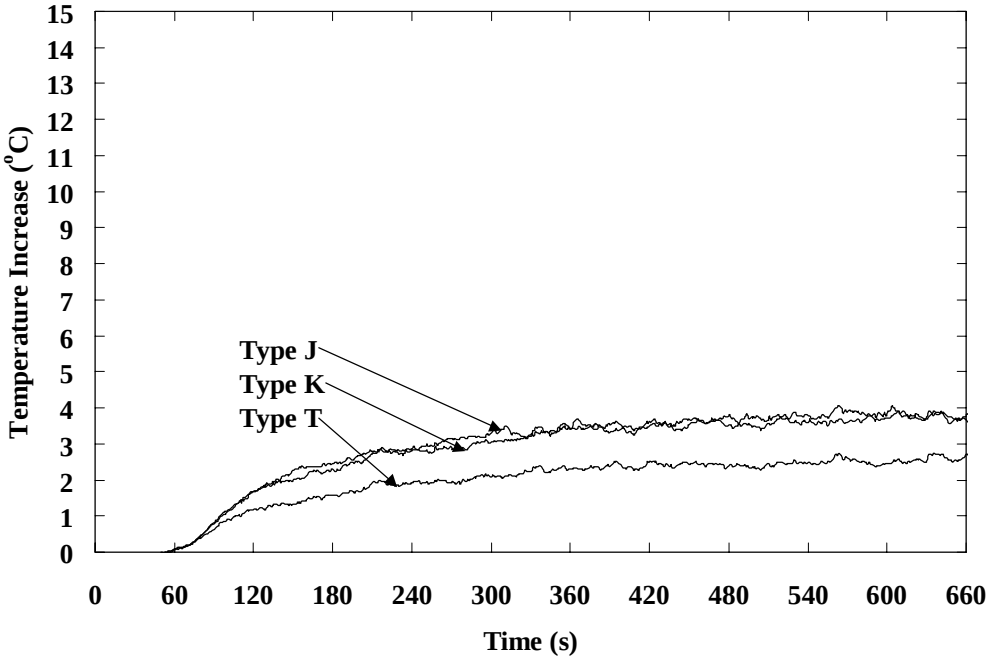

Figure 66. Response of type J, K, and T thermocouples, 0.81 mm wire diameter, fabric-exposed-space, 1.2 kW/m^2.

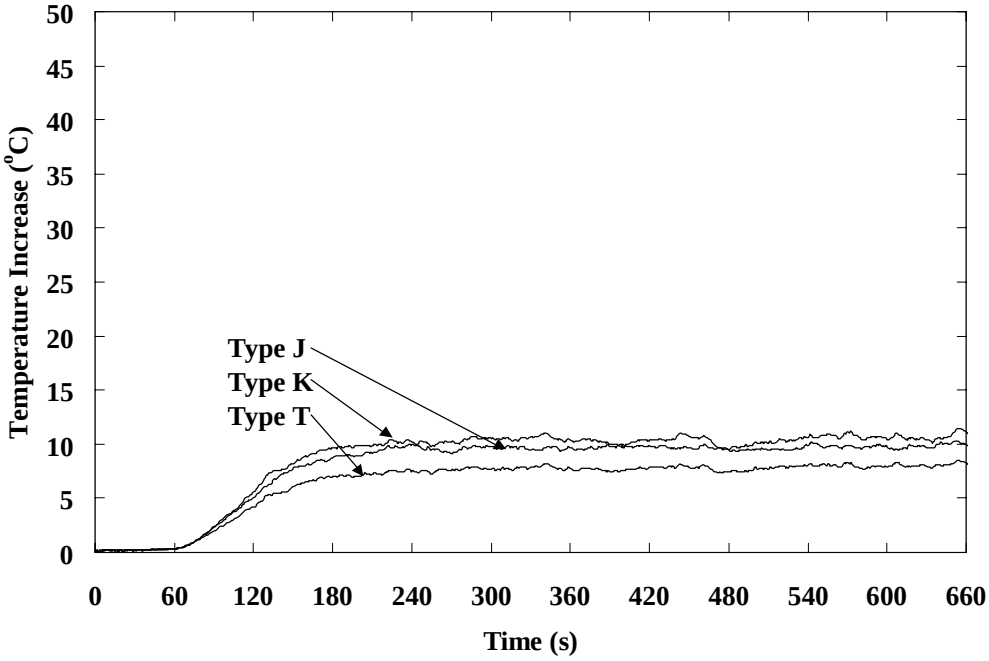

Figure 67. Response of type J, K, and T thermocouples, 0.81 mm wire diameter, fabric-exposed-space, 5.0 kW/m^2.

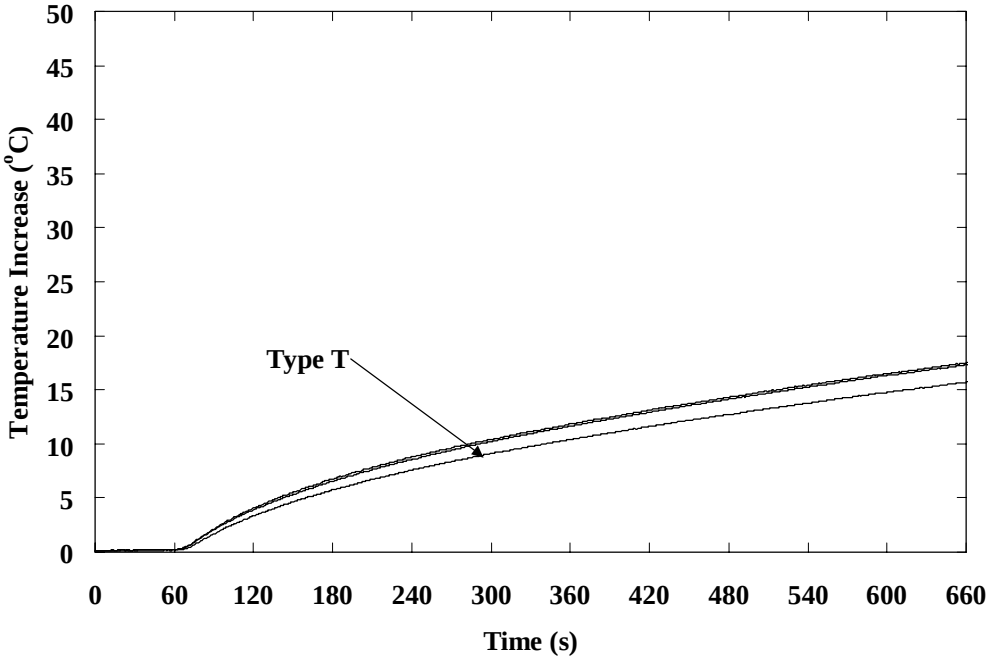

Figure 68. Response of type J, K, and T thermocouples, 0.13 mm wire diameter, fabric-substrate-no space, 1,25 kW/m^2.

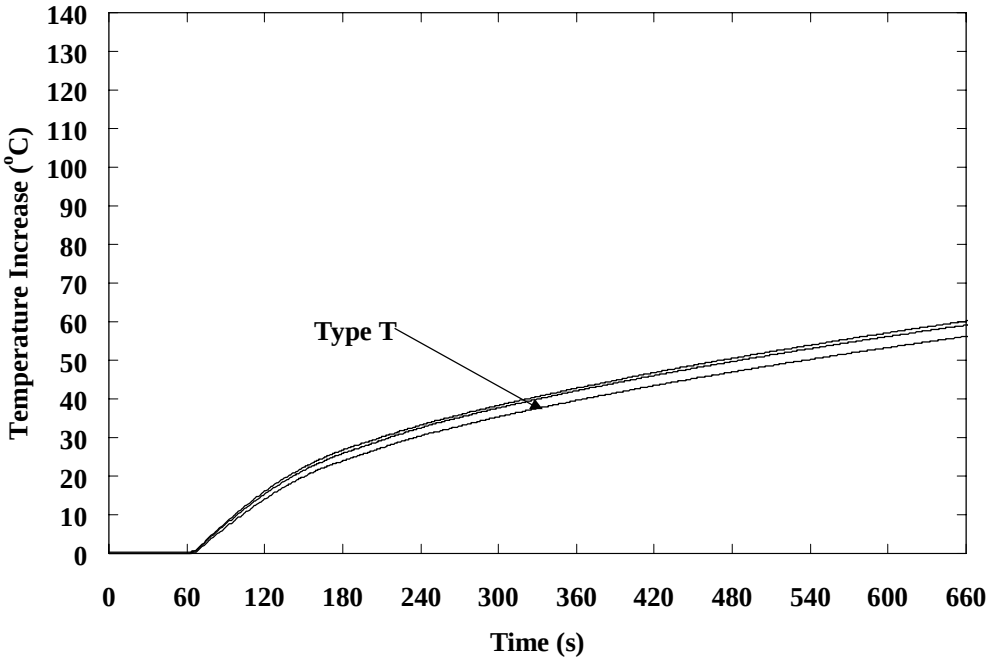

Figure 69. Response of type J, K, and T thermocouples, 0.13 mm wire diameter, fabric-substrate-no space, 5.0 kW/m^2.

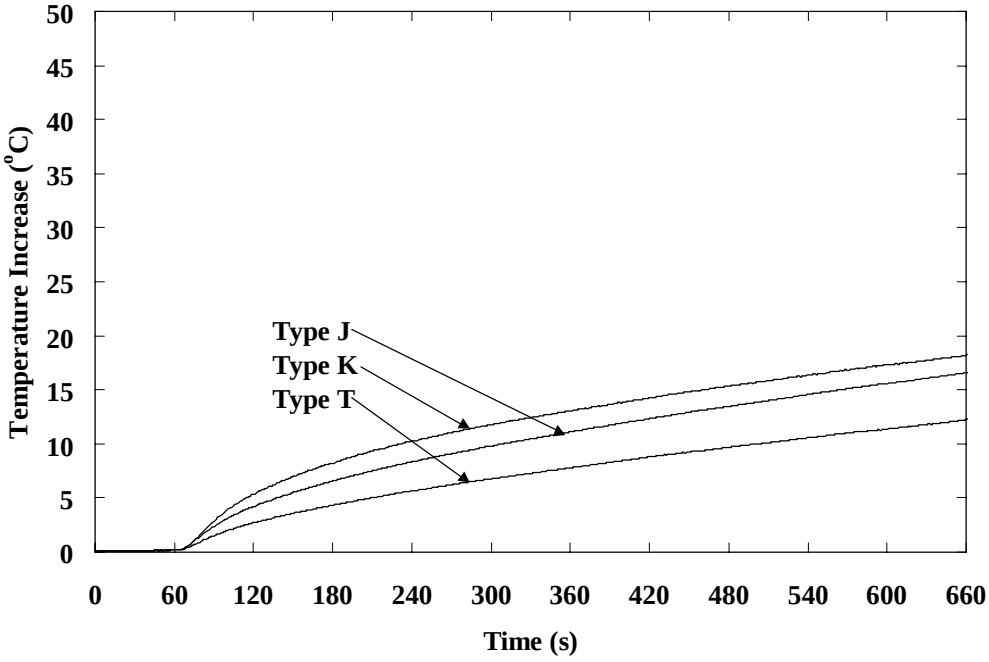

Figure 70. Response of type J, K, and T thermocouples, 0.81 mm wire diameter, fabric-substrate-no space, 1.2 kW/m^2.

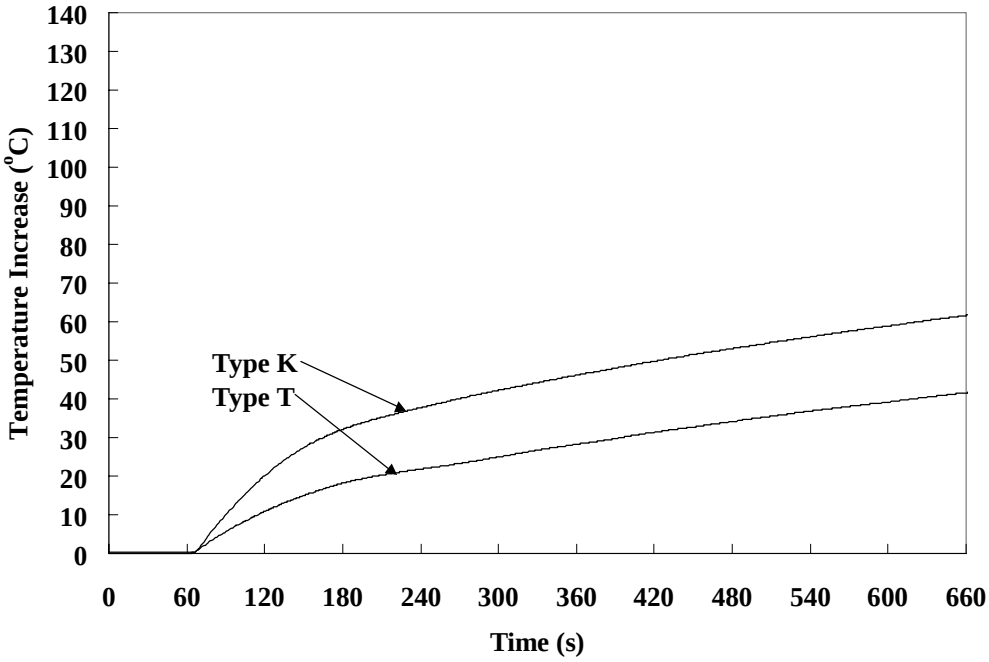

Figure 71. Response of type K, and T thermocouples, 0.81 mm wire diameter, fabric-substrate-no space, 5.0 kW/m^2. No data for type J thermocouple.

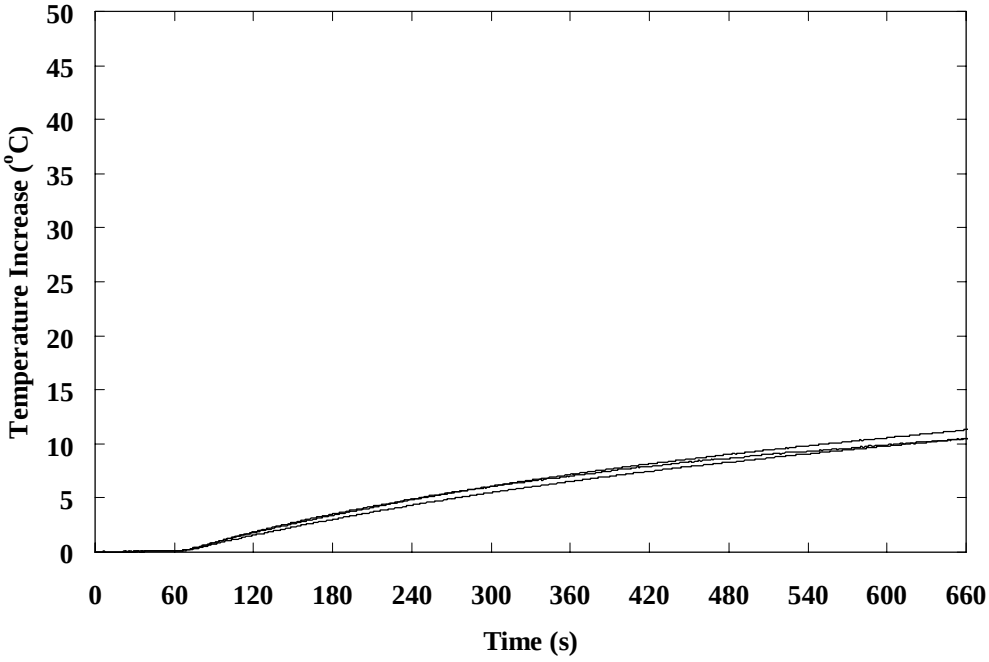

Figure 72. Response of type J, K, and T thermocouples, 0.13 mm wire diameter, fabric-substrate-space, 1.2 kW/m^2.

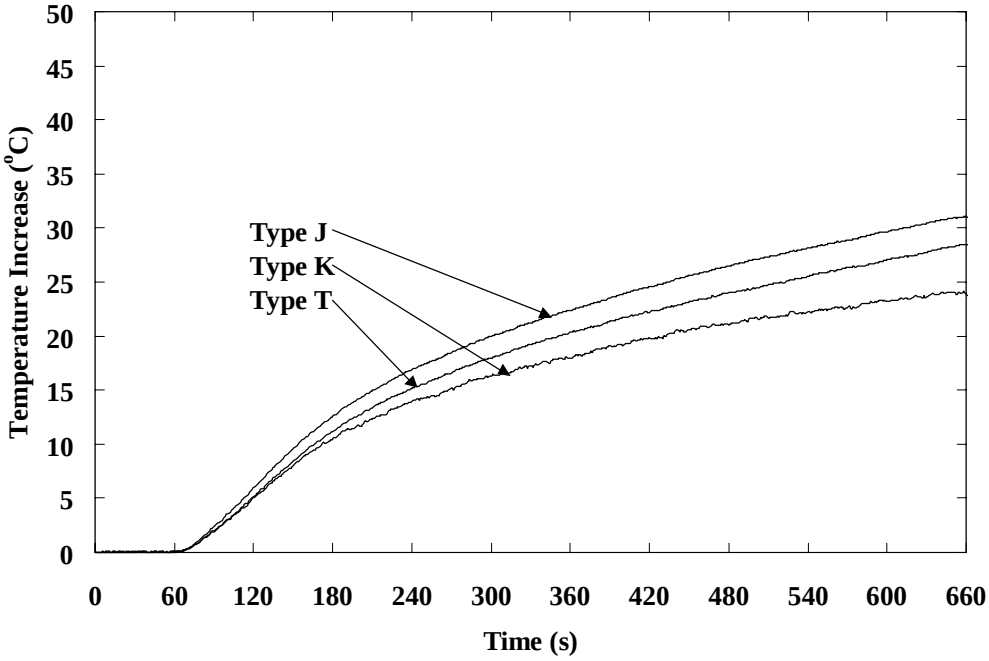

Figure 73. Response of type J, K, and T thermocouples, 0.13 mm wire diameter, fabric-substrate-space, 5.0 kW/m^2.

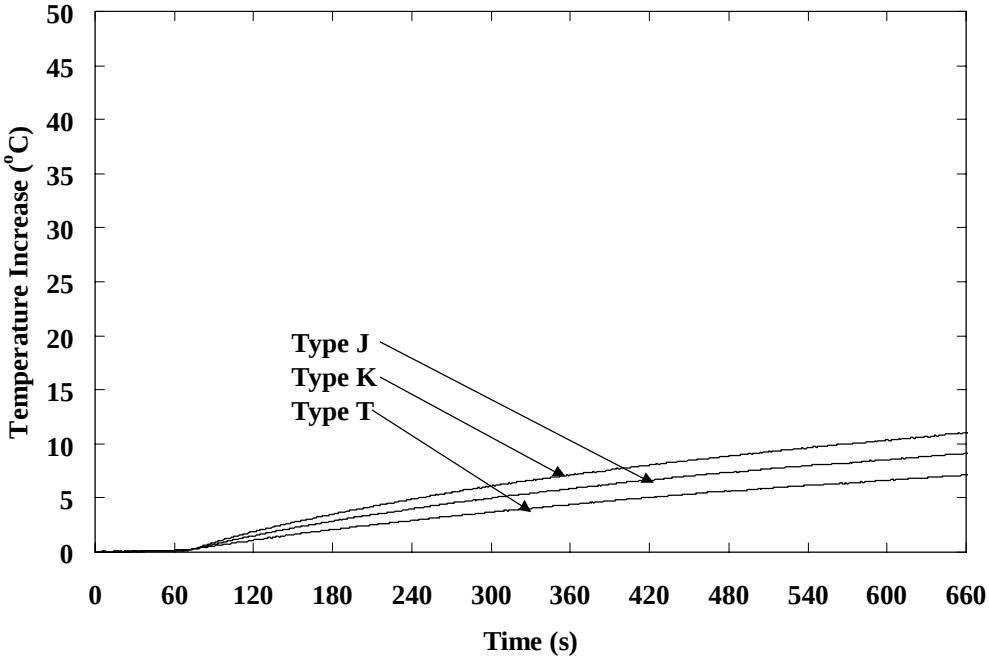

Figure 74. Response of type J, K, and T thermocouples, 0.81 mm wire diameter, fabric-substrate-space, 1.2 kW/m^2.

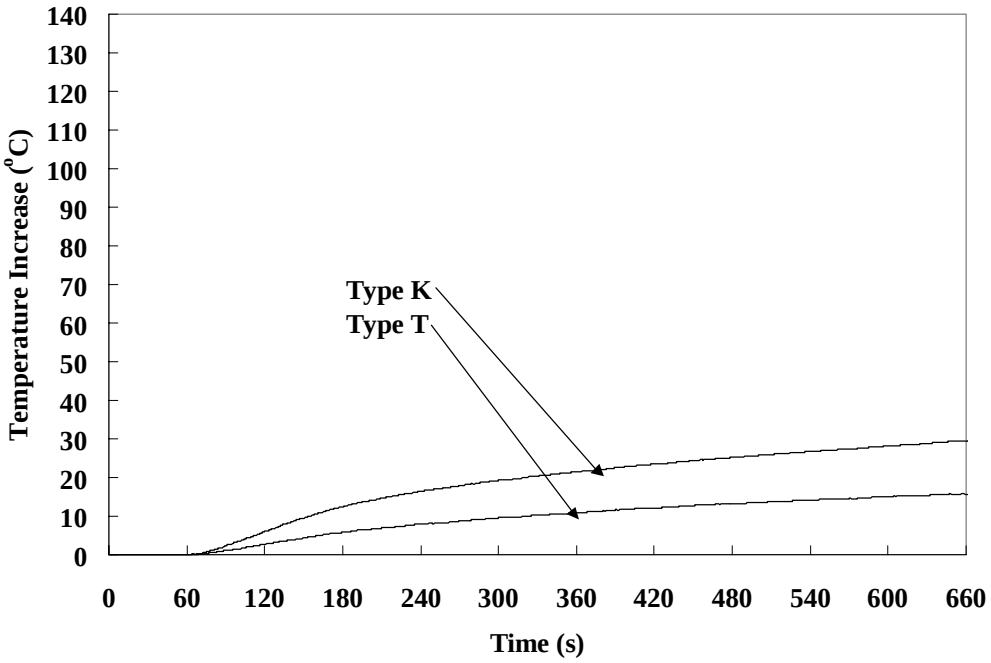

Figure 75. Response of type K, and T thermocouples, 0.81 mm wire diameter, fabric-substrate-space, 5.0 kW/m^2. No data for type J thermocouple

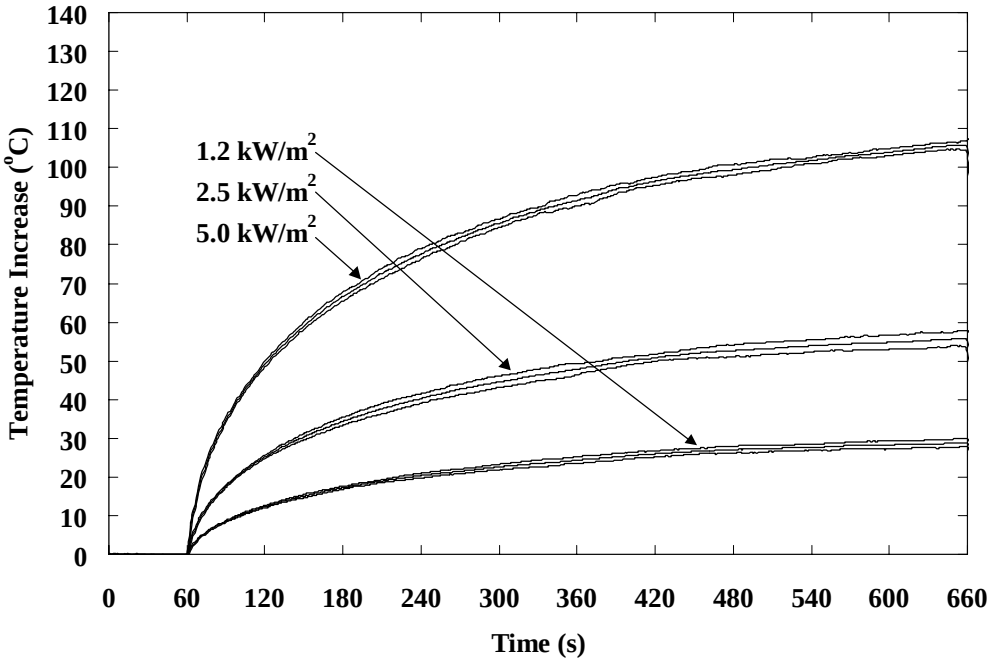

Figure 76. Response of encapsulated type T thermocouple, exposed, all three heat flux levels, with error bars.

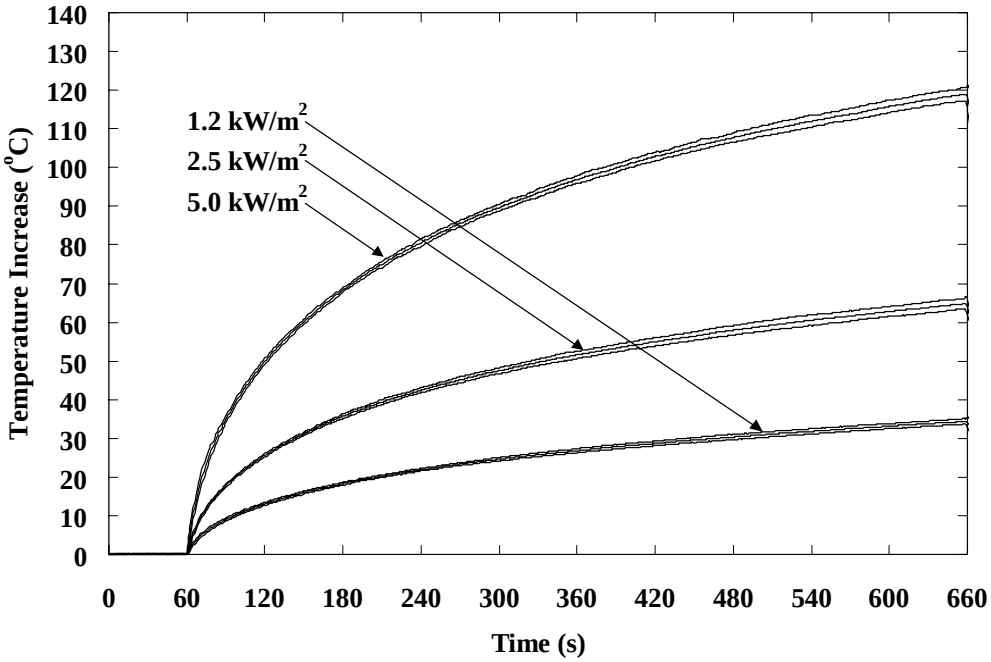

Figure 77. Response of encapsulated type T thermocouple, substrate, all three heat flux levels, with error bars.

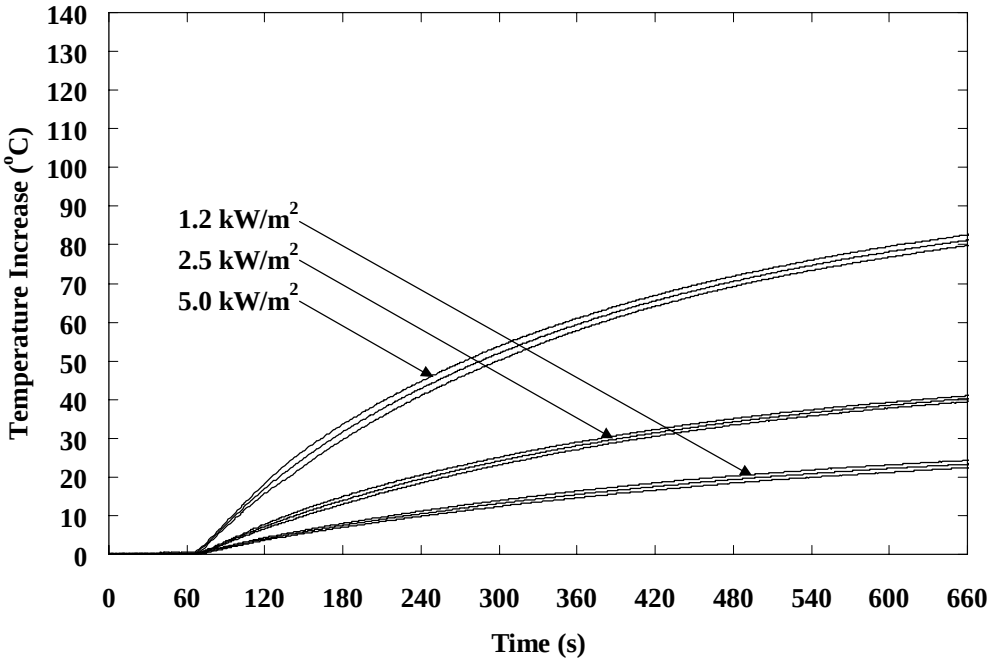

Figure 78. Response of encapsulated type T thermocouple, fabric-exposed-no space, all three heat flux levels, with error bars.

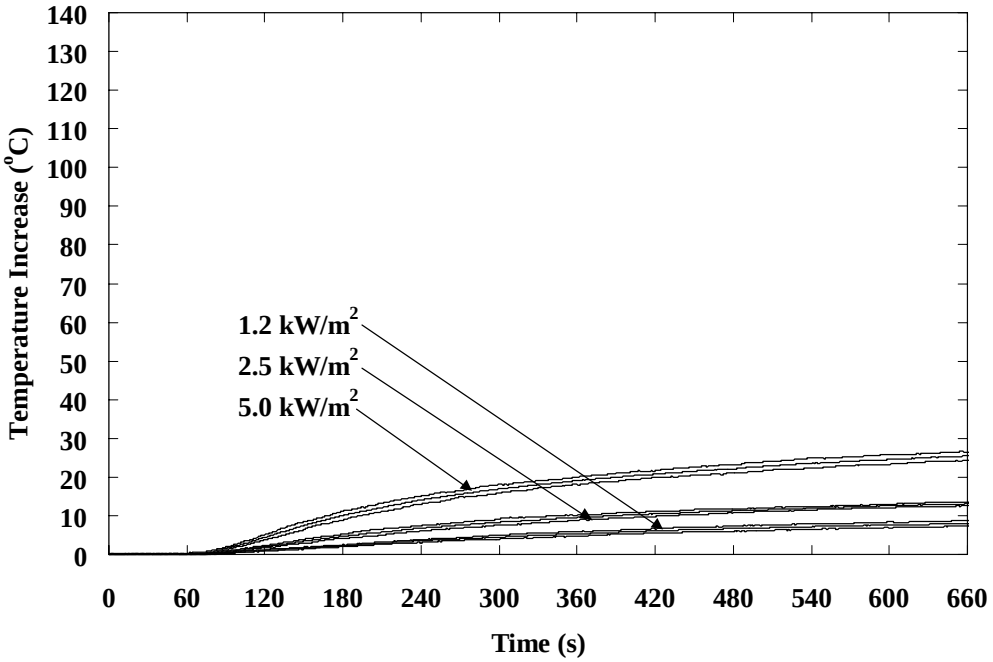

Figure 79. Response of encapsulated type T thermocouple, fabric-exposed-space, all three heat flux levels, with error bars.

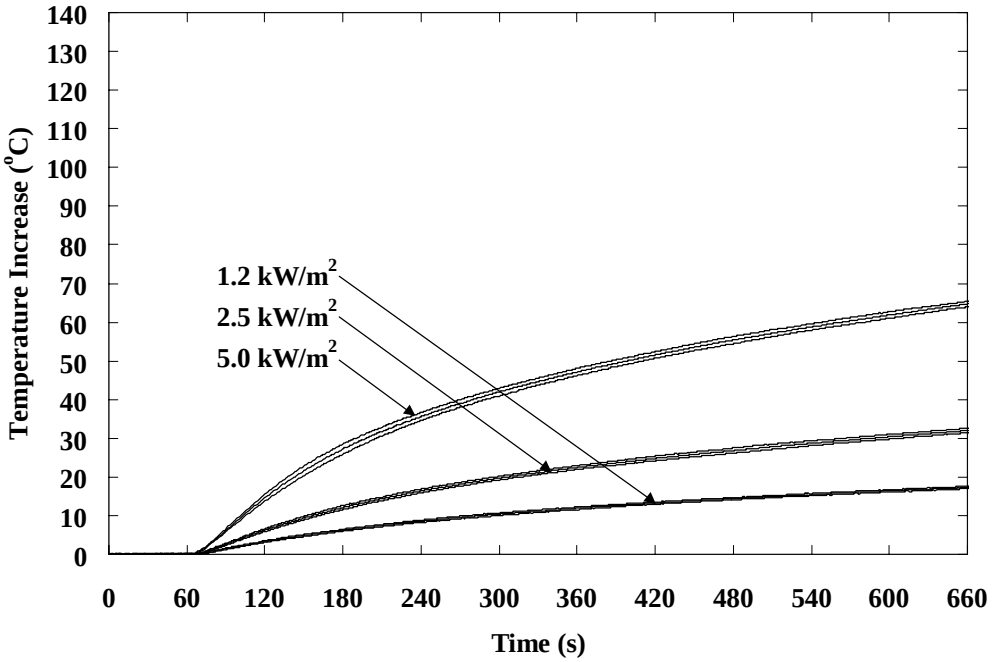

Figure 80. Response of encapsulated type T thermocouple, fabric-substrate-no space, all three heat flux levels, with error bars.

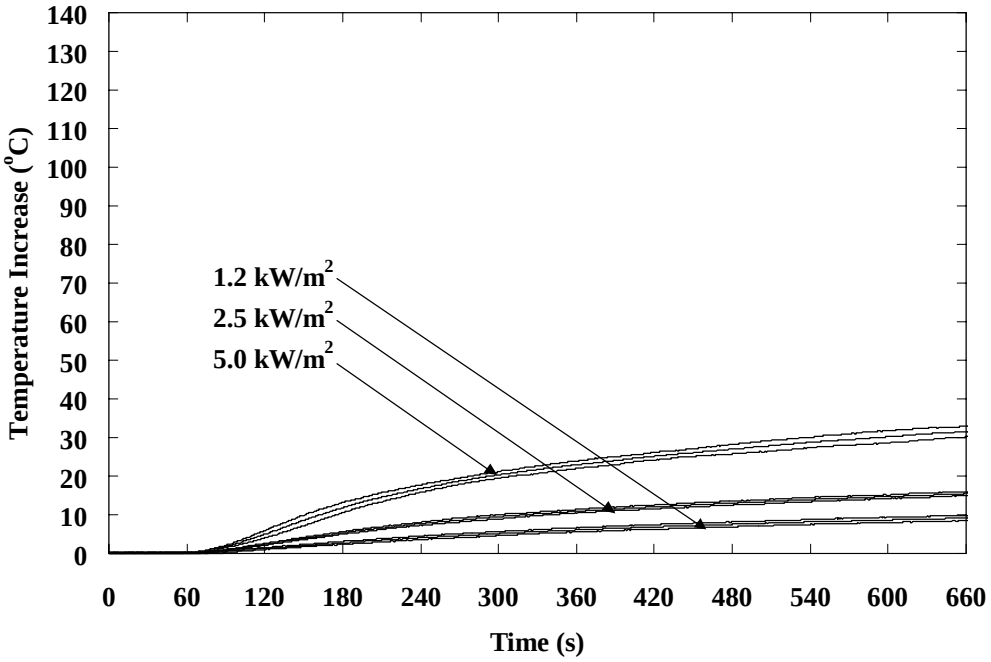

Figure 81. Response of encapsulated type T thermocouple, fabric-substrate-space, all three heat flux levels, with error bars.

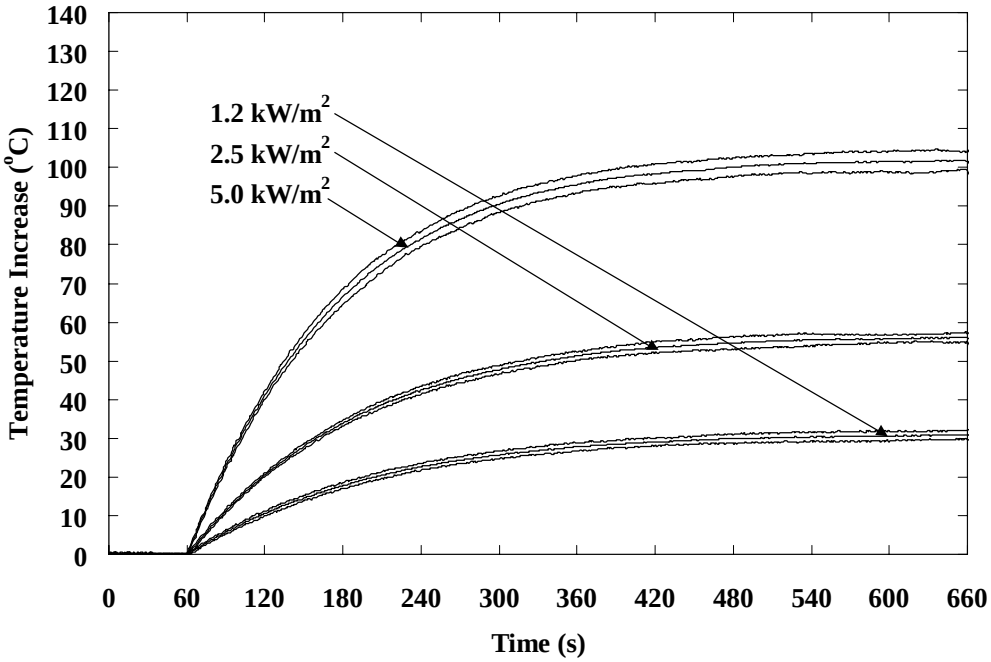

Figure 82. Response of copper disk with 4 type J thermocouples, exposed, all three heat flux levels, with error bars.

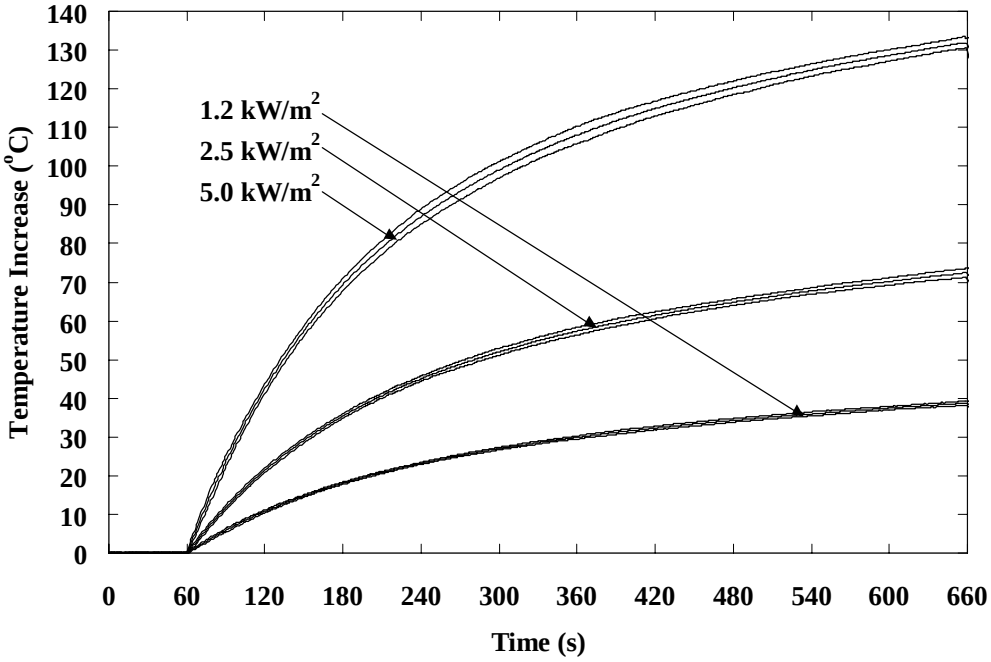

Figure 83. Response of copper disk with 4 type J thermocouples, substrate, all three heat flux levels, with error bars.

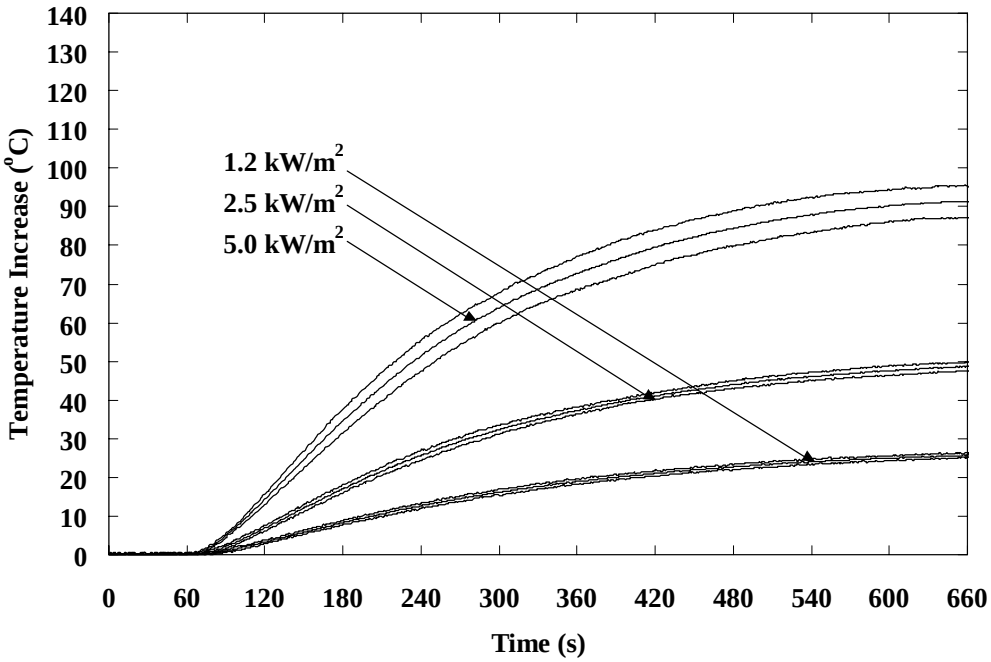

Figure 84. Response of copper disk with 4 type J thermocouples, fabric-exposed-no space, all three heat flux levels, with error bars.

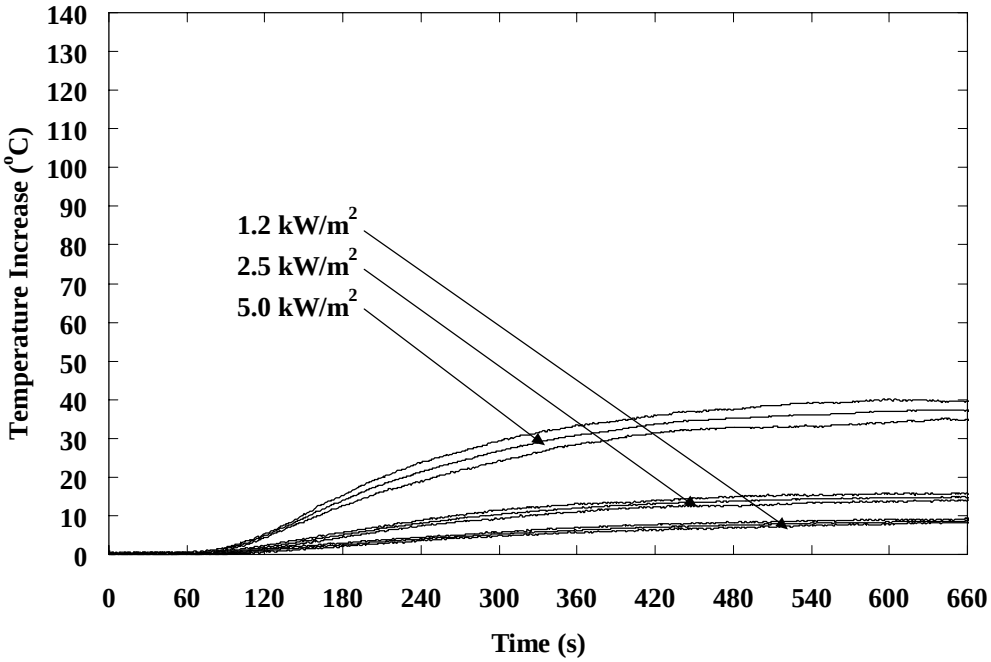

Figure 85. Response of copper disk with 4 type J thermocouples, fabric-exposed-space, all three heat flux levels, with error bars.

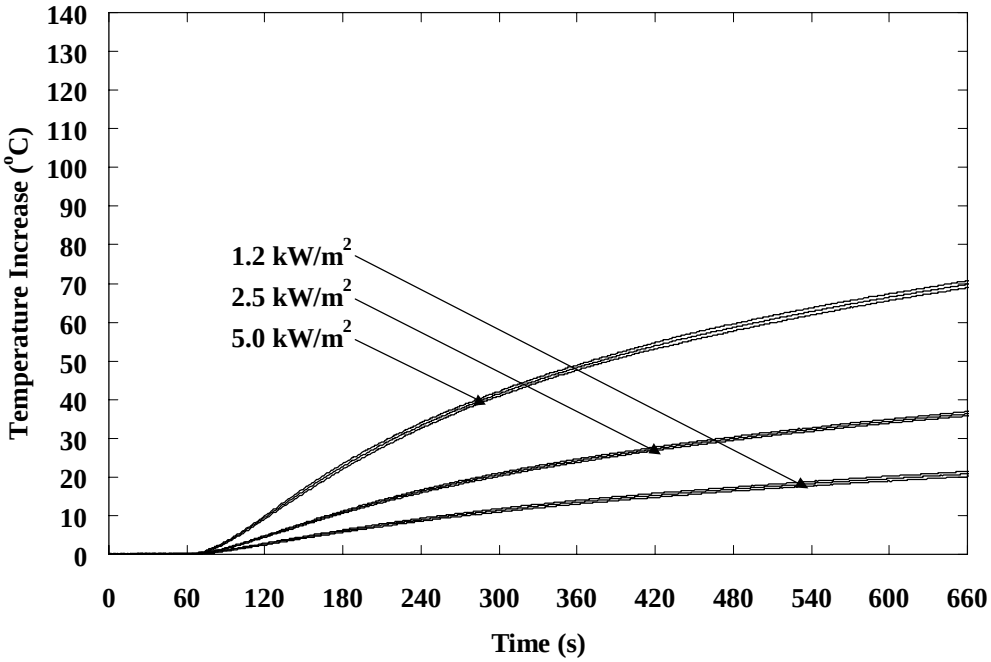

Figure 86. Response of copper disk with 4 type J thermocouples, fabric-substrate-no space, all three heat flux levels, with error bars.

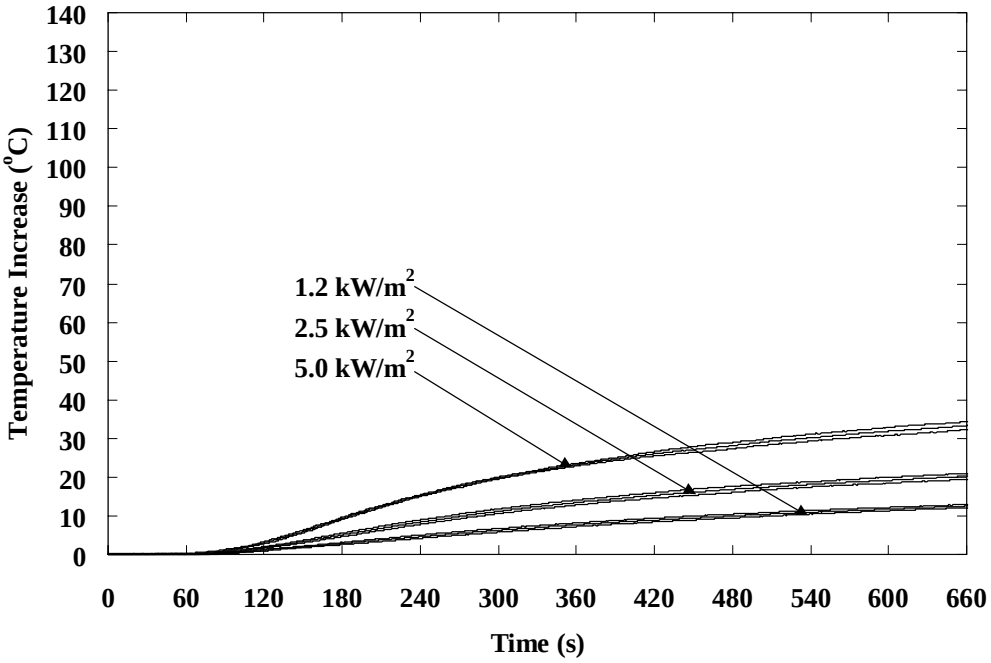

Figure 87. Response of copper disk with 4 type J thermocouples, fabric-substrate-space, all three heat flux levels, with error bars.

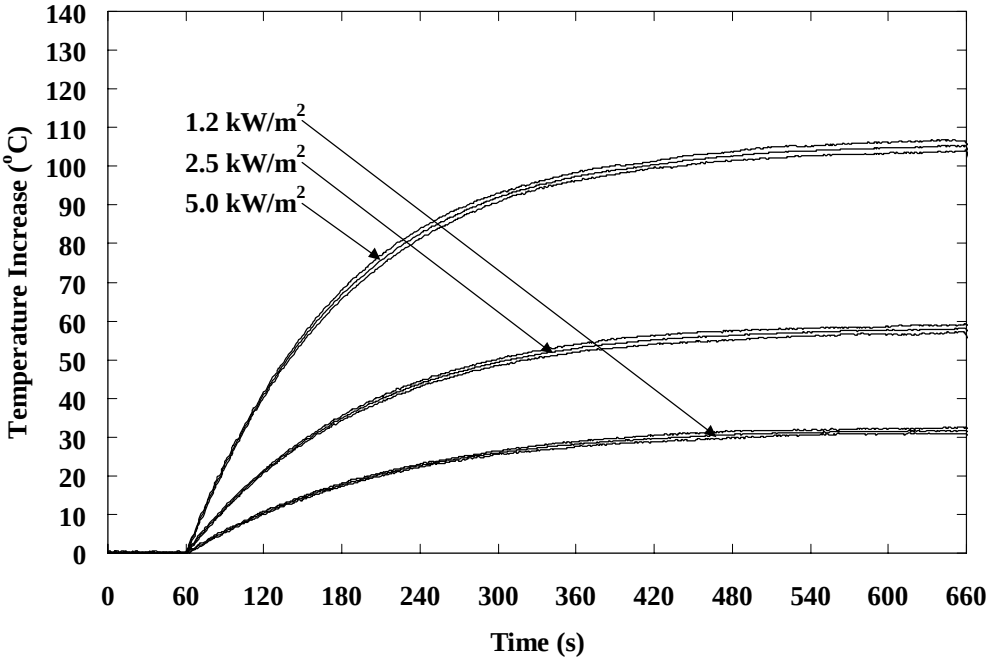

Figure 88. Response of copper disk with 1 type J thermocouple, exposed, all three heat flux levels, with error bars.

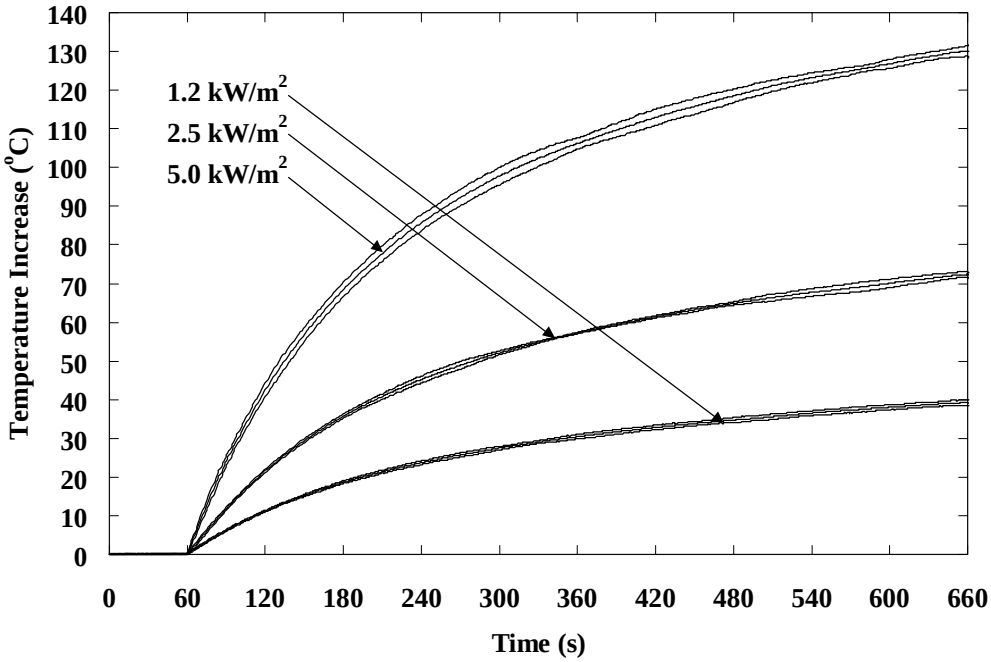

Figure 89. Response of copper disk with 1 type J thermocouple, substrate, all three heat flux levels, with error bars.

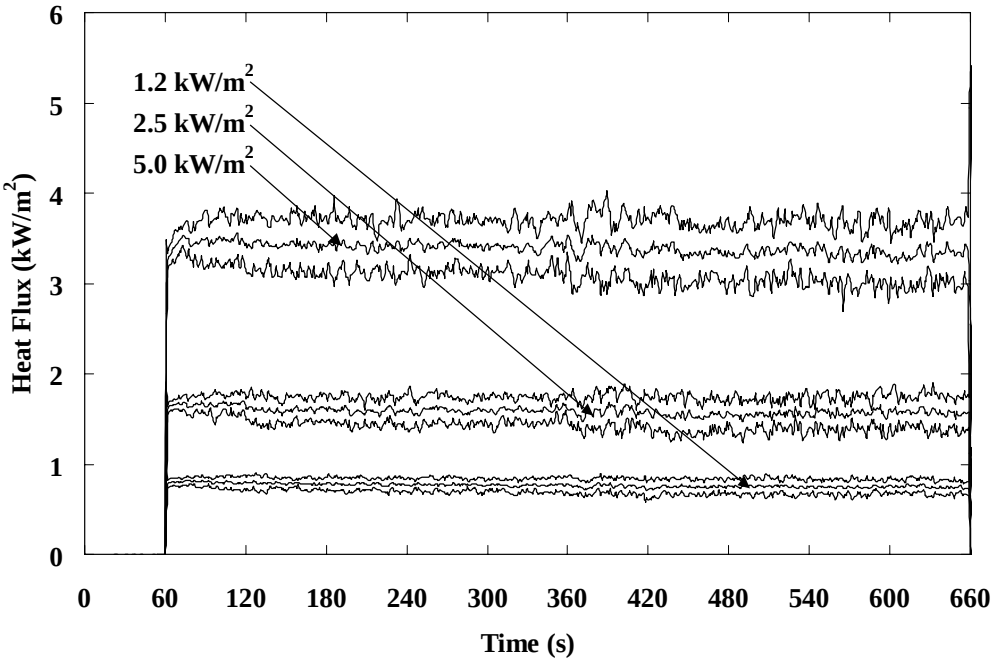

Figure 90. Response of thin film heat flux gauge, exposed, all three heat flux levels, with error bars.

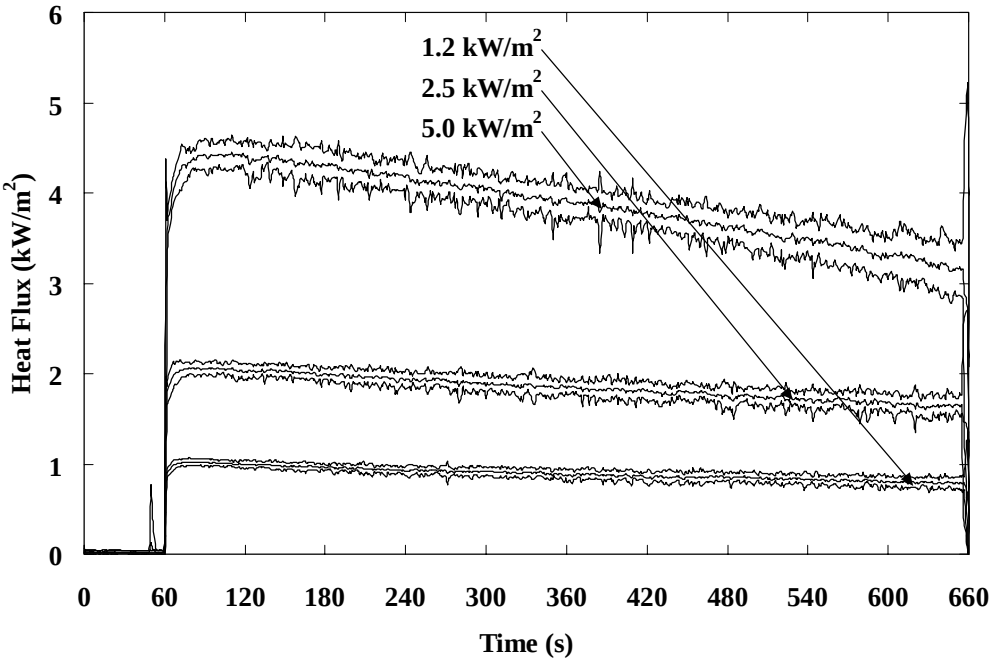

Figure 91. Response of thin film heat flux gauge, substrate, all three heat flux levels, with error bars.

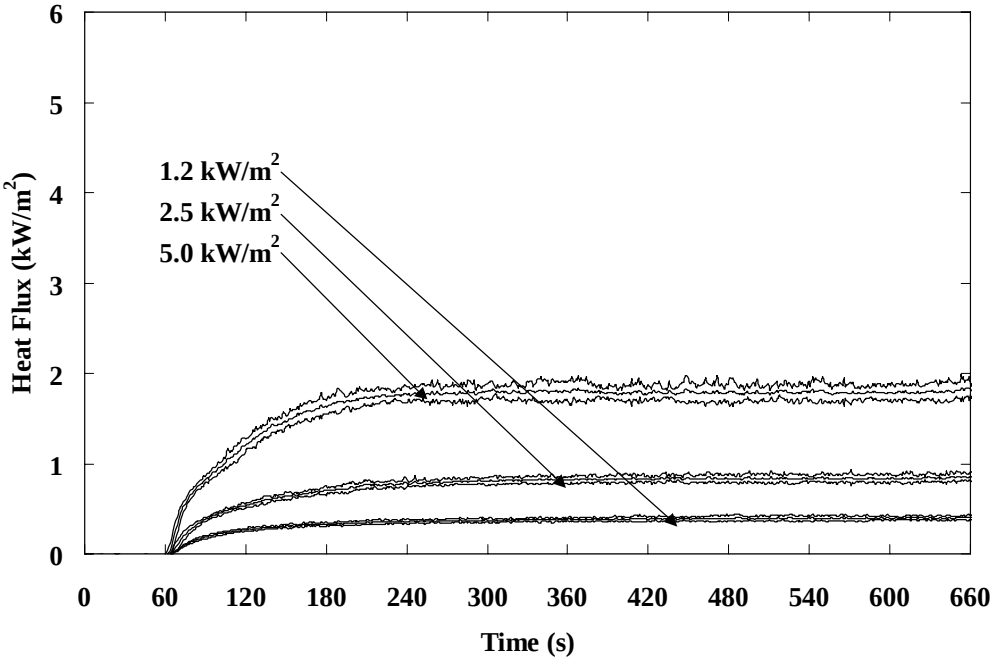

Figure 92. Response of thin film heat flux gauge, fabric-exposed-no space, all three heat flux levels, with error bars.

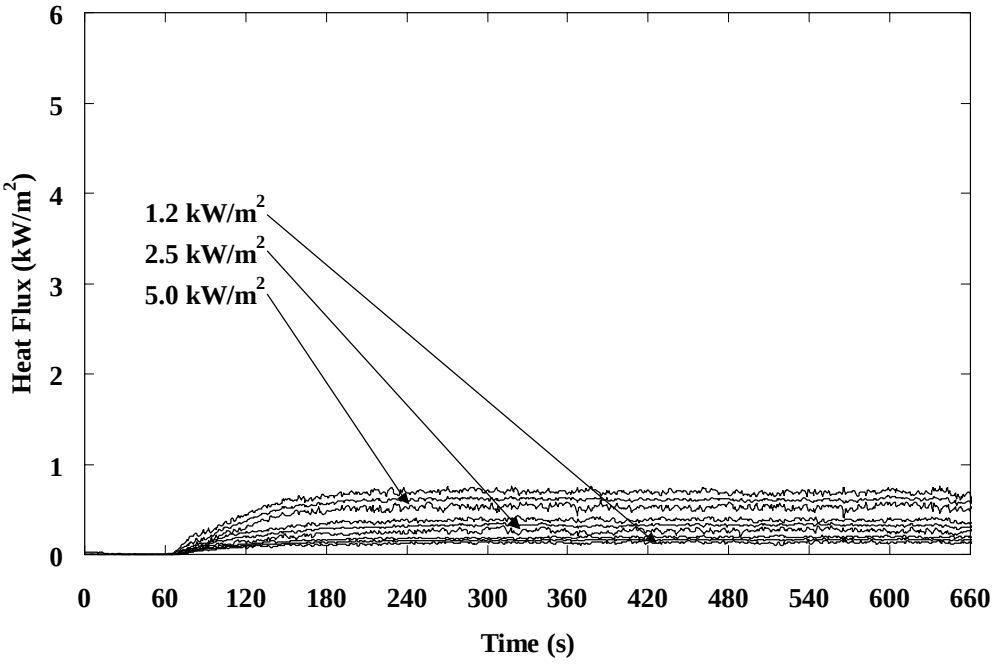

Figure 93. Response of thin film heat flux gauge, fabric-exposed-space, all three heat flux levels, with error bars.

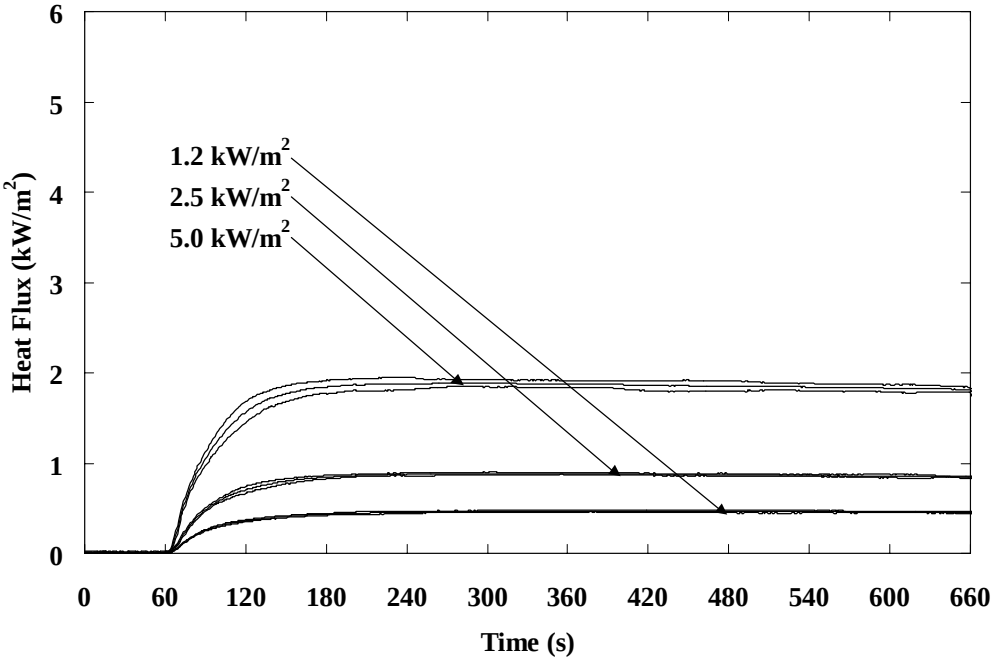

Figure 94. Response of thin film heat flux gauge, fabric-substrate-no space, all three heat flux levels, with error bars.

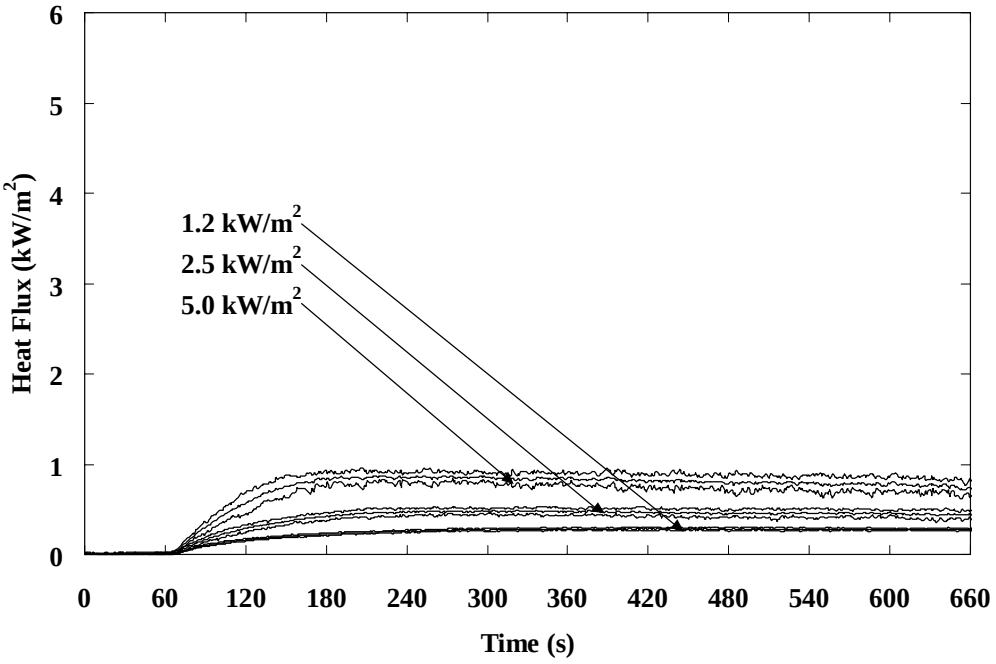

Figure 95. Response of thin film heat flux gauge, fabric-substrate-space, all three heat flux levels, with error bars.

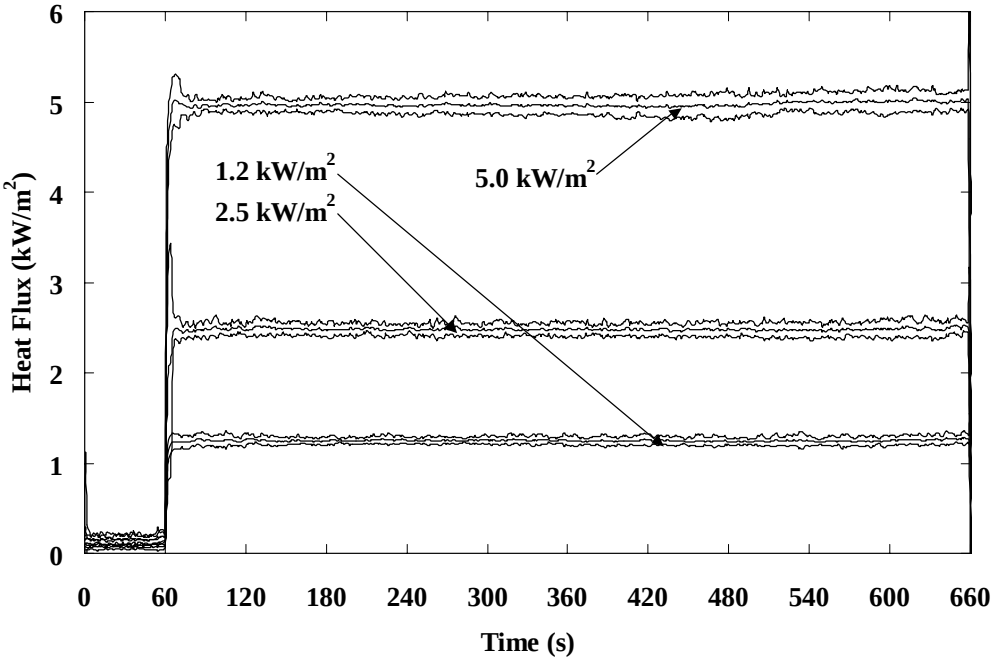

Figure 96. Response of Schmidt-Boelter total heat flux gauge, exposed, all three heat flux levels, with error bars.

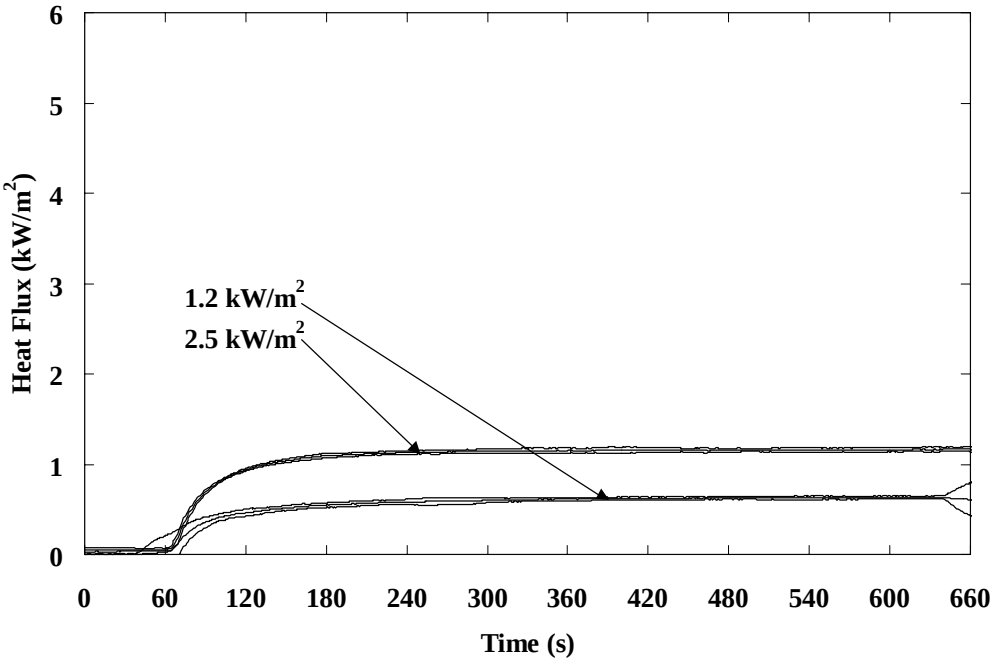

Figure 97. Response of Schmidt-Boelter total heat flux gauge, fabric-exposed-no space- two heat flux levels, with error bars.

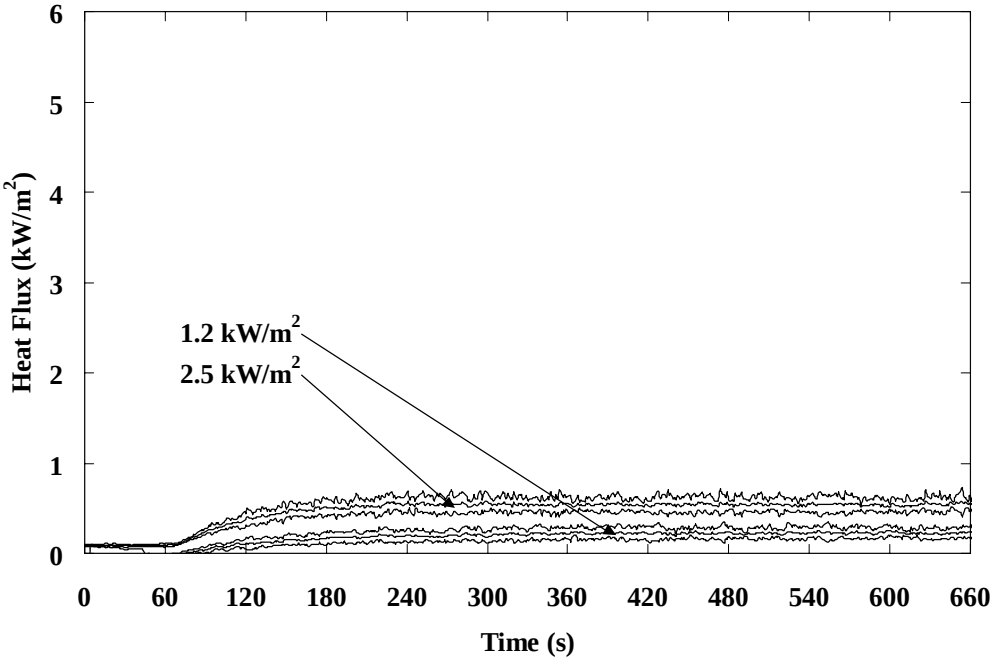

Figure 98. Response of Schmidt-Boelter total heat flux gauge, fabric-exposed-space, two heat flux levels, with error bars.

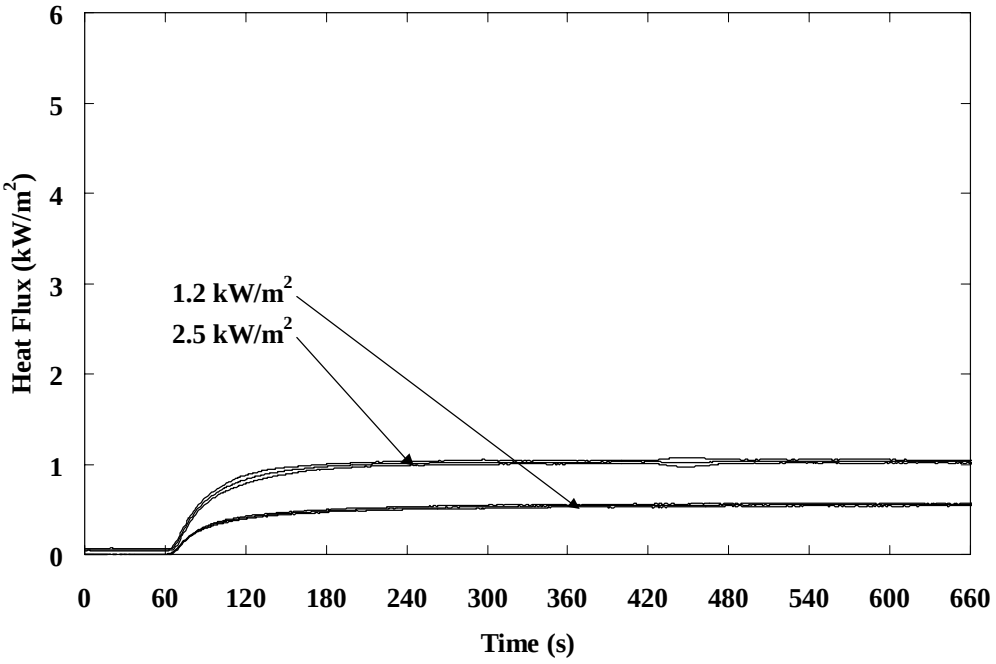

Figure 99. Response of Schmidt-Boelter total heat flux gauge, fabric-substrate-no space, two heat flux levels, with error bars.

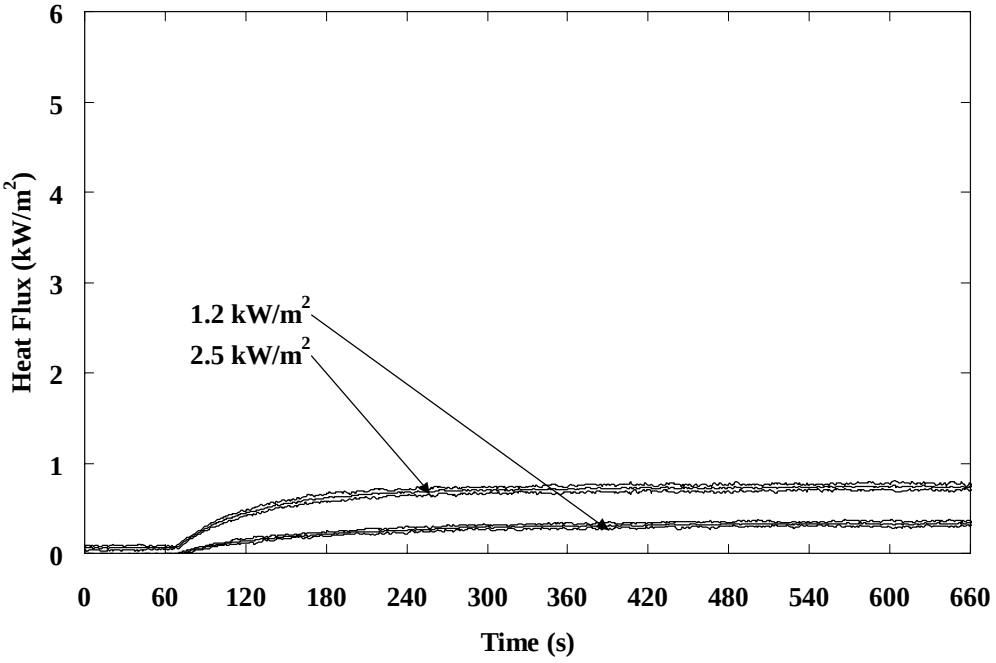

Figure 100. Response of Schmidt-Boelter total heat flux gauge, fabric-substrate-space, two heat flux levels, with error bars.

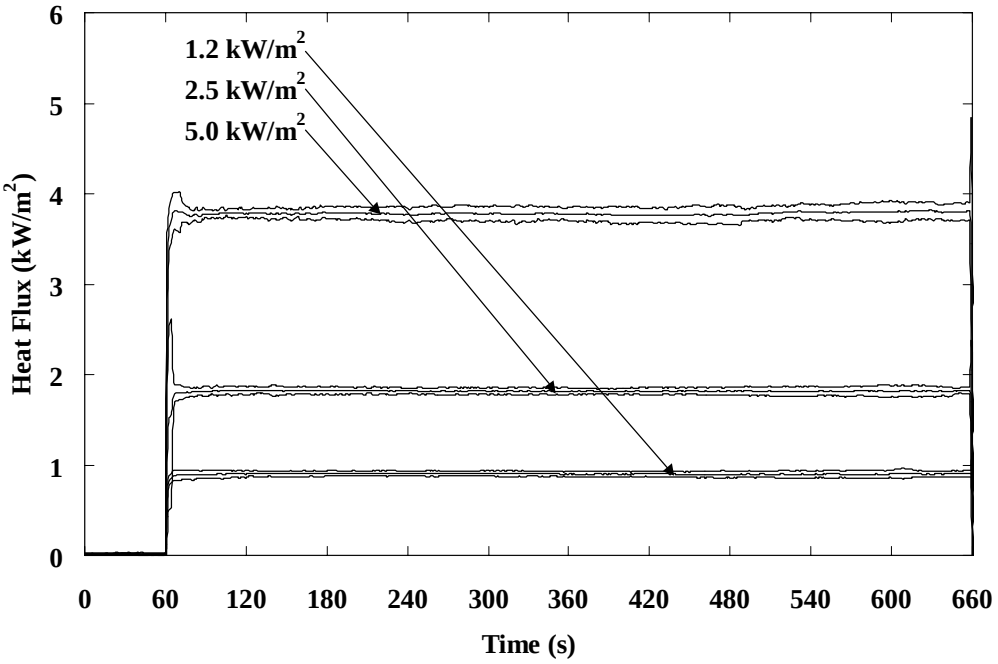

Figure 101. Response of sapphire window radiometer, exposed, all three heat flux levels, with error bars.

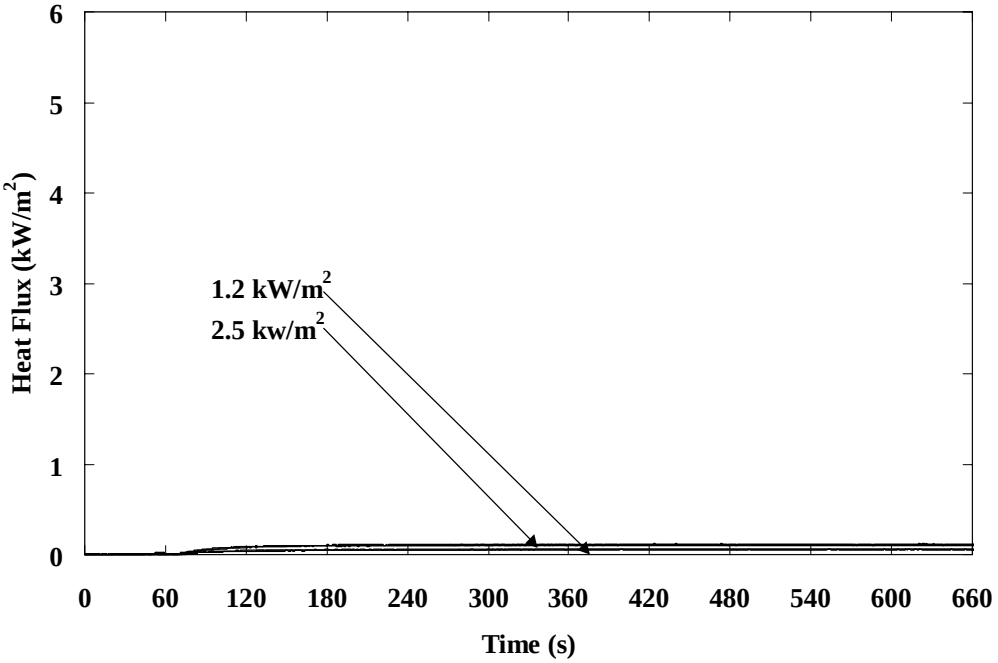

Figure 102. Response of sapphire window radiometer, fabric-exposed-no space, two heat flux levels, with error bars.

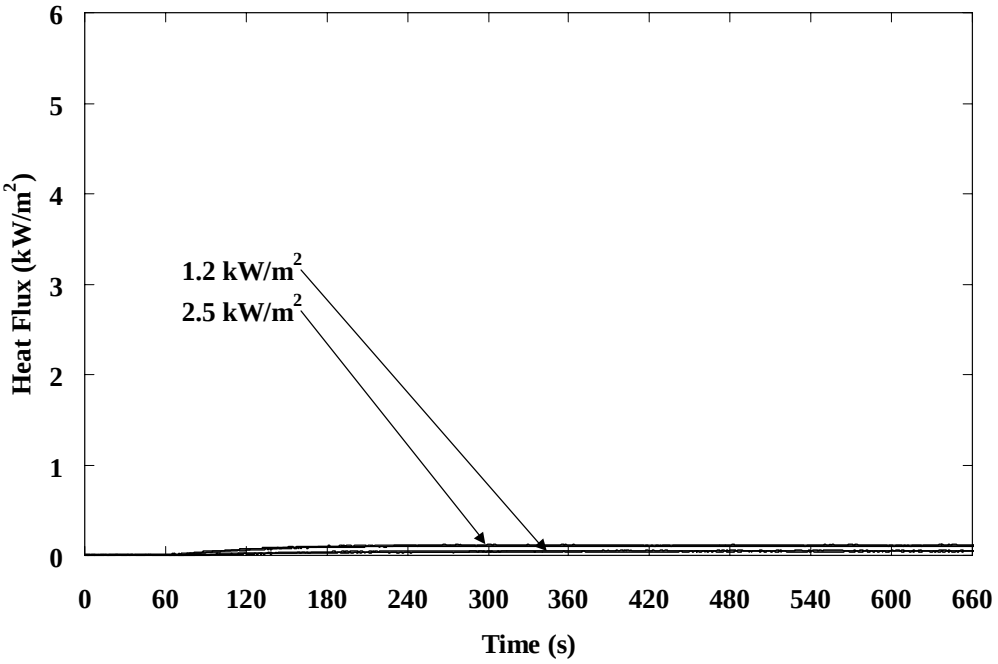

Figure 103. Response of sapphire window radiometer, fabric-exposed-space, two heat flux levels, with error bars.

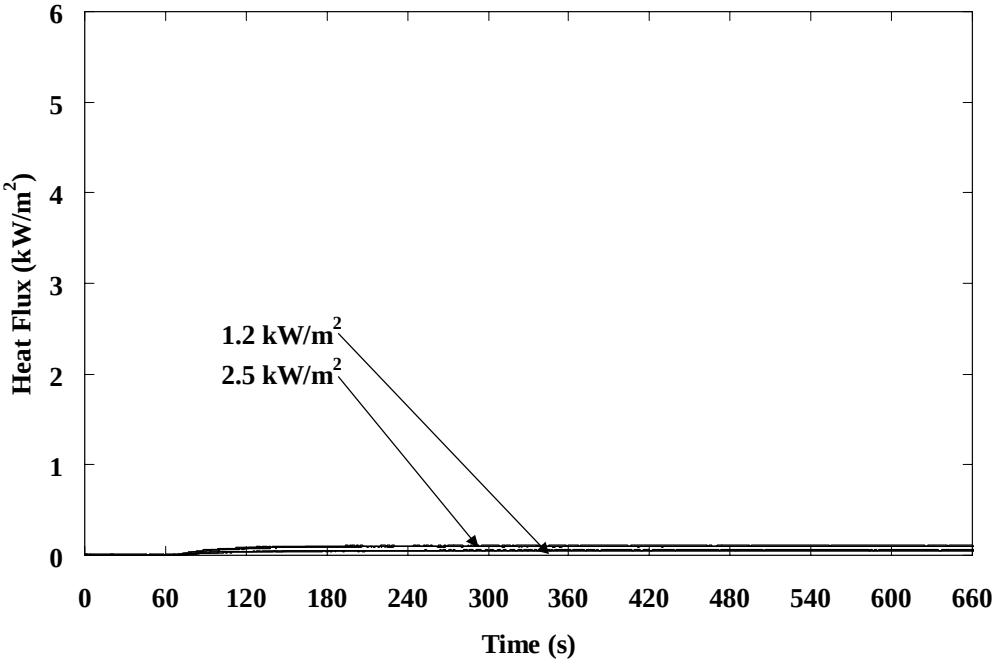

Figure 104. Response of sapphire window radiometer, fabric-substrate-no space, two heat flux levels, with error bars.

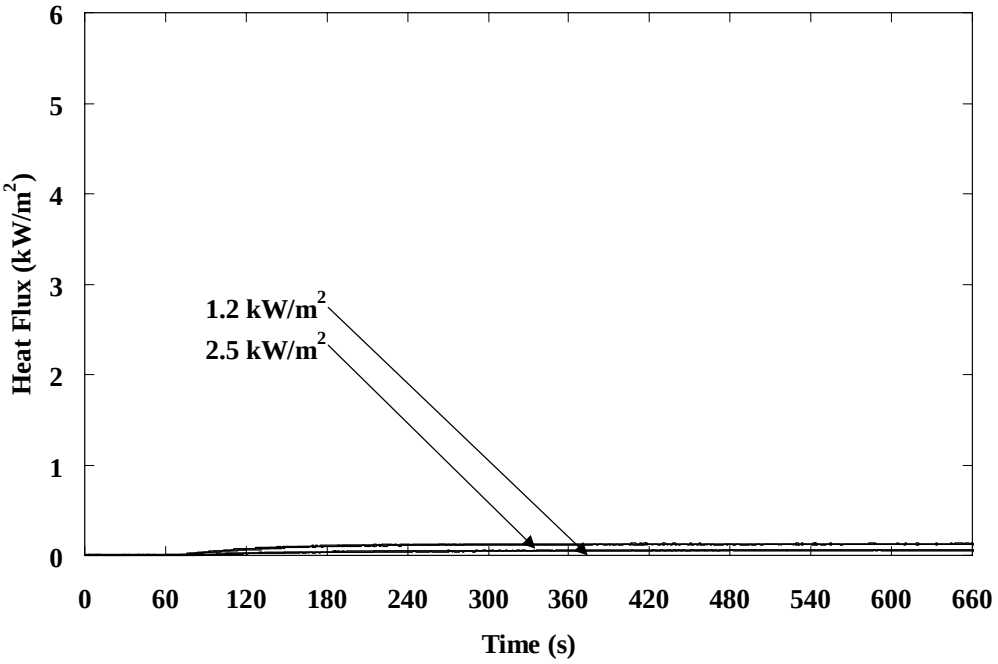

Figure 105. Response of sapphire window radiometer, fabric-substrate-space, two heat flux levels, with error bars.

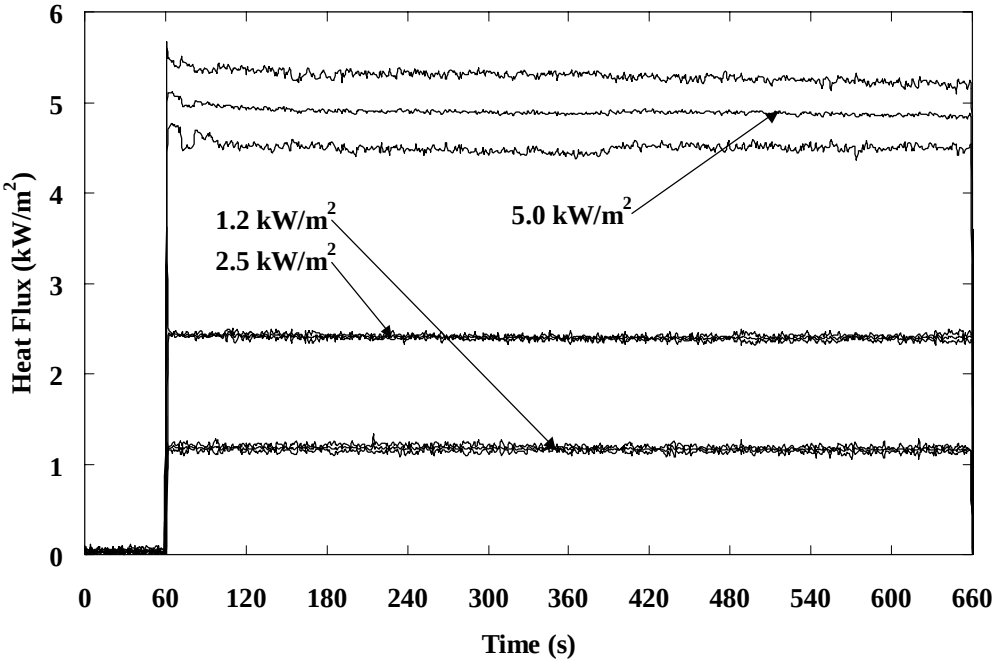

Figure 106. Response of zinc selenide window radiometer, exposed, all three heat flux levels with error bars.

11.0 References

1 National Fire Protection Association, "National Fire Protection Association 1971 Standard on Protective Ensemble for Structural Fire Fighting," 2000 Edition, National Fire Protection Association, Quincy, MA 02269.

2 Lawson, R. L., "Fire Fighter's Protective Clothing and Thermal Environments of Structural Fire Fighting," NISTIR 5804. National Institute of Standards and Technology, Gaithersburg, MD, August 1996.

3 Foster, J. A., and Roberts, G. V., "Measurements of the Firefighting Environment – Summary Report," Fire Engineers Journal. Vol. 55, No. 178, September 1995, pp 30-34.

4 Abbott, N. J., and Schulman, S., "Protection from Fire: Non Flammable Fabrics and Coatings," Fire Retardants: Proceedings of 1976 International Symposium on Flammability and Fire Retardants, May 6-7, 1976, pp 64-80.

5 Henriques, F.C., and Moritz, A. R., "Studies of Thermal Injury: I. The Conduction of Heat to and Through Skin and the Temperatures Attained Therein. A Theoretical and an Experimental Investigation," American Journal of Pathology, Vol. 23, p. 531, 1947.

6 Stoll, A. M., and Greene, L.C., "Relationship Between Pain and Tissue Damage Due to Thermal Radiation," Journal of Applied Physiology, Vol. 14, pp 373, 1959.

7 Chianta, B. A., and Stoll, A. M., "Heat Transfer in Protection From Flames," Aerospace Medicine, Vol. 34, p 7-11, January 1964.

8 Barker, R. L., Hamouda, H., Shalev, I., and Johnson, J., "Review and Evaluation of Thermal Sensors for use in Testing Fire Fighters Protective Clothing," NIST GCR 99-773, National Institute of Standards and Technology, Gaithersburg, MD 20899, March 1999.

9 Dale, J. D., Crown, E. M., Ackerman, M. Y., Leung, E., Rigakis, K. B., "Instrumented Mannequin Evaluation of Thermal Protective Clothing," Performance of Protective Clothing: Fourth Volume, ASTM STP 1133, ASTM Philadelphia 1992.

10 Vettori, R. L., "Effect of an Obstructed Ceiling on the Activation Time of a Residential Sprinkler," NISTIR 6253, National Institute of Standards and Technology, Gaithersburg, MD 20899, November 1998.

11 Lawson, J. R., and Twilley, W. H., "Development of an Apparatus for Measuring the Thermal Performance of Fire Fighter's Protective Clothing," NISTIR 6400, National Institute of Standards and Technology, Gaithersburg, MD 20899, October 1999.

12 American Society for Testing and Materials, "E162 Standard Test Method for Surface Flammability of Materials Using a Radiant Heat Energy Source," Annual Book of ASTM Standards, Vol. 04.07, West Conshohocken, PA, 1997.

13 American Society for Testing and Materials, "E1321 Standard Test Method for Determining Material Ignition and Flame Spread Properties," Annual Book of ASTM Standards, Vol. 04.07, West Conshohocken, PA, 1997.

14 McGuire, J., H., "Heat Transfer by Radiation," Department of Scientific and Industrial Research and Fire Offices Committee, London, 1953.

15 Incropera, F. P., and Dewitt, D. P., "Fundamentals of Heat and Mass Transfer Fourth Edition," John Wiley and Sons, New York, NY, 1996.

16 Taylor, B.N., Kuyatt, C. E., "Guidelines for Evaluating and Expressing the Uncertainty of NIST Measurements Results," NIST Technical Note 1291, National Institute of Standards and Technology, Gaithersburg, MD 20899, 1994.
17 American Society for Testing and Materials "Manual on the Use of Thermocouples in Temperature Measurement Fourth Edition," ASTM, 1916 Race Street, Philadelphia, PA 19103, 1993.
18 Lawson, J. R., Pinder, T. A., "Estimates of Thermal Conductivity for Materials used in Fire Fighter's Protective Clothing," NISTIR 6512, National Institute of Standards and Technology, Gaithersburg, MD 20899, May 2000.
19 Stoll, A. M., and Hardy, J. D., "Direct Experimental Comparison of Several Surface Temperature Measuring Devices," Review of Scientific Instruments, Vol. 20 No. 9 September 1949.
20 American Society for Testing and Materials, "E-457 Standard Test Method for Measuring Heat Transfer Rate Using a Thermal Capacitance (Slug) Calorimeter," Annual Book of ASTM Standards, Vol. 04.07, West Conshohocken, PA, 1997.